December 2014

Project Report No. 537

Inorganic polymer bio-composites

Edited by AS Matharu, University of York
on behalf of the consortium members:
University of Bangor, Velcourt R&D, AHDB-HGCA, C S Process Engineering Ltd, PQ Silicas UK, Velcourt Ltd Farm Management, Eccleshall biomass, EPR Ltd, E4 Structures Ltd, Envirowall Ltd, B&Q Plc

This is the final report of a 58 month project (RD-2007-3368) which started in November 2008. The work was funded by Defra and a contract for £120k from HGCA.

HGCA is the cereals and oilseeds division of the Agriculture and Horticulture Development Board.

CONTENTS

1. ABSTRACT

The aim of this project was to develop a generic production methodology with sound underpinning science and technology, leading to pre-commercial prototypes of general purpose boards (herein termed ‘bioboards’) that are wholly derived from sustainable resources and which make maximum use of agricultural lignocellulosic residues (Figure 1). Ideally, all bioboard components: aggregate (straw), binder (biosilicate) and hardener (by-product wastes) were to be derived from agricultural residues. The resultant bioboards were envisaged to have advantages of being inexpensive, environmentally benign, chemically and biologically resistant, and physically and mechanically stable. By employing a variety of agri-derived raw materials the project aimed to minimise its impact on the environment and biodiversity and maximise socio-economic benefits through optimum resource utilisation and added value to farming communities and the manufacturing and retail industry.

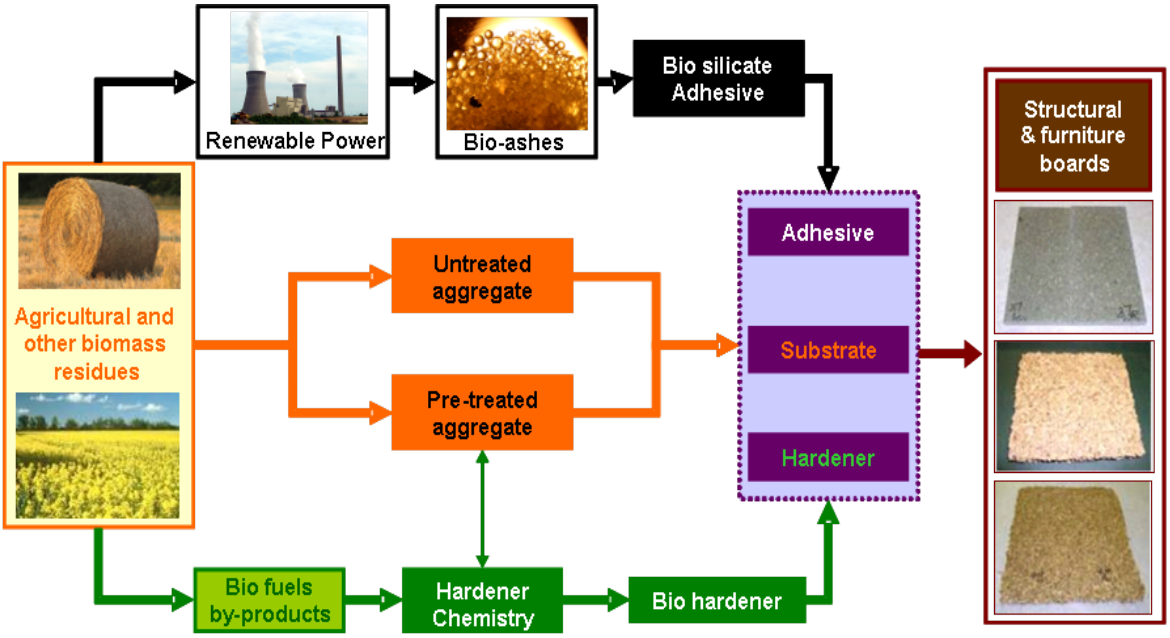

Figure 1. Schematic of overview of the project: Agricultural residues to bioboards via biosilicate adhesives and by-product derived hardeners

The project led by the University of York brought together a full supply chain consortium, each with given roles and responsibilities (Figure 2): B&Q – furniture manufacturer and DIY retailers; CS Process Engineering – panel production systems (Compak) developer and manufacturer; PQ Corporation - silicate manufacturer; Bioflame waste biomass power plant manufacturer and provider of biomass ash (withdrew in 2011) and Velcourt Farm and Management and Bical – Raw Materials producers (withdrew 2011); EPR Ltd – provider of biomass ash (joined 2011); Eccleshall Biomass Ltd – provider of biomass ash (joined 2011); E4 Structures – composite materials manufacturers (joined 2012); Envirowall Ltd – composite materials manufacturers. University of York, Bangor University and Velcourt R&D provided the R&D support. The programme was sponsored by Defra

through the Renewable Materials LINK programme and by research grant from AHDB-HGCA.

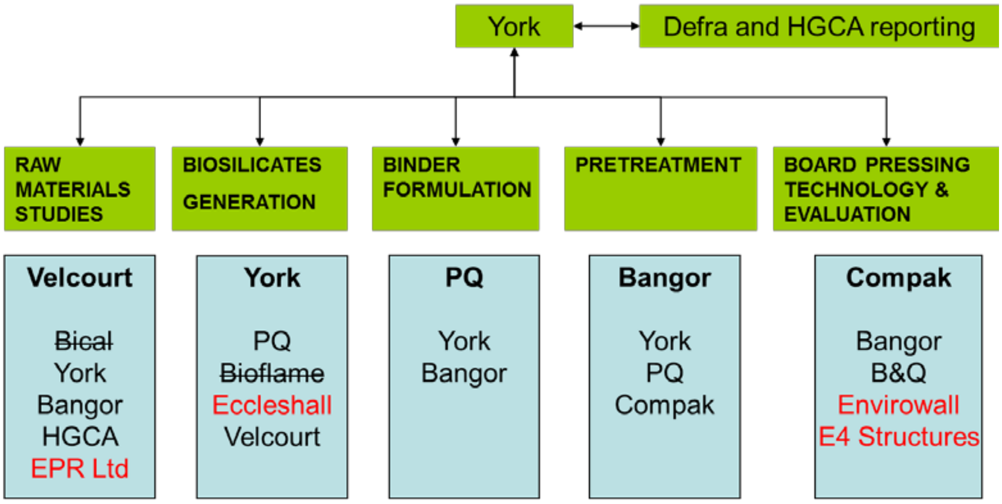

Figure 2. Division of roles and responsibilities organogramme

The technical standard (P3, see Table 1) and target application for the bioboards were set by B&Q based on their market research in the area of kitchen cabinet doors, carcases and worktops, which were based on chipboard/wood/MDF, i.e. troubled resources based on competition for wood with other markets and health concerns with respect to use of formaldehyde, urea and isocyanate adhesives.

Table 1. Values for a board of over 6 to 13 mm thickness at P3 classification according to EN 312:2003 Particleboards - specifications.

Parameter	Value	Standard method
Internal Bond Strength (N/mm^2)	0.45	EN 319
Thickness swelling (%)	14	EN 317
Bending strength (N/mm^2)	15	EN 310
Modulus of elasticity in bending (N/mm^2)	2050	EN 310

Achievements against milestones

1. *First set of bioderived Auxiliary (in-situ) hardeners (see Section 2.5)*

The need for a protein-containing source as an auxiliary hardener was established very early on in the project. The first set trialled were skimmed milk, waste milk (from Arla, Leeds, UK) and whey protein. The latter produced best boards. Unfortunately, we were not successful in attaining any suitable auxiliary hardeners from the bio-diesel industry so this aspect was curtailed very early on in the project. However, glycerol, a by-product from biodiesel production, was trialled not in the context of an auxiliary hardener but as a replacement for water in the formulation, not with much success.

2. *Portfolio of bioderived Auxiliary (in-situ) hardeners (see Section 2.5)*

We have established a portfolio of hardeners in addition to the three mentioned above that include: sodium lignosulfonate; calcium lignosulonate; ammonium lignosulfonate; tannic acid; glucose-tannic acid; tannic acid-hydroxymethyl furfural (HMF); wheat gluten; defatted wheat gluten; wheat gluten-zein; wheat gluten-polylactic acid; wheat gluten-glyoxal.

3. *Development of biosilicate binders (see Section 2.4)*

Biosilicate has been successfully leached from laboratory-generated ash derived from a variety of pretreated straws and wood chip, and commercial ashes from EPR (miscanthus) and Eccleshall (green waste/wood chip). The latter contain very low silica concentration and are not useful as biosilicate binders. A large proportion of silica can be extracted utilising the inherent alkalinity of the ashes formed. The additional alkali required can be calculated from the initial inorganic content of the straw. However, less than 100% of the silica is completely solubilised.

4. *Application of biosilicate binders (see Sections 2.4 and 2.5)*

Biosilicate binders have been used successfully to make bioboards albeit not of P3 standard. In a formulation with dewaxed wheat straw, whey protein and either biosilicate solution or commercial KI20, the biosilicate solution(s) outperformed K120 (see Table 24).

5. *Surface pretreatment methodology (see Sections2.3, 2.4, 2.5, 2.6)*

Agronomy trials based on altering PGR and nitrogen levels with respect to Hereward and Viscount varieties had limited effect on ash production for biosilicate leaching or board making. However, dewaxing using ethanol (Soxhlet) is an important pre-treatment together with milling of the straw to sizes of 1 and 2 mm (preferably a 50:50 mix). Waxed or natural straws fail to bind. De-waxed straw, although an additional processing step, offers a mixture of waxes, lipids and esters, as a potential revenue side-stream. Pretreatment of straws with respect to minerological content of the resultant ash post combustion and extractability of silica was significant. Acid washing removes salts and calcium, and results in silica with a greater amorphous character but a less alkaline solution following combustion and extraction. Water washing and ethanol Soxhlet extraction both remove salts (particularly KCl). However, ethanol extraction does not affect the alkalinity of the extraction solution formed after combustion with similar levels of silica extracted.

6. *Initial boards processing methodology, system optimized boards processing methodology, laboratory scale boards (Sections 2.5 and 2.6)*

Work both at York and Bangor, and subsequently Compak, allowed the progression from 5 x 5 cm to 30 x 30 cm to 50 x 50 cm boards being manufactured. De-waxing was undertaken at large scale (50 L) as well as milling. Press times and profiles prior to scale-up were optimised by Bangor. Efficient thermal transfer, curing and steam egress all affected the final properties of the board. For example, significant variations in density were noted for some formulations. Silicate distribution was investigated by scanning electron microscopy but did not yield anything significant.

De-waxed rapeseed straw gave stronger boards than wheat straw (all varieties). Although boards of P3 standard have been made with respect to internal bond strength, water swelling (failure to get it less than 14%) is still problematic. The speed of cure still needs improving.

7. *First and Second commercially viable prototypes (Section 2.7)*

Boards of 12 mm and 18 mm thickness were successfully manufactured by Compak. Production preparation and actual production and then subsequent cleaning of equipment took approximately one week per board thickness. Particular care had to be taken cleaning resin systems after use of the silica resins because of their alkalinity, a risk to metal pipework. 2% solids silica resin was used in the formulation. Unfortunately, a small amount of MDI (2.5%) had to be added so that the press cycle could operate at curing speeds to commensurate with traditional MDI-lines.

Dissemination

The work within has reported at:

i. Renewable Resources and Biorefineries 6 (RRB 6), 7-9 June 2010, Dusseldorf.'Towards an integrated wheat straw biorefinery'. Jennifer Dodson, V. Budarin, P. Shuttleworth, A. Hunt, R. Marriott, K. Milkowski and J. Clark. Best poster/presentation Award.
ii. Bioten, 21-23 September 2010, Birmingham. Poster and Oral presentation - 'The elemental value of ash'.
iii. Enhanced Landfill Mining, 4-6 October 2010, Molenheide, Belgium. Poster - 'The elemental value of ash'
iv. Cereals 2010. HGCA Research brief: Biocomposites incorporating wheat straw.
v. NORSC: Northern Universities for Sustainable Chemistry, 28 September 2010, York Poster - 'The elemental value of ash'
vi. NNFCC's Green Supply Chain 2010, 4-5 November, York. Poster - 'The elemental value of ash'.

vii. Jennie Dodson, PhD 2012, University of York.

viii. “The chemical value of wheat straw combustion residues. / Dodson, Jennifer R.; Hunt, Andrew J.; Budarin, Vitaly L.; Matharu, Avtar S.; Clark, James H. *RSC Advances*, **1**, No. 3, 2011, p. 523-530.

ix. “Alkali silicates and structured mesoporous silicas from biomass power station waste: the emergence of bio-MCMs.” MacQuarrie, Duncan James; Clark, James Hanley; Matharu, Avtar Singh; Cooper, Emma Cecelia; Dodson, Jennifer Ruth; Hunt, Andrew John.; Cole, John; Minihan, Alan. *Green Chemistry*, **15**, No. 5, 2013, p. 1203-1210.

2. BACKGROUND

Wood based panels are an ubiquitous part of office and home design with just over 6 million $m^3 y^{-1}$ used in the UK every year (Figure 3a)(FAOSTAT).* The major types used are plywood, MDF and particleboard, with only the latter two produced in the UK (Figure 3b). These two materials are, therefore, most relevant to this study.

Particleboard has been defined as a “sheet material manufactured from small pieces of wood or other ligno-cellulosic materials (e.g. chips, flakes, splinters, strands, shreds etc.) agglomerated by use of an organic binder together with one or more of the following agents: heat, pressure, humidity, a catalyst, etc. MDF is defined as a “type of fibreboard with a density exceeding 0.50 g cm^{-3} but not exceeding 0.80 g cm^{-3}”. Fibreboard is “a panel manufactured from fibres of wood or other lignocellulosic materials with the primary bond deriving from the felting of the fibres and their inherent adhesive properties. Bonding materials and/or additives may be added. It is usually flat pressed but may also be moulded.” (FAOSTAT)

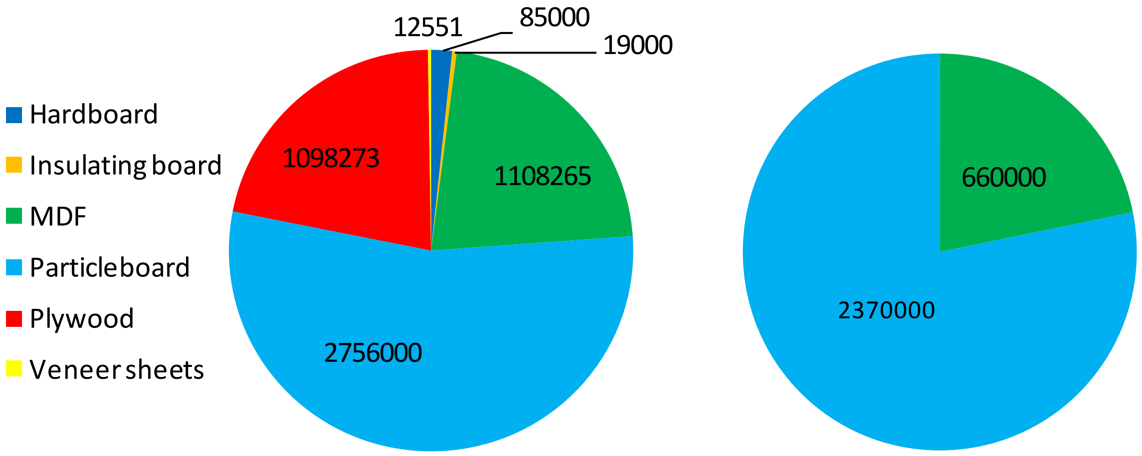

Figure 3: Distribution of wood-based panelling used in the UK in 2009 (a) and production of wood-based panelling in the UK in 2009 (b) (Data from FAOSTAT) (Originally in colour)

The manufacturing processes for MDF and particleboard are shown in Figure 4. Although the overall the process is similar for both products, the manufacturing process for MDF requires the production of fine fibres prior to pressing.

---

* Data shown relevant at the time in the project

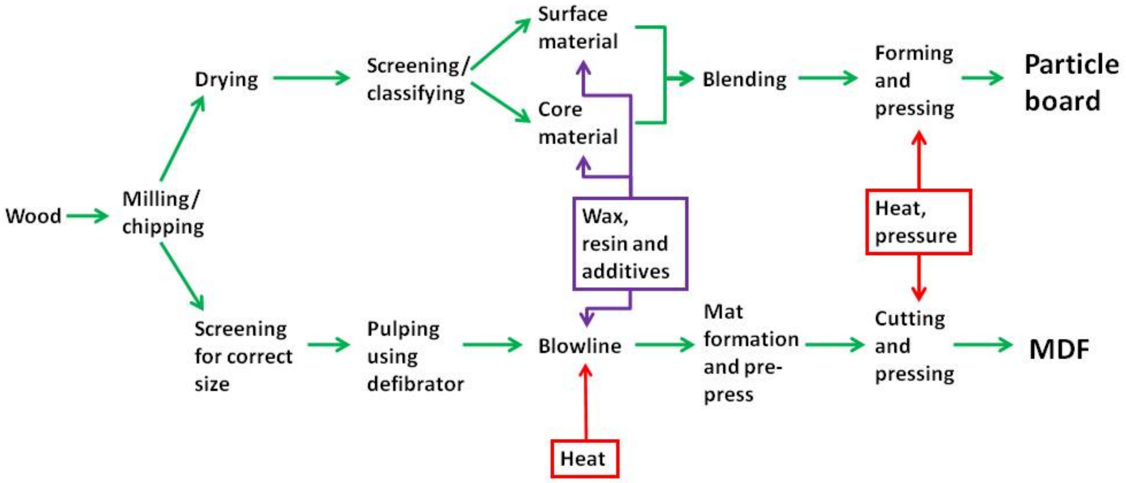

Figure 4. Main steps in the manufacture of particle board and MDF (Originally in colour)

2.1. Environmental impacts and challenges

There are three major environmental issues related to the current manufacture of these lignocellulosic construction materials: the binder; the use of wood as the substrate; and inefficiencies in the manufacturing process.

Urea formaldehyde (UF) is used as the binder for over 90% of particleboard and is also the main binder for many other wood-based panels due to the strong bonds formed at low cost (Nemli and Öztürk, 2006). However, formaldehyde has been classified as a 'probable carcinogen' by the International Agency for Research on Cancer (Ghost and Sain, 2006), is linked to eye, nose and respiratory irritation and can cause contact dermatitis (Isaksson *et al.,* 1999), thereby posing a significant health risk to people working in the composite board manufacturing industry. In addition, formaldehyde emissions continue to be released following manufacture due to the presence of free formaldehyde, which has resulted in many countries applying stringent limits on formaldehyde release from composite boards (California Air Resources Board, 1985). Urea formaldehyde is also manufactured from fossil fuel sources (Dutta and Shieh, 1985). With around 10% of urea formaldehyde present in particleboard by weight, and a higher content in MDF (Environmental Protection Agency),the production of boards worldwide puts pressure on the dwindling fossil fuel resources.

Currently, both particleboard and MDF are overwhelmingly made from wood-based material, usually waste from sawmills, although some virgin wood is used. However, with an estimated increase of MDF production of 4% year-on-year from 2006-2010 in Europe (Halvarsson *et al.* 2008), competition from other products for the same raw material and environmental imperatives to reduce virgin wood consumption, the demand for non-wood lignocellulosic substrates will increase.

2.2. Opportunities for alternative resins

Due to these challenges with conventional production, many researchers have been searching for alternative binders or production methods. Melamine modified urea formaldehyde (Chung-Yun *et al.,* 2008), phenol-formaldehyde (Rammon, 1997), and methylenediphenyl isocyanate (MDI) all show reduced formaldehyde emissions. However, similar concerns remain as for UF since they are fossil-fuel derived and often require corrosive or irritating starting materials.

In search of sustainable alternatives, other researchers have looked to renewable binders based on, for instance, soy flour (Columbia Forest Products), forest-floor biomass (depolymerised lignin)(Ghosh and Sain, 2006), cashew nut shell liquid (Lubi and Thachil, 2007) and sugarcane bagasse lignin (Hoareau *et al.,* 2006). Mostly these are phenolic substitutes, although they usually cannot entirely replace the fossil fuel phenol source. An alternative approach is to eradicate the need for binders altogether. High strength-high density low cost binderless boards have been formed from coconut husk via the melting of the high lignin content pith residue binding the coir fibres (van Dam *et al.,* 2004).

Inorganic composites that are highly resistant to fire and insects have been developed using gypsum and Portland Cement (English, 1994). These boards usually contain between 10–70 wt% wood particles and consequentially require 30–90 wt% binder due to the high viscosity of the inorganic binders (Simatupang and Geimer, 1990; Giancaspro *et al.,* 2008). They can also require long cure times, although they are often set at ambient conditions. Research using potassium aluminosilicate as an alternative binder showed that with 70% binder by weight and curing at ambient temperature and pressure, highly fire-resistant materials could be formed (Giancaspro *et al.,*2008).

One possible binder system is the use of silicate binders; silicates are inorganic, polymeric, alkaline silica based materials. Alkali silicates have been utilised as adhesives in many applications including cardboard packaging and foil laminate (PQ Corporation Bulletin, 2006). Commercial silicates contain three basic components: silica (SiO_2), which can be obtain using sand; an alkali material (Na_2O or K_2O), which are obtained from soda ash or potash; and water. The silica and alkali materials are fused in a furnace at temperatures of 1200 °C and the resultant glass can be converted into liquids, or hydrous or anhydrous powders. The silicate binder can act as either a film binder or as a chemical binder, it depends on what material is being agglomerated, which property of the silicate is being utilised and what properties are desired in the final product. The weight ratio of

SiO_2:Na_2O or KCO is an important property for defining the final silicate binder; this will determine the solubility of salts and powders, as well as the reactivity of the silicate and other physical properties such as viscosity, and the desired ratio is between 1.5 and 3.3 (Gill, 1997; Rabbii, 2001). Silicate binders offer many advantages over the more traditional UF based systems; they emit no Volatile Organic Compounds (VOCs), they have a high tensile strength, they are water and heat resistant, readily available, and they are resistant to bacteria and vermin attack. One problem, however, with the traditional method of producing silicate is that it requires a lot of energy in order to heat the material up to 1200 °C, and so an alternative bio-derived silicate feedstock has been proposed, which is the use of wheat straw in which to produce the silicate.

Herein, the subsequent information is mainly based on primary information from Ms J Dodson's PhD thesis (2012), sponsored by this programme and HGCA, and information from consortium partners. This report is structured as follows:

1. Introduction: A detailed introduction is given based on literature relevant at the time of the project. Different straws and their composition are considered. Combustion ashes generated from commercial operations, their minerological content and uses are discussed. Silica in biomass, silicates and their uses are reported.
2. Raw materials and pretreatment: results of agronomy trials based on wheat (Hereward, Viscount) and oilseed rape (Castille, Dimension) straws are discussed. Analysis and characterisation of straws and resultant ashes is reported. Dewaxing trials both at small and large scale with differing solvents are described.
3. Biosilicate generation and binder formulation: A significant volume of work pertinent to understanding the changes occurring in the inorganic species in wheat straw during the combustion and extraction of wheat straw ashes and chars on a laboratory scale is reported. Both laboratory-derived and commercially-derived ashes are discussed. Optimisation methods for silica extraction and subsequent analysis are reported.
4. Binder formulation and board making trials: A variety of binder formulations are described based on protein-derived auxiliary hardeners, lignosulfonates, tannic acid, wheat gluten. Optimistion trials are discussed and transfer of technology/cross-collaboration between York and Bangor
5. Board pressing technology (Bangor): A significant volume of work is reported in trying to optimise a process amenable for large-scale manufacture of boards at P3 standard. Press time versus temperature for a variety of formulations is investigated with respect to P3 standards. The internal and external surfaces are interrogated by SEM.

6. Commercial manufacture of boards (Compak): A brief overview and protocol for manufacture of 12 and 18 mm boards is described.

3. INTRODUCTION

The 21st century is, and will be, gripped by several, inter-linked, global economic and environmental crises that, unless mitigated, represent an unsustainable future. Crude oil (and fossil fuel) continues to be our cornerstone for energy and feedstock chemicals but for how long? As emerging economic countries become more successful, coupled with increasing industrialisation and urbanisation, future oil production will be unable to meet the anticipated energy, materials and feedstock chemicals demand. Utilisation of biomass, at best non-food competitive, and where it is produced as a waste or low value resource represents an outstanding opportunity for our next generation feedstocks for the chemical industry. According to Pike Research green chemistry markets represented a market opportunity of $2.8bn in 2011 and are expected to reach to $98.5bn by 2020 (Pike Research, 2011). Judicious use of the 12 principles of green chemistry (Anastas and Warner, 1998) (waste as a resource, bio-based or renewable materials) is expected to save the chemical industry $65.5bn by 2020.

3.1. Agricultural residue availability in the UK[*]

In 2008, Copeland and Turley studied the national and regional supply/demand balance of agricultural straws in the UK, reporting a potential total annual straw yield of 11.9 million tonnes from wheat (54%), oilseed rape (21%), barley (20%), oats (4%), other cereals (1%) and linseed (0.1%) (Copeland and Turley, 2008). Allowing for the current straw use in the livestock and mushroom industries, they estimated approximately 3 million tonnes annual cereal straw surplus (mainly wheat), concentrated in the East of England. In addition, 2.5 million tonnes of oilseed rape straw could be available that is not presently recovered. The decision to focus on an understanding of the utilisation of indigenous agricultural residues therefore led to the choice of wheat straw as the main focus of this investigation, with some comparisons to other crop residues. As one of the main staple crops grown across the world, the results and lessons learnt from this study may also be applicable more widely.

3.2. Biomass composition

The composition of biomass varies depending both on the species and the geographic location in which it has been grown. Nevertheless, in general, crop residues such as cereal straws consist of five main components: cellulose, hemicellulose, lignin, extractives

---

[*] Literature is based at the time of writing deliverables for this report.

and ash. Typical values for herbaceous plants range from 40–50% cellulose, 20–40% hemicellulose, 15–20% lignin and 5–10% extractives (Barneto *et al.,* 2009). Woody biomass generally has a higher lignin but lower hemicellulose content.

In terms of energy production, the polysaccharide content of biomass makes the material much more oxygen rich than coal, than with materials with a higher lignin content having a lower O/C ratio and a corresponding higher calorific value (Jones *et al.,* 2006).

Additionally, in comparison to coal, biomass contains more moisture, has a lower density, contains less sulphur, less nitrogen, more silica, potassium and chlorine, less aluminium and iron and has a lower heating value (Demirbas, 2004). Some of these differences are beneficial, whilst others create technological challenges. High moisture contents reduce the thermal efficiency of combustion, can cause problems during ignition and lower the maximum flame temperature (Khan *et al.,* 2009). The optimal moisture content is around 15%, although furnaces can usually cope with a maximum of 65% moisture (Klas, 1998). Chopped straw has a bulk density of 50–120 kg m^{-3} compared to 800–900 kg m^{-3} for bituminous coals (Werther *et al.,* 2000). This increases both the carbon and monetary costs of transportation, reduces the heating value per unit volume, and makes it difficult to continuously feed the straw and control the rate of burning (Khan *et al,* 2009;Werther *et al.,* 2000). Densification of biomass to 500–1000 kg m^{-3} is possible using several different technologies, such as pelletisation, however it increases the production cost (Werther *et al.,*2000).

A wide variation in the ash content and distribution of inorganic species can be observed both within agricultural residue types and between them (Table 2). Irrigation and fertiliser usage in the growth of herbaceous plants leads to higher contents for almost every inorganic species in comparison to wood (Dayton *et al.,* 1999). The alkali content is, in particular, much higher in the herbaceous materials in comparison to the woody and coal sources. Silica and potassium are the two major ash forming species for all of the agricultural residues, excluding rape straw. The mix of inorganic species within each material affects both the combustion properties of the fuel and the design and operation of combustion systems.

Table 2. Ash content, elemental composition and calorific value data for a variety of biomass materials and coal

Residue type		Ash (wt%	SiO_2	Al_2O_3	Fe_2O_3	CaO	Mg	Na_2O	K_2O	SO_3	P_2O	Cl	HHV	Alkali	Ref
Wheat straw	Imperial Valley	12.8	35.8	2.5	1.0	4.7	2.5	10.5	18.4	5.5	1.5	14.7	17.2	2.15	10
	(China)	10.0	36.9	8.0	6.3	8.1	3.0	9.2	17.4	4.5	2.0	5.2	16.2	1.64	11
	2000 (Denmark)	4.8	35.3	1.1	0.1	10.2	2.4	0.5	30.1	6.2	2.6	3.4	16.8	0.88	12
	Soisson (Spain)	5.7	64.0	0.3	0.2	5.4	1.8	0.1	17.0	1.8	1.6	2.8	16.3	0.60	12
	2001 (Denmark)	4.8	67.0	0.2	0.2	8.7	2.2	0.1	14.0	2.2	2.4	2.1	17.4	0.39	12
	Marius (Spain)	4.9	65.0	0.8	0.6	11.0	1.7	0.1	9.1	2.5	2.3	1.2	17.1	0.26	12
Other agri-straws available in UK	Winter barley	6.9	25.2	0.2	0.1	6.9	2.2	5.1	40.2	5.1	1.9	6.9	16.5	1.89	12
	Spring barley	5.7	37.2	nd	nd	12.5	1.0	0.9	17.8	2.7	1.4	1.4	nd		12
	Oat straw	3.8	15.2	0.3	0.1	26.5	3.3	4.5	17.4	6.4	6.7	0.8	17.4	0.48	12
	Rape straw	2.7	2.4	4.2	1.6	48.7	3.1	0.2	15.2	3.8	1.4	0.5	17.0	0.24	12
Agri-residues around the world	Rice straw	20.9	72.3	0.1	0.3	2.1	2.1	2.7	11.8	1.1	1.8	4.1	14.7	2.05	10
	Cotton straw	7.4	17.7	10.8	2.4	9.0	7.3	6.8	30.2	5.8	4.3	4.9	15.9	1.73	11
	Maize	7.1	33.0	3.7	1.6	17.0	4.4	0.4	22.0	1.7	1.9	5.4	16.4	0.97	12
	Sugarcane bagasse	8.5	42.6	23.2	16.2	3.0	2.0	0.6	3.0	0.5	1.3	0.1	17.7	0.17	10
	Switchgrass	3.8	62.8	0.3	0.9	6.2	1.7	0.4	11.7	1.5	4.2	0.1	18.7	0.24	10
Wood	Wood fuel	4.5	37.5	14.1	0.6	7.6	17.	3.6	1.4	2.2	6.0	2.2	18.7	0.12	10
	Red Oak	1.2	38.3	8.1	7.6	12.8	1.0	0.4	8.6	1.8	1.0	<0.0	19.0	0.06	13
Macroalgae	*Laminara digitata*	25.8	0.4	0.1	1.0	5.0	5.2	19.6	14.8	-	6.7	-	17.6	3.23	14
Coal	Eastern Kentucky	7.6	51.6	32.5	4.5	1.1	0.4	0.2	1.3	1.3	0.3	2.3	31.0	0.04	13

3.3. Combustion of biomass and the impact of inorganic species

The stoichiometric equation for the combustion of biomass using the basic empirical formula for cellulose can be represented as:

$$(C_6H_{10}O_5)_n + 6nO_2 \longrightarrow 6nCO_2 + 5nH_2O$$

Thermogravimetric analysis has been used to identify the stages of biomass combustion (Barneto *et al.,* 2009). An initial mass loss of up to 120 °C is caused by evaporation of the contained moisture along with high-energy volatiles. The main mass loss occurs between 180 – 375 °C as the solid lignocellulosic material begins to decompose and devolatilise releasing organic compounds that burn in the gas phase (Klass, 1998). This step is similar to the processes occurring during pyrolysis. Research within the latter area has given rise to a 3-component model: hemicellulose and cellulose decompose in parallel and are mainly responsible for the mass loss, whilst lignin decomposes over a broader temperature range and is responsible for the majority of the char formed (Barneto *et al.,*2009). At higher temperatures (375–525 °C) in an oxygen-rich atmosphere, the residual chars combust at a slower rate (Klass, 1998).

3.4. Combustion technologies

The main aims in combustion systems are to maximise boiler efficiency for the production of steam and to minimise undesirable gas emissions (Klass. 1998). The two main biomass combustion technologies in use are grate-fired and fluidised bed combustion (FBC) boilers (Yin *et al.,* 2008)

3.4.1. Grate fired combustion

Grate-fired boilers vary in capacity from around 4-200 MW and consist of (Figure 5):

1. A fuel feeding system
2. Grate assembly
3. Secondary air supply
4. Ash discharge system
5. Heat exchange system

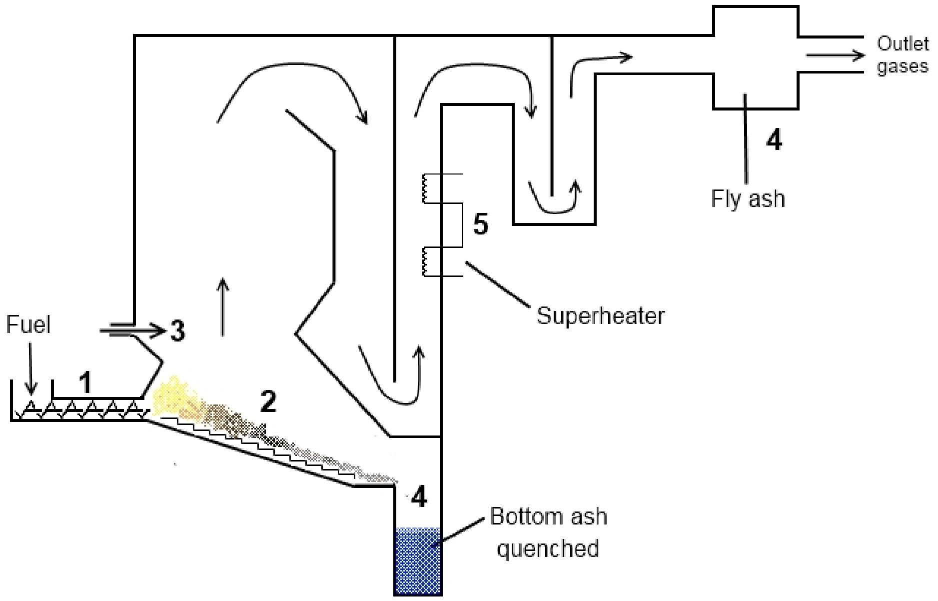

Figure 5. Basic grate-fired biomass combustion plant design (Originally in colour)

The grate assembly is responsible for ensuring good mixing of the fuel and that there is a sufficient air flow and residence time for the complete combustion of slower burning chars. Generally a residence time of 20–40 minutes is required (Knudsen *et al.,*2004). The top layer of the fuel ignites due to radiant heat from the furnace and flames above the bed (van der Lans *et al.,* 2000). The flame front moves down through the bed against the primary air supply. After reaching the grate, a char burnout front moves in the opposite direction. Primary air is injected up through the grate. In modern systems a sub-stoichiometric amount of air is likely to be added, with a secondary air supply added higher up in the furnace box (Klass*,* 1998; Blander and Pelton, 1997)This helps to ensure complete combustion to prevent emissions of pollutants such as hydrocarbons (C_xH_y), CO, particulates and polyaromatic hydrocarbons (Obernberger *et al.,* 2006). It can also prevent NO_x emissions and volatilisation of inorganic species by enabling a lower temperature and less air to be used at the fuel bed (Staiger *et al.,* 2005).

The hot flue gases transfer heat to water cooled tubes in the superheaters. Additional economisers capture the waste heat by heating the boiler feedwater. The bottom ash that falls through the grate is discharged to an ash receptacle and is often quenched in water. Fine particulate fly ash, which has followed the flue gases, is collected in bag filters (Sander and Andren, 1997).

Few studies indicate the actual grate temperature in industrial combustion units, however, furnace gas exit temperatures and furnace temperatures are typically between 800 – 900 °C; flame temperatures above the grate may be higher (Jenkins *et al.,* 1996). In Denmark, the Government's requirement to burn large volumes of straw since 2004, has led to the development of dedicated straw-fired co-generation plants which can operate at lower furnace exit gas temperatures of 640 – 760 °C (Olanders and Steenari, 1995). An additional superheater, utilising gases from straw pyrolysis, can be used to superheat the steam for power generation.

3.4.2. Fluidised bed combustion

In fluidised bed combustion (FBC) an inert refractory material, usually silica sand (Pettersson *et al.,* 2009), is used as the bed material, with the fuel suspended within it. Air is added through a hole under the bed, which increases the volume of the bed, causing it to become 'fluidised' (Klass, 1998). The constant movement of the bed material improves the temperature distribution, ensures intimate mixing of the fuel and oxidant and enables the addition of additives, such as limestone, to minimise pollutants(Klass, 1998).

Both of these technologies are flexible to a wide variety of fuels and are used at dedicated biomass facilities around the world with FBC, a more recent technological development. However, despite some advantages, the latter is prone to bed agglomeration when using high alkali fuels, such as straw, and the initial capital and maintenance costs are higher (Yin *et al.,* 2008). The research contained within this report does not study fluidised bed combustion further as the travelling grate boiler is the most common design for biomass combustion and produces an ash material based only on the initial elemental composition of the fuel is formed (Miles *et al.,*1996) .

3.5. Impact of inorganics during grate-firing of herbaceous biomass

Within the past decade, extensive investigations have been undertaken into the combustion of wheat straw (Wu *et al.,* 2009;Blander and Pelton, 1997; Olanders and Steenari, 1995; Gupta *et al.,*1999; Knudsen *et al.,* 1998; Arvelakis *et al.,* 2003; Thy *et al*.,2006; Vamkuva *et al*., 2006; Jones *et al*.,1963). The combustion of wheat straw has been found to differ greatly to coal and woody biomass sources. This is primarily due to its distinct ash chemistry, including higher total ash content, alkalinity, chlorine and silica content (Table 2), resulting in lower ash melting points (Llorente and Garcia, 2005). The impact of this can be severe slagging, fouling and corrosion.

Fouling is the deposition of solid materials on heat transfer zones, such as superheaters, beyond the furnace cavity (Bryers, 1999). Slagging is the formation of fused or sintered materials on radiant heat transfer surfaces within the furnace cavity, or of agglomeration of fluidised-bed materials. These problems have been found to occur extensively during the combustion of wheat straw, in particular, decreasing the thermal efficiency of the system and, at its worst, causing the shutdown of boilers (Arvelakis *et al.,* 2004; Jenkins *et al.,*1996; Olanders and Steenari, 1995; Miles *et al.,* 1996; Arevlakis *et al.,* 2003; Thy *et al.,* 2006). The impacts of the three main ash forming components in wheat straw are discussed in more detail below.

3.5.1. Potassium

Studies indicate that potassium is present in biomass as cations associated with oxygen-containing functional groups or precipitated as chloride, carbonate, oxalate or sulphate salts (Jones *et al.,* 2007). Chemical fractionation suggests that 70–80% of the potassium present is either water soluble or ion exchangeable (Miles *et al.,* 1996). In comparison, in coal the alkali metal is usually bound within stable minerals (Zolin *et al.,* 2001).

In laboratory studies, potassium losses during wheat straw combustion positively correlate with temperature (Thy *et al.,*2006). Evolution has been observed to occur over two stages: a small amount at lower temperatures (180–500 °C), suggested to be due to release of potassium associated with organic species (Jones *et al.*, 2007); and 50–90% at higher temperatures (> 700 °C) (Knudsen *et al.*, 2004). Correlation with chlorine losses intimates that the majority of this is due to the vaporisation of sylvite, with KCl amongst the most stable gas-phase alkali containing species, however, some of the potassium is still retained in the ashes (Thy *et al.*, 2006). Simultaneous Thermal Analysis (STA) studies imply that this is a result of the reaction of K_2CO_3 with SiO_2,(Arvelakis *et al.,*2004) with more potassium captured in the bottom ashes in higher silica content straws (Knudsen *et al.,*2004; Thy *et al.,*2006)

Potassium can also influence the combustion and pyrolysis processes, with the onset of devolatilisation and the char burnout phase observed to occur at lower temperatures when even a small amount of potassium is present.

3.5.2. Chlorine

Laboratory-scale studies differ in their observations of the temperature of chlorine loss. Some have noted 25–70% of chlorine to be released at < 500 °C with the remainder above 700 °C (Knudsen *et al.,*2004). Others have only detected chlorine losses to occur above 770 °C due to the vaporisation of sylvite (Thy *et al.,* 2006). Many researchers have highlighted that chlorine, rather than alkali concentration in fuels, can be the limiting factor in controlling the total amount of alkali volatilised by supporting the transfer of alkali to the surface of the fuel (Miles *et al.,*1996).

3.5.3. Silicates

Potassium silicate eutectics formed in the combustion bed can melt or soften at temperatures as low as 700 °C. Ternary silicates, containing a small quantity of sodium, can have liquidus temperatures as low as 540 °C. Equilibrium calculations of the combustion of wheat straw indicate the presence of liquid silicates from 500 – 1200 °C (Blander and Pelton, 1997). By studying the solubility of potassium from wheat straw chars at 700 – 900 °C, significant amounts of potassium silicate were hypothesised to be formed above 700 °C (Jensen *et al.,*2000). As mentioned previously, these low melting silicates can cause bed agglomeration in FBC or, if present on refractory surfaces, can capture fly ash through inertial impaction and sticking, leading to the build-up of deposits.

All of these issues depend on the melting point and evaporation of inorganic species within the solid fuel. Ash fusion tests are therefore frequently used to try and predict the behaviour of biomass ash during combustion (Llorente and Garcia, 2005). The slagging index, which measures the mass of alkali within the material as a ratio of the calorific value, was developed for coal to predict the risk of problems during combustion of different coals. Levels of < 0.17 kg GJ^{-1} indicate a low slagging risk and levels > 0.34 kg GJ^{-1} indicate that the fuel is virtually certain to cause melting, vaporisation and condensation of deposits on surfaces. High slagging indices are observed in wheat straw samples from around the world (Table 2).

3.6. Current uses of residues from thermochemical conversion of biomass

The large-scale utilisation of wheat straw, and similar biomass materials, in combustion systems will result in the formation of a significant quantity of new waste: biomass fly ash and bottom ash. The valorisation of these waste materials is vital to ensure recovery and reuse of the inorganic species, in line with an elemental sustainability and biorefinery vision, and to add economic value. In large-scale combustion tests on wheat straw the total ash produced has been found to be as much as 12% by weight of the initial straw, with fly ash making up 28% of the ash (Sander and Andren, 1997). In countries where the utilisation of biomass residues is more developed, particularly in Scandinavia where wood is widely used, the increasing amount of ash residue is leading to the search for utilisation methods other than landfilling (Sarenbo, 2009).

The most frequently cited alternative applications for biomass ashes are in: 1) agriculture, as a fertiliser or soil amendment; and 2) construction, by partly replacing cement or as an aggregate in road building (Gómez-Barea *et al.,* 2009).

3.6.1. Agriculture

The return of biomass ashes to soils is considered invaluable to reduce fertiliser usage and recycle the nutrients removed with the plant. Nutrients of particular importance are phosphorous, potassium, magnesium and calcium. Nitrogen is almost totally lost during combustion. However, landfilling is currently the primary disposal method for combustion residues (Elliot and Mahmood, 2006). In the US, currently a substantial amount of ash from the combustion of paper production residues goes to landfill (Pitman, 2006). The overwhelming majority of research on the reutilisation of ash has been carried out on wood ash, particularly in the US, Sweden, Finland and Denmark, specifically to return it to forest soils. This has led to the development of standards for threshold values of components in ash for recycling on forest floors (Table 3) (Sarenbo, 2009). Combustion ashes are also considered as potential liming agents to reduce acidity in soils (Vesterinen, 2003).

The specific mineral and organic content of the ashes formed affects its use, with these varying even between wood species. The mineral content of herbaceous biomass is higher than wood and therefore produces a proportionally larger amount of ash following combustion, and also has a significantly different elemental distribution. Lab-scale studies in Germany have recently shown that rye straw ash can have a beneficial impact on yields of ryegrass and maize (Schiemenz and Eichler-Lobermann, 2010). Rape straw ash contains more calcium and has been observed to have a higher liming effect than wheat straw ash (Sander and Andren, 1997).

Table 3: Recommendations of the Swedish Forest Agency on threshold values for constituents in ash aimed for recycling on forest soils (Sarenbo, 2009)

	Minimum	Maximum
Macronutrients		
Ca	12.5	
Mg	1.5	
K	3.0	
P	0.7	
Micronutrients		
B		800
Cu		400
Zn	500	7000
As		30
Pb		300
Cd		30
Cr		100
Hg		3
Ni		70
V		70

3.6.2. Construction

The vast quantities of coal fly ash produced have led to the development of its use as a standard additive in concrete as a pozzolan (Wang and Baxter, 2006); approximately 6.7 million tonnes of coal fly ash were used in this way in the US in 1994 (Janos *et al.,* 2003). A pozzolan is a siliceous material that by itself has little or no cementious property, but will react with calcium hydroxide in the presence of water to form a material with cementing properties (Nair *et al.,* 2008). However, fly ash from biomass does not meet the current standards, due to the high alkali and chloride concentrations and lower alumina levels in the ashes. Therefore, further research is required to study the use of biomass ashes for this application and others. Researchers have found that several agricultural waste ashes are suitable for use as a component of concrete including rice husk ash (Chindaprasirt and Rukzon, 2008), sugarcane ash (Frias *et al.,* 2007), palm oil fuel ash (Tangchirapat *et al.,* 2007), and wheat ash (Biricik *et al.,*1999).

This highlights several potential opportunities for the utilisation of wheat straw and other agricultural ashes. The inorganic composition of the waste ashes should be the starting point for directing the potential applications, with silicon (Si) and potassium (K), the most abundant elements in wheat straw ash (Table 2).

3.7. Silica from biomass

Silicon is one of the most abundant minerals present in plant tissues(Hodson *et al.,* 2005) Within soil, silicon is mostly found in the form of insoluble crystalline silica and silicates with soluble silicic acid present at around 0.1 – 2.0 mM (Casey *et al.,* 2004).

The ability of plants to accumulate silica to a higher concentration than that of the soluble silica in the soil is not uniform throughout the plant kingdom and neither are the silica structures formed and the location of them within the plant. Silica accumulation ability appears to be highly dependent on the high-level phylogenetic position of the plant, mainly present in primitive land plants and monocot angiosperms, particularly the family *Poaceae*, also known as grasses. This family includes the major agricultural species such as rice, wheat and other important plants such as bamboo. Studies have shown that of various different grass species, uptake of silicon from a solution of silicic acid is in the order rice > wheat > triticale > sorghum > rye > maize > barley (Tamai and Ma, 2003).. In these plants, silicon is actively taken up by the roots in the form of silicic acid, although efflux and influx transporter genes have so far only been identified for rice. Once in the root, the silicic acid is transported to the xylem and then to the shoot, stem and leaves by the transpiration stream, where it becomes concentrated due to evaporation and polymerisation and is deposited as a thin layer of amorphous silica in the cell walls below the cuticle layer. The effect of the strong pull of the transpiration stream is that the silicon concentration is higher in older tissues, leaves and the shoot than in the stem (Table 7a) (Mecfel et al.,2007).

The relative Si shoot concentrations vary across different agricultural and energy crops (Table 7b) (Hodson *et al.,*2005). Of the species cultivated in the UK, miscanthus and wheat display the highest uptake of silica.

Table 7 a. Percentage of silica found in different parts of the wheat plant (Mecfel *et al.,* 2007) b. Relative silica concentration in the shoots of several agricultural and energy crops (Hodson *et al.,* 2005).

a.

Wheat organ	SiO_2 (%)
Culm/stem	1.5±0.2
Leaf sheath	5.8±0.9
Leaf blade	5.7±1.4
Rachis	1.1
Influorescence	3.8±0.9
Bulk	2.3±0.3

b.

Species	Common name	Mean relative shoot [Si]
Oryza sative	Rice	4.12
Equisetum arvense	Horesetail	3.99
Miscanthus sinensis	Miscanthus / Elephant grass	2.86
Triticum aestivum	Wheat	2.46
Panicum virgatum	Switchgrass	2.01
Hordeum vulgare	Barley	1.82
Quercus robur	English oak	1.54
Saccharun officinarum	Sugarcane	1.51
Avena sativa	Oat	1.51
Secale cereal	Rye	1.26
Brassica napus	Oilseed rape	-0.12

3.7.1. Composition and inorganic distribution

Potassium is generally also present at high levels, and at a much higher level than sodium, resulting in a varying SiO_2:K_2O molar ratio for each different biomass source, both between different species and from different studies of the same species (Table 7c). The results for wheat straw show a ratio generally in the range of commercially produced alkali silicates. Where they are not, this is probably due to the loss of potassium by rain leaching prior to harvesting (Hald, 1994). This data indicates the potential for the production of alkali silicates from the ashes of these biomass materials using only the inherent inorganic species.

Table 7c. Main element concentrations of initial dry biomass and silica:alkali ratios.

	SiO_2 (%)	K_2O (%)	SiO_2:K_2O(wt)	Cl (%)	CaO (%)	Ref
Wheat straw	4.6	2.4	1.9	1.9	0.6	2
Wheat straw	3.7	1.7	2.1	0.5	0.8	32
Wheat (Marius)	3.6	1.0	3.8	0.2	0.3	33
Wheat Denmark 2001	3.2	0.7	4.8	0.1	0.4	33
Wheat (Soisson) Spain	3.2	0.4	7.1	0.1	0.5	33
Wheat Denmark 2000	1.7	1.4	1.2	0.2	0.5	33
Winter barley	1.7	2.8	0.6	0.5	0.5	33
Spring barley	2.1	1.0	2.1	0.1	0.7	33
Oat straw	0.6	0.7	0.9	0.0	1.0	33
Rape straw	0.1	0.4	0.2	0.0	1.3	33
Rice straw	15.1	2.5	6.1	0.8	0.4	2
Sugarcane bagasse	3.6	0.3	14.4	0.0	0.2	2
Switchgrass	2.4	0.4	5.4	0.0	0.2	2
Wood fuel	1.7	0.1	26.4	0.1	0.3	2
Laminara digitata	0.1	3.8	0.0	0.0	1.3	34
Eastern Kentucky Coal	3.9	0.1	39.7	0.2	0.1	35

3.8. Alkali silicates – chemistry and uses

Alkali silicates are solutions or solids of silicate anions and alkali metal cations. These systems can be expressed as M_2SiO_3 but are more usually defined by the molar ratio or $xSiO_2$:M_2O, where M = Li, Na or K. It is this molar ratio together with the solids concentration in solution and the alkali metal used that defines the physical and chemical properties of the alkali silicate system. Since the molar ratio and solids concentration is highly variable and can be controlled, this produces a system with a wide variety of applications.

3.8.1. Structure of alkali silicates

A wide variety of different silicate structures are formed in solution. Evidence indicates that the species are all compact and tetrahedrally co-ordinated with many similar species in dynamic equilibrium (Knight *et al.,* 2007). The condensation processes that occur to form polymeric species are still not fully understood and are of particular interest for researchers understanding sol-gel chemistry and zeolite synthesis (Mora-Fonz et al.,2007).

Condensation is generally believed to be catalysed by hydroxyl ions from both theoretical and experimental studies (Trinh *et al.,* 2006; Munoz Aguado and Gregorkiewitz, 1997). The mechanism suggested involves deprotonation by a hydroxyl ion followed by a two-step condensation reaction with silicic acid via a five-coordinate reaction intermediate stabilised by three strong hydrogen bonds, followed by loss of water (Figure 9) (Trinh *et al.,* 2006). The anionic species formed may be charge-stabilised by an alkali cation.

3.8.2. Analysis by ^{29}Si NMR

The specific species that are formed in solution and during polymerisation under different conditions are not well understood. Engelhardt *et al.* (1975) developed a Q^i description to describe the connectivity of silicon atoms and help identification by ^{29}Si nuclear magnetic resonance spectroscopy (NMR). Q^0 represents silicate structures in which the silicon atom is not connected to any other silicon atoms through an oxygen bridge (monomeric species), whilst Q^4 denotes a silicon atom that is connected to four other silicon atoms at each tetrahedral linkage (Figure 10). ^{29}Si NMR peaks have been assigned to the different Q^i species in solution (Table 4) (Engelhardt and Michel, 1987).

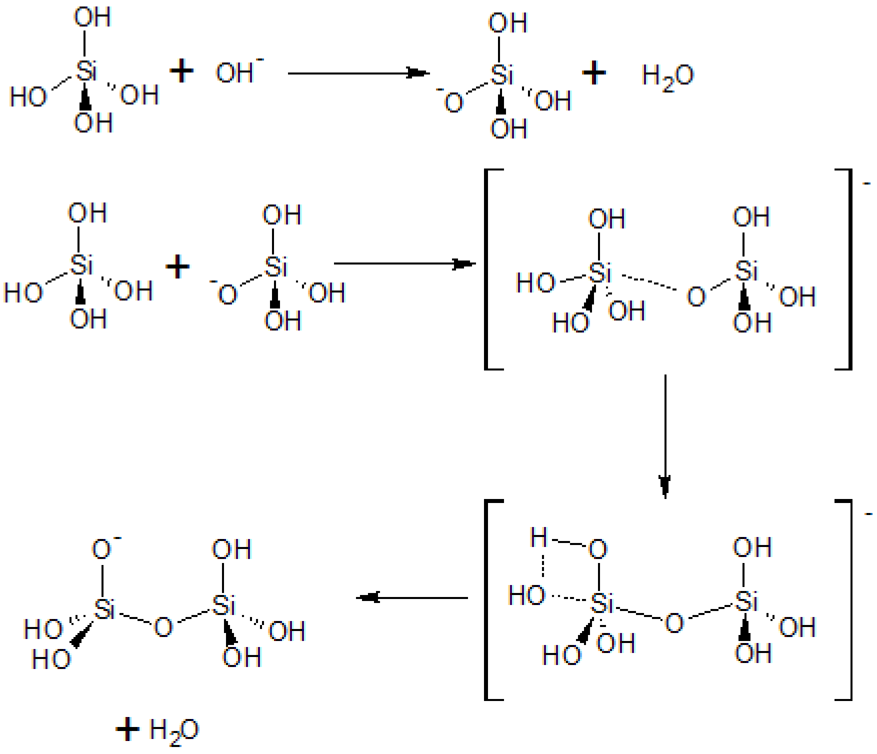

Figure 9. Proposed mechanism for the condensation of silicic acid (Trinh *et al.,* 2006)

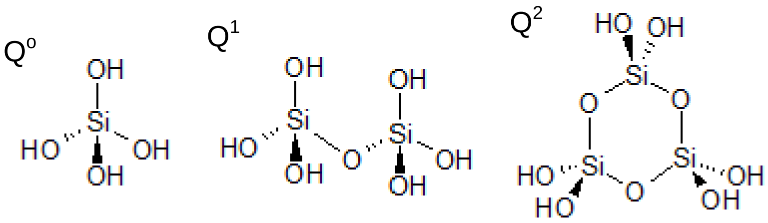

Figure 10. The structure of a few species identified in silicate solutions by ^{29}Si NMR

Table 4. Assigned ^{29}Si NMR shifts for silicate species with different connectivities in solution (with respect to tetramethylsilane) (Engelhardt and Michel, 1987)

Q^i connectivity	-δ(ppm)
Q^0	~ 72
Q^1	~ 79
$Q^2_{(3R)}$ (cyclic trimer)	~ 82
$Q^2_{(4R)}$ and $Q^3_{(3R)}$ (three ring)	~ 87 – 92
$Q^3_{(4R)}$ (four ring)	~ 96 – 98
Q^4	~ 108 (broad)

Identifying specific species in solution using ^{29}Si NMR is made difficult due to the presence of many similar species in dynamic equilibrium and due to the low abundance of ^{29}Si which prevents the visibility of ^{29}Si-^{29}Si coupling. Greater success has been achieved by studying the changes in the integrated band intensities of the different Q^i peaks with changing silicon concentration (Bass and Turner, 1997), cation type (Engelhardt and Michel, 1987), pH (Weber and Huntm 2003), and molar ratio (Figure 11) (Bass and Turner, 1997; Svensson *et al.,* 1986; Provis *et al.,* 2005). These indicate that at a pH above ~10.7 and as solutions become more siliceous, more complex polymeric species, Q^3 and Q^4, are formed at the expense of the monomer and dimer (Provis *et al.,* 2005). It is also noticeable that cyclic species are favourably formed during condensation processes. In addition, it has been found that decreasing the concentration of the solution decreases the degree of polymerisation and *vice versa* (Engelhardt and Michel, 1987).

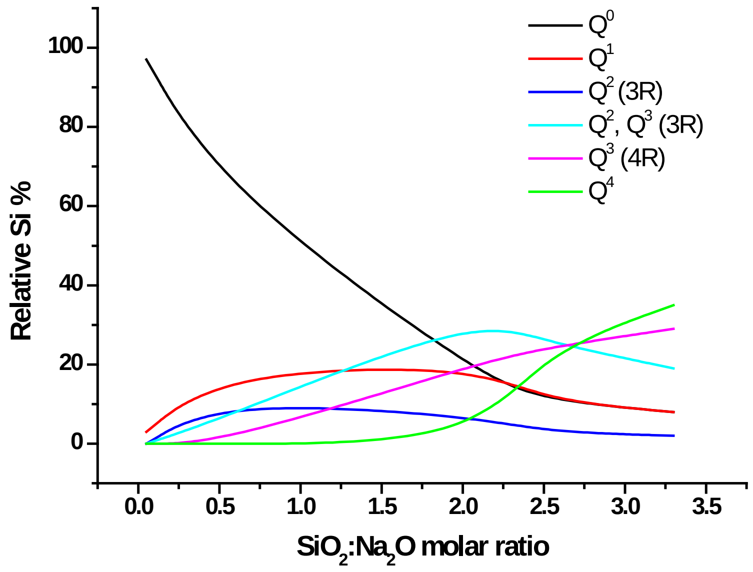

Figure 11. Changes in silicate species distribution with changing SiO_2:Na_2O molar ratio at a SiO_2 concentration of 0.4 M. (Data from Bass and Turner (1997))

3.8.3. Analysis by infrared

IR can enable the characterisation of silicate solutions, albeit at a much lower resolution and with some controversy remaining around assignments of bands to specific vibrational modes (Halasz *et al.,* 2007; Halasz *et al, 2007a)*. The main infrared absorption bands of alkali silicates are observed between 1250 and 700 cm^{-1} with a strong broad band due to asymmetric Si-O-Si stretching vibrations, usually centred around 1000 cm^{-1}. Bass and Turner (1997) have correlated the changes in silicate speciation observed by ^{29}Si NMR with the changing peak structure observed in the infrared (IR) spectra by deconvolution (Table 5), proposing that higher wavenumber sections of the band correspond to more complex anionic species. They then observe that as the molar ratio decreases the high frequency edge of the band shifts to lower frequency, suggesting a reduction in the complexity of the anionic species present. Bands in the range 950–1020 cm^{-1} appear to more sensitive to the local silicate environment (Falcone *et al.*, 2010). However, band assignment was undertaken by comparing low concentration solutions due to better resolution of the ^{29}Si NMR peaks at 0.4 M concentrations.

Table 5. Bass and Turner's (1997) assignments of components of main sodium silicate infrared band to different silicate anion types

Assignment	Wavenumber (cm^{-1})
SiO- small anions	850-900
Monomer + dimer	910-950
Linear Q^1	965-985, 995-1005
SiO^- cyclic anions	1010-1020
$Q^2_{(3R)}$ rings	1020-1050
$Q^3_{(3R)}$, $Q^2_{(4R)}$ rings, linear Q^2	1030-1070
$Q^3_{(4R)}$ rings	1050-1120
Polymer	1100-1300

Osswald and Fehr attempted to assign IR bands of concentrated potassium silicate solutions based on a comparison with IR studies of silica gels (Osswald and Fehr, 2006). They correlated the shift of the frequency of the main band to the presence of surface Si-O-K groups, weakening neighbouring Si-O-Si bonds, and the high frequency shoulder of the mainband to the situation where neighbouring oxygen atoms asymmetrically vibrate 180° out of phase with each other, rather than to the presence of more highly polymerised species (Kirk, 1988). Halasz *et al*. (2007) tried to distinguish between bands related to monomeric and polymeric silicate species by using aqueous solutions of Na_2SiO_3, which almost exclusively contain monosilicate ions at pH's > 10. Their aqueous ATR FTIR spectra showed broad bands, without a high frequency shoulder, that shifted to lower wavenumbers with decreasing concentration or increasing alkali content, which they related to the degree of dissociation in the solution.

3.8.4. Setting processes

The chemical and physical properties of alkali silicates vary depending on their molar ratio and solids concentration. Of particular interest, with respect to this project, are the properties relating to the use of alkali silicates as a binder. There are three setting reactions that alkali silicates can undergo, which each impart different characteristics on the final material. In addition, compatibility with the substrate material must be considered, with the solutions performing most effectively on hydrophilic, non-oily surfaces, where they can achieve proper wetting and, hence, maximum adhesion.

Dehydration

Viscosity increases rapidly as moisture is removed and more rapidly for higher ratio silicate solutions (PQ Corporation, 2004). The glassy nature of the bond formed imparts strength and rigidity, however, the insolubility of the bond is dependent on the ambient temperature and humidity (Gill, 1997). Heating to around 250 °C is required to cross-link the silicate species and impart a high moisture resistance (PQ Corporatin, 2006).

Precipitation

Soluble silicates react almost instantly with multivalent metal cations such as Ca^{2+} and Mg^{2+} to form either insoluble metal silicate networks or hydrated silica with adsorbed metal oxides or hydroxides (PQ Corporation, 2004). This mechanism is used to form pigments and surface coatings.

Gelation

Silicate solutions are stable to condensation above pH ~10.7, due to the presence of repulsive highly charged anionic silicate species or stabilised ion-paired species (Iler, 1979). As the pH decreases, fewer silicate anions are supported in solution, and the polymerisation of these species occurs with the expulsion of water due to a reduction in electrostatic repulsive forces (Nasr-El-Din and Taylor, 2005). There are three stages recognised in the polymerisation process (Iler, 1979):

1. Polymerisation of the monomer to form small particles
2. Growth of particles
3. Linking of particles into chains and then networks which extend through the solution, thickening it to a gel.

The extent of polymerisation is dependent on the solids concentration, salt content, temperature and pH of gelation. In general, the rate of gelation increases as the pH decreases to a maximum at pH 6–7. Initially small polymerised species are formed, maximising the number of internal siloxane bonds and minimising the number of surface silanol groups. The resulting small particles are the nuclei for larger particles which form the backbone of the silica gel. A dynamic equilibrium is present in which smaller, more soluble particles dissolve releasing silica which can react with the nucleating particles resulting in growth of the particles in a process known as Ostwald ripening (Iler, 1979). The main driving force for this is the reduction in surface free energy. Both simultaneously with and following particle growth, aggregation of the particles may occur dependent on diffusion rates and electrostatic forces between the particles until a gel network is formed. During this process, the gel continues on a macroscopic scale to have the same concentration of silica and water as the surrounding sol. However, if coagulants, such as polyvalent metal ions or substantial amounts of salts are present, a white precipitate or opaque gel will be formed.

The bond formed via gelation is usually not as strong as that caused by dehydration but can have a higher degree of water resistance (McDonald and LaRosa Thomson). A wide variety of different setting agents are available that can be used to induce gelation by reducing the pH of the solution. For controlled gelation a chemical that will be hydrolysed over time to induce acidity is often used. For binding purposes a higher ratio silicate solution is often particularly valuable since less additional chemical is required to neutralise the solution to a pH below 10.7 and begin to induce gelation.

3.9. Utilising silica from biomass

Sodium silicate is generally formed by the fusing of sand (SiO_2) with sodium carbonate or ‘soda ash’ at around 1100–1200 °C. The resulting glass is then dissolved using high pressure steam (Iler. 1979). A large amount of energy is used during this process and there are environmental issues associated with the extraction of sand from mining or dredging, as well as the release of CO_2 due to carbonate decomposition. It is only in the past few years that the extraction and use of silicon present in biomass has seriously been considered. The main resource studied has been rice husk ash (RHA) due its high content of relatively pure silica, as described later.

3.9.1. Dissolution of silica

Silica can either be dissolved by strong alkaline solutions or by HF. In alkaline solutions, the reaction that is occurring during dissolution is essentially depolymerisation, the reverse of the polymerisation reaction described earlier. This reaction is also catalysed by hydroxyl ions which can react with silica to form a five co-ordinate centre, thereby weakening the other oxygen linking bonds. The rate at which dissolution occurs depends on the ability of the hydroxyl ion to catalyse this reaction, particularly the silica structure and the pH of the solution. At atmospheric pressure, the main crystalline silica phases formed are quartz, tridymite, cristobalite, with the transformation between them fully reversibly if the temperature change is slow (Figure 12) (Iler. 1979). The structures of tridymite, cristobalite and silica melts (glass) will be preserved at low temperatures if they are quickly cooled beyond their transition temperature. Interestingly, as silica glass is heated it is transformed directly to β-cristobalite rather than quartz. Amorphous unstructured silicas, including glass, opal and biogenic silica, have much greater dissolution rates than the crystalline phases due to the openness of the structure, enabling greater access to hydroxyl ions. The dissolution rate and maximum saturation level for all silica phases increases with increasing alkalinity, particularly above a pH of 9, due to the increasing presence of silicate ions influencing the silica saturation equilibrium, with the rate of dissolution correlated to the density of the material (Vogelsberger *et al.,*1992). The dissolution rate and total solubility are also affected by surface area (Vogelsberger *et al.,*1992), temperature and pressure (Zotov and Keppler, 2002).

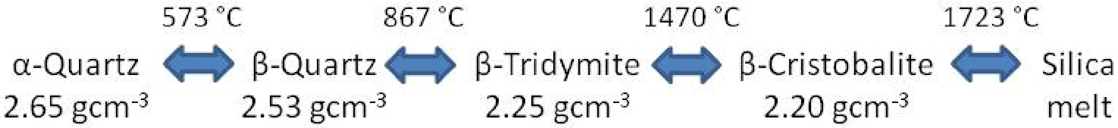

Figure 12. Silica phase transformations

3.9.2. Silica from Rice Hull Ashes (RHAs)

Most silica in biomass is thought to exist in inorganic linkages as amorphous silica. X-Ray diffraction studies and solid state ^{29}Si NMR have identified amorphous silica in rice hull ashes (RHAs) up to 800 °C, with cristobalite and tridymite phases present at higher temperatures (Nair *et al*., 2008). Therefore, generally, extraction of silica from RHAs uses material combusted, gasified or pyrolysed below 800 °C. By boiling RHAs in 1M NaOH for 1 h, Kalapathy *et al.* (2000) demonstrated that 91% of the silica present could be extracted This methodology is now being used by AgriTec Systems to produce sodium silicate solutions from gasified rice hulls with a high value activated carbon co-product (USA patent 6524543, 1998). It has also been used to study the production of silicate thermal insulation material and the formation of flexible silicate films from RHAs (Kalapathy, 2003; Kalapathy, 2000).

By purely heating RHAs to 700 °C for 6 h, Della *et al.* (2002) found that they could produce a material that contained 95% amorphous silica with a surface area of 54 – 81 m^2 g^{-1} This method was also used by Rodrigues (2003) to create a pozzolanic material for cement production.

Silica has also been formed from rice hulls, rice straw and wheat straw by chemical pulping of the material with H_2SO_4 followed by combustion of the residue at 500 °C. The materials formed contained 99% SiO_2 and had BET surface areas ranging from 186 – 291 m^2 g^{-1} (Ubukata *et al.,* 2010). The only other studies that have examined the utilisation of silica in wheat residues have investigated, briefly, the use of ashes as an additive in cement production and for the formation of autoclaved mortar (Biricik *et al.,* 1999; Zhang *et al.,*2009, Al-Akhras and Abu-Alfoul, 2002). These studies found that wheat straw ash (WSA) or wheat hull ash can produce a pozzolanic material. However, the formation of alkali silicates utilising the inherent inorganic species has not been explored.

4. RAW MATERIAL STUDIES AND PRETREATMENT

Agronomy trials (raw materials studies) were conducted by Velcourt Farm Management and Velcourt R&D attempting to alter straw characteristics using different plant growth regulators (PGR) and nitrogen (N) approaches. Trials were undertaken with winter wheat and winter oilseed rape. All trials were harvested using a small plot combine to cut the straw. Straw was collected from the back of the combine and stored in bags until ready to be collected by the University of York and Bangor University.

The received straw was hammer milled to a 9 mm screen, then milled twice to pass a 0.5 mm screen using either a Glen Creston or Wiley mill. Wax was removed via continuous reflux extraction (Soxhlet) for 6 h using a 2:1 v/v solution of toluene and ethanol. The dewaxed fibre was used for analysis, with 1 g being used for holocellulose determination by the acid chlorite method, and 1 g for Klason lignin determination. After holocellulose determination, the proportion of α-cellulose and hemicellulose was determined by reaction with sodium hydroxide, and precipitation of the hemicellulose.

The ash content (heating in a muffle furnace for at 595 °C for 16 h) was assumed to be part of the hemicellulose and α-cellulose fraction, as any silica would be insoluble in both the acid chlorite and the sodium hydroxide steps.

Thermogravimetric analysis was run for 100 mg of sample mass on a NETSCH 409 STA with a heating rate of 10 K min^{-1} up to a maximal temperature of 700 °C under a gas flow of 150 ml min^{-1} air and 50 ml min^{-1} nitrogen. Analysis was undertaken using the NETSCH Proteus ® Software for Thermal Analysis.

Infrared spectroscopic analysis of samples of straw and ashes was undertaken on Verrtex 70 FT-IR-Spectrometer equipped with a MKII Golden Gate Single Reflection ATR System with a 45° diamond crystal. 46 scans with a spectral resolution of 4 cm^{-1} were recorded and analyzed using the Bruker OPUS software.

The carbon, hydrogen and nitrogen content of the samples were analyzed using an Exeter Analytical (Warwick, UK) CE440 Elemental Analyzer. These were carried out by Dr Graeme

MacAllister at the University of York. Additionally, XRF analyses of samples were carried out by the Materials Analysis and Research Service at Sheffield Hallam University.

4.1. Field Trials: Winter wheat (2010 harvest)

Three trials were conducted with varieties Viscount and Hereward at sites near Nuneaton, Warwickshire with respect to PGR and nitrogen application (Table 6): two with Viscount (one planted as 250 seeds/m^2 and; one planted at 400 seeds/m^2), and; the third with Hereward (planted at 300 seeds/m^2).

Table 6. Treatment matrix for PGR and N application rates

	PGR application			Nitrogen (N) application (kg/ha)			Total N (kg/ha)
				1st	2nd	3rd	
Treat No.	T0 (GS30/31)	T1 (GS32/33)	T2 (GS37/38)	Mid Feb	Mid-March	Mid-April	
1	Untreated	-	-	40	40	40	120
2	Hive 1.0	Hive 1.0	Terpal 1.0	40	40	40	120
3	Moddus 0.2 + Hive 1.0	Moddus 0.2 + Hive 1.0	Terpal 2.0	40	40	40	120
4	Untreated	-	-	40	100	100	240
5	Hive 1.0	Hive 1.0	Terpal 1.0	40	100	100	240
6	Moddus 0.2 + Hive 1.0	Moddus 0.2 + Hive 1.0	Terpal 2.0	40	100	100	240

Treatments 1 and 4 had no PGRs applied, treatments 2 and 5 had a moderate PGR applied and treatments 3 and 6 had strong PGR applied. These treatments were all tested at N rates of 120 (low nitrogen) and 240 (high nitrogen) kg N per hectare.

The straw from each field plot was compared before milling (see photograph for Hereward, Figure 13) and the following observations were noted. The Hereward stems appeared quite strong and had generally resisted breaking when packed, whilst Viscount straw (not shown) tended to suffer a greater degree of damage. Many of the Viscount straw samples were actually longer than the Hereward.

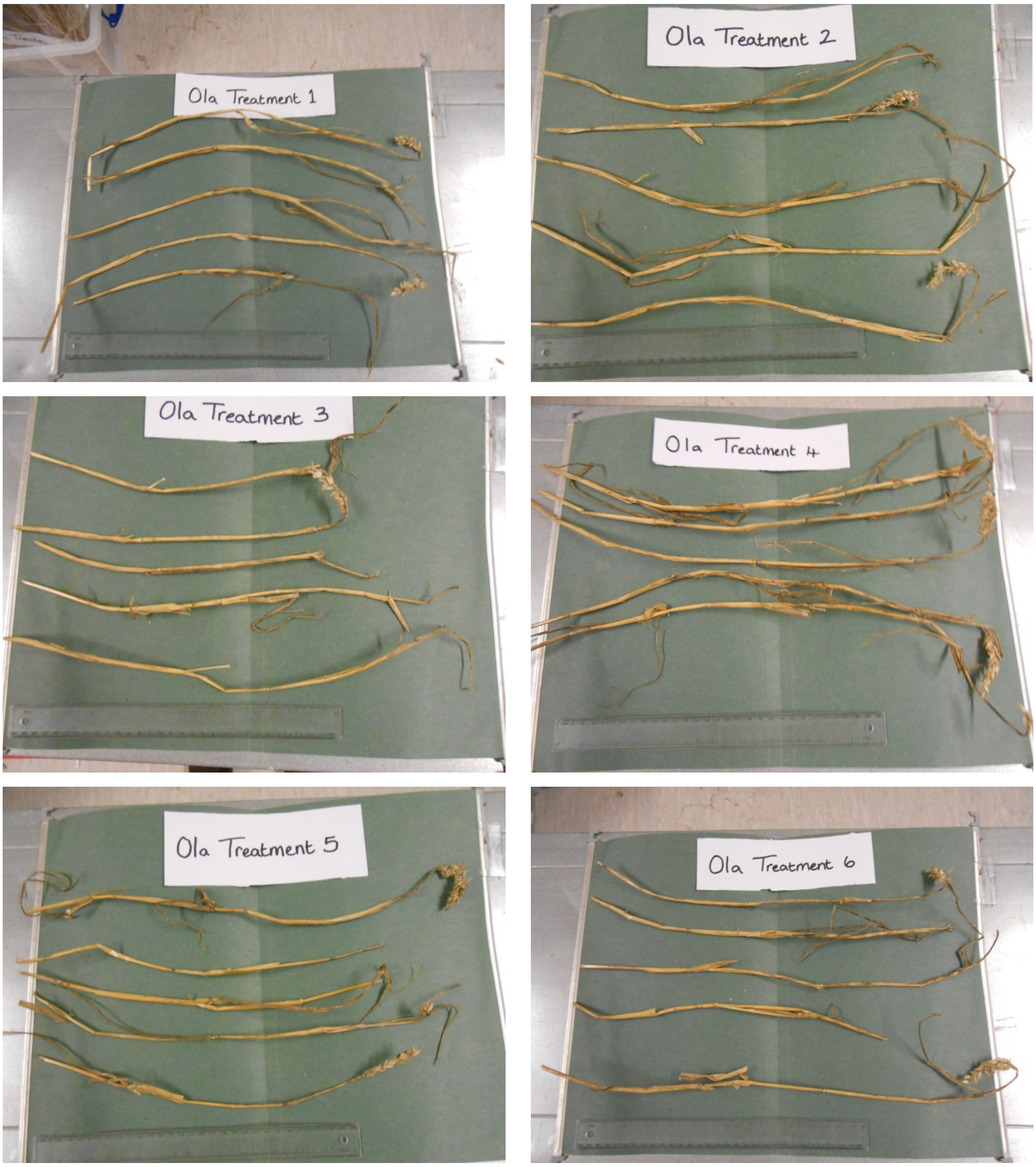

Figure 13. Hereward straw 2010 harvest

The total composition is listed in Table 8a(Hereward) and b (Viscount). No significant difference in applied treatment was noted either for Hereward or Viscount varieties.

Table 8 a) Composition (%) of Hereward wheat straw from six treatment regimes.

b) Composition (%) of Viscount wheat straw from six treatment regimes (low seed rate shown in black, high seed rate shown in brackets, where applicable).

Treatment	Ash	Wax	α-cellulose	hemicellulose	lignin
1	3.17	1.02	42.25	39.24	15.33
2	3.35	1.23	43.93	38.81	14.56
3	3.86	2.12	41.02	40.68	14.44
4	3.62	1.91	43.32	38.08	14.97
5	3.75	1.13	44.79	35.98	15.48
6	3.51	2.23	52.05	28.35	16.07

b)

Straw	Ash	Wax	α-cellulose	hemicellulose	Lignin
1	3.25 (3.12)	1.64	48.99	30.36	17.40
2	2.80 (3.30)	1.62	45.14	33.93	18.13
3	2.97 (3.04)	1.92	41.14	40.07	15.82
4	2.98 (2.99)	1.56	46.46	33.01	17.54
5	3.21 (3.03)	2.01	43.18	33.30	20.31
6	2.83 (3.05)	1.77	45.07	34.00	18.10

Ear count data for the field plots indicated that in the higher planting density wheat, the rate of secondary tillers was lower. For Viscount, the ear counts were very similar at low and high seed rate for each treatment (Table 9). Thus, for the lower seed rate, the better spaced plants had produced a greater number of tillers.

Table 9. Ear counts from the field plots where the straw was produced.

Treatment	Hereward, 300	Viscount, 250	Viscount, 400
1	437	420	430
2	437	421	402
3	430	414	429
4	443	419	432
5	441	423	467
6	441	433	453

4.1.1. Combustion and Thermogravimetric Analysis (TG)

The ash content measured via thermogravimetric analysis (TGA) is slightly higher than the one observed after combustion. However, for both techniques the amount of residual ash seems to be higher for Hereward straw (ca. 3.1 % to ca. 35 % for the TG measurement) than for Viscount straw (ca. 2.1 % to 3.1 % for the TG measurement, Table 10). Thus the amount of residual ash is comparable to the results of McKendry (2002) who measured 4% of residual ash or Ergudenler and Ghaly (1992) who observed 3.9 % to 4.8 % of ash for wheat straw combustion.

During the TG as temperature increases, water evaporates causing the initial loss of weight. In a next step at 200 °C – 400 °C the hemicellulose, which is the least stable component, starts to decompose. The temperature of this initial degradation seems to be similar (200°C and 220 °C) for all treatments of all species. Regarding the rest of the combustion file of the different species only slight differences can be observed between the different treatments. However the differences between the different species can be observed. There is a shift of the temperature for the maximal degradation rate between the Hereward and the Viscount straw from 282 °C –284 °C to 307 °C – 311 °C, respectively. Additionally the form of the graph differs as the Hereward straw shows one single peak (exception for T2 which shows a shoulder) and the Viscount straw shows an additional shoulder (Figure 14).

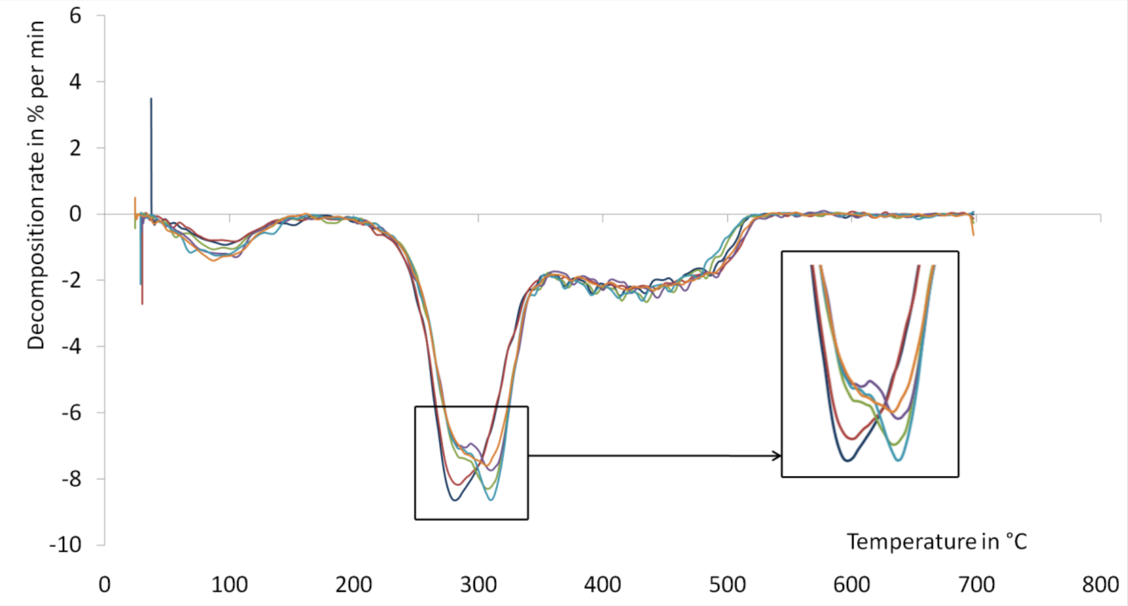

Figure 14. Decomposition rate of T1 and T6 of the different species. dark blue: Hereward-T1, red: Hereward-T6 , green: Viscount (low)-T1, purple: Viscount (low)-T6, light blue: Viscount (high)-T1, orange: Viscount (high)-T6

A lower temperature for the maximal degradation correlates well with the higher amount of hemicelluloses or cellulose as seen for Hereward straw (Ergudenler and Ghaly, 1992). The slight differences at higher temperatures could be assigned to differences in the cellulose or lignin content which decompose at 280 to 400 °C and 300 °C to 500 °C, respectively (Rao and Sharma, 1998; Raveendran *et al*., 1996) However, the inorganic compounds present in biomass are said to have a strong influence on the combustion characteristics (Raveendran *et al.,* 1996). Minerals could influence the way hemicelluloses and cellulose components interact with lignin. Especially the potassium and chlorine content are of interest as they, together with silica (SiO_2), which is considered not to catalyze pyrolysis reaction, make up the major fragment in wheat straw ash (Jensen and Dam-Johansen, 1998). As differences in the inorganic composition could already be noticed in the results of the XRF analysis, it is likely that the differences in the TG analysis are not only caused by variations in the organic composition but also by the differences of the inorganic composition.

4.1.2. Attenuated Total Reflectance IR Spectroscopy

Attenuated Total Reflectance Fourier Transform Infrared (ATR FTIR) spectroscopy was used to further analyse straw surface. No variations were observed between the straw species and the different treatments. Only slight differences in absorption bands that are assigned to the lignin (1243 cm^{-1}, the 1512 cm^{-1}, 1595–1654 cm^{-1}, and the 1738 cm^{-1}) (Sun *et al.,* 1996; Yao *et al*., 203; Jung and Himmerlsbach, 1989) or surface-wax (2850 cm^{-1} and 2916 cm^{-1})(Tazber *et al.,* 2005) content occur (Figure 15). Confirming the CHN analysis it seems that the treatments do not have a huge influence on the organic compounds of the wheat straw and that the differences between species of wheat straw in the organic composition are rather small.

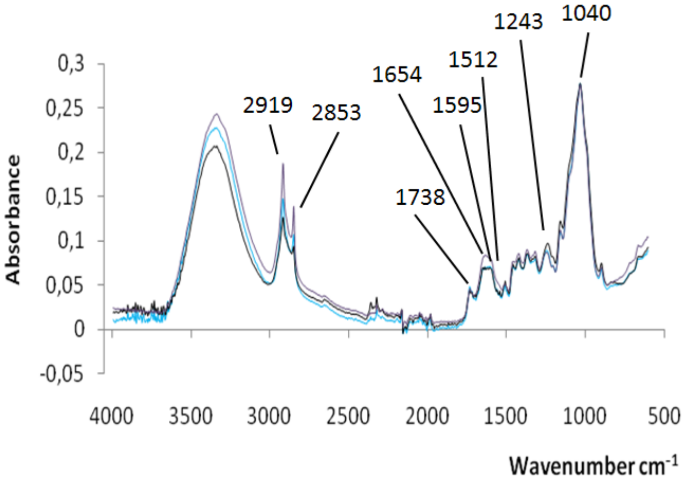

Figure 15. IR analysis of the wheat straw. blue: Hereward-T1, black: Viscount (low)-T1, purple: Viscount (high)-T1.

However, the changes in the ashes of the wheat straw seem to be more clearly apparent. T4, T5 and T6 of all species show higher absorption bands at 1415 cm^{-1} which can be allocated to a higher calcium carbonate content (Taztber *et al.,*2005) Moreover the absorption bands assigned to Si-O (960 cm^{-1}, 970 cm^{-1}, 790 cm^{-1}, 1031 cm^{-1} and 1100 cm^{-1}) (Hannah and Su, 1964; Ferraro and Manghani, 1972) vary for the different treatments and species (Figure 16).

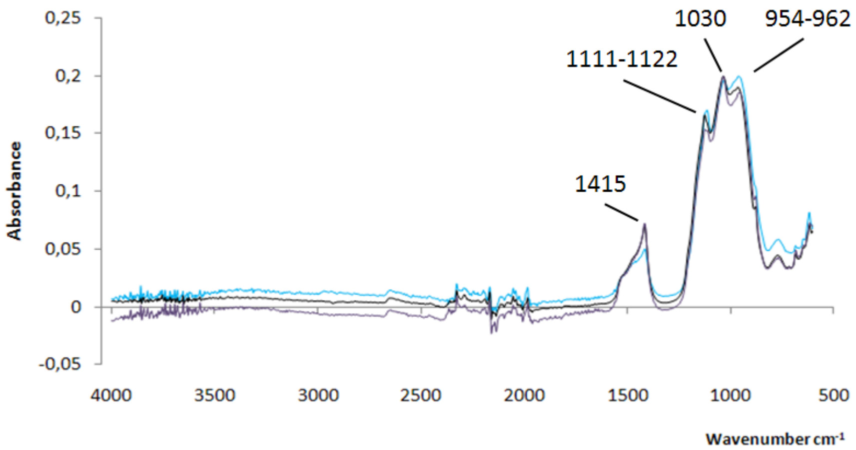

Figure 16. IR analysis of the wheat straw ash- comparing T1 of each species. Differences in the silica peaks can be observed. blue: Herward-T1, black: Viscount (low)-T1, purple: Viscount (high)-T1

Table 10. Combustion, TG and CHN results of the wheat straw and XRF results of the wheat straw ash

Compound	**Unit**	**VISCOUNT (LOW)**						**VISCOUNT (HIGH)**			**HEREWARD**					
		T1	**T2**	**T3**	**T4**	**T5**	**T6**	**T1**	**T4**	**T6**	**T1**	**T2**	**T3**	**T4**	**T5**	**T6**
Residual ash	%	2,98	2,38	2,45	2,52	3,06	3,1	2,11	2,57	2,79	3,5	3,23	3,11	3,17	3,04	3,05
Water content	%	5,51	5,39	6,01	7,26	6,68	6,88	6,95	6,24	7,05	5,3	5,78	4,91	4,71	4,61	4,71
Max.degradation	° C	308	310	314	310	312	311	311	310	307	282	283	282	284	282	282
Na_2O	%	0,32	0,32	0,28	0,24	0,24	0,28	0,44	0,12	1	0	0,28	0,24	0,08	0,08	0,3
MgO	%	4,58	4,36	4,73	4,47	4,8	4,78	4,83	4,51	4,61	4,03	3,92	3,82	3,4	4,44	4,51
Al_2O_3	%	-0,02	0,01	-0,01	0,01	0,02	1,15	0,04	0,04	0,23	0,08	0,06	0,01	0,01	0,04	0,06
SiO_2	%	46,43	50,3	47,83	42,96	40,02	42,19	46	43,01	41,86	48,75	49,78	42,38	42,47	41,88	45,21
P_2O_5	%	1,9	2,05	2,13	2,04	2,08	1,9	2,12	2,69	2,47	1,56	1,55	1,57	1,53	1,84	1,7
SO_3	%	4,15	5,11	4,68	4,17	6,05	4,92	3,8	5	3,12	2,54	3,64	1,64	2,44	3,4	2,3
K_2O	%	15,76	12,99	12,56	13,89	15,04	15,2	15,9	16,67	14,61	19,71	15,73	21,56	20,81	22,24	19,7
CaO	%	18,19	17,94	19,82	19,07	19,68	19,59	19,53	18,99	20,38	13,89	15,6	14,38	14,78	14,38	15,69
Cr_2O_3	%	0,15	0,08	0,06	0,02	0,03	0,02	0,19	0,127	0,254	0,16	0,04	0,88	0,14	0,08	0,14
Mn_3O_4	%	0,07	0,05	0,06	0,08	0,06	0,06	0,1	0,12	0,1	0,15	0,06	0,14	0,07	0,12	0,14
Fe_2O_3	%	0,77	0,49	0,33	0,18	0,21	0,14	0,82	0,58	1,38	0,79	0,26	3,73	0,7	0,44	0,74
ZnO	%	0,31	0,33	0,5	0,26	0,26	0,22	0,25	0,2	0,34	0,26	0,29	0,33	0,27	0,28	0,33
Cl	%	0,133	0,199	0,0701	0,104	0,166	0,112	0,144	0,156	0,125	0,197	0,177	0,0973	0,0787	0,158	0,197
SnO_2	%	0,0096		0,0089	0,0067		0,0124		0,044					0,033	0,074	0,0318
MnO	%	0,0692	0,0661	0,0677	0,0693	0,0731	0,0123	0,0918	0,118	0,0932	0,129	0,0712	0,0759	0,0583	0,0875	0,133
NiO	%	0,0371	0,0291	0,0162	0,0128	0,0139		0,0626	0,0501	0,876	0,0543	0,0144	0,0604	0,0243	0,0156	0,429
CuO	%	0,0146	0,0148	0,0123	0,0136	0,0155	0,0147				0,0151	0,016				0,0204
C	%	45,808	45,477	45,149	45,122	44,95	44,786	45,008	44,88	45,116	45,857			45,694		44,815
H	%	5,892	5,969	5,847	5,714	5,769	5,886	5,784	6,207	5,749	5,86			6,168		5,981
N	%	0,285	0,335	0,418	0,285	0,391	0,615	0,427	0,431	0,309	0,357			0,254		0,323

These differences are most likely due to Na, K and other cations. Na and K within the Si-O network can cause the formation of a double band due to non-bridging oxygens facing sodium or potassium. Furthermore, a certain ratio of calcium to aluminium can cause the formation of a double band or a shift to lower frequencies (Hanna and Su, 1964). The IR data affirms the differences in the inorganic composition which could be seen in the XRF data (Table 10).

In summary, there seems to be no cohesion between the different treatments and the variations of the wheat straw samples that could be observed in the measurements. It appears that the variation of wheat straw has the biggest impact on the composition. For the organic composition the differences between the samples were rather small. Marginal variations, such as the slight differences in the hemicelluloses, lignin or surface wax content, might not have a huge influence on the board properties.

4.2. Field Trials: Oilseed Rape

In the first year only one variety of oilseed rape was supplied (Dimension), but this had been grown with high and low nitrogen inputs, and with two different fungicide treatments which also have a growth regulating effect, Folicur and SunOrg Pro (Table 11). The compositional analysis is shown in Table 12 and inorganic speciation in Table 13.

Table 11. Treatments applied to Winter Oilseed Rape trial in 2010

	Fungicide/ PGR	Nitrogen (N) Application (kg/ha)			Total N (kg/ha)
		1st	2nd	3rd	
Treat No.	Stem Extension stage	Late Feb	Late March- Early April	Green- Yellow Bud	
1	Untreated	70	50		120
2	Folicur 1.0	70	50		120
3	SunOrg Pro 0.8 + Folicur 1.0	70	50		120
4	Untreated	70	85	85	240
5	Folicur 1.0	70	85	85	240
6	SunOrg Pro 0.8 + Folicur 1.0	70	85	85	240

Table 12. Composition (%) for oil seed rape straw from field trials (2010)

Treatment	Ash	Wax	α-cellulose	hemicellulose	lignin
1	5.04	1.94	43.61	40.86	10.49
2	6.62	3.01	41.13	34.24	18.01
3	6.29	3.35	37.34	38.75	17.62
4	6.15	1.85	36.03	39.99	17.83
5	6.49	3.47	39.78	38.06	15.67
6	6.32	1.95	35.36	43.58	14.74

The ash content of oilseed rape straw was higher than that of wheat straw, almost double in some cases. This greater ash content is problematic for biomass energy producers; however, from the point of view of creating a biosilicate binder based on ash by-products from bioenergy generation, the greater ash content of oilseed rape may be useful. However, as shown from the speciation data in Table 13, oilseed rape has very low silica content and not useful for this project.

Table 13. Oxide speciation with oilseed rape with respect to treatment applied

Species (%)	Treatment					
	1	2	3	4	5	6
Na_2O	**8.5**	**7.6**	**6.4**	**12.4**	**13.7**	**12.0**
MgO	1.0	1.6	1.5	1.1	0.9	1.1
Al_2O_3	0.0	0.0	0.0	0.1	0.4	0.0
SiO_2	0.0	0.2	0.1	0.4	2.4	0.5
P_2O_5	1.0	1.6	1.5	1.8	0.6	1.0
SO_3	**21.6**	**16.0**	**14.0**	**14.5**	**13.7**	**19.6**
K_2O	**24.4**	**26.5**	**27.6**	**25.1**	**19.9**	**20.1**
CaO	**27.8**	**35.2**	**35.1**	**31.2**	**22.5**	**31.1**
TiO_2	0.0	0.0	0.0	0.0	0.0	0.0
V_2O_5	0.0	0.0	0.0	0.0	0.0	0.0
Cr_2O_3	0.0	0.0	0.0	0.0	0.0	0.0
Mn_3O_4	0.0	0.0	0.0	0.0	0.0	0.0
Fe_2O_3	0.3	0.1	0.1	0.1	0.1	0.1
ZnO	0.1	0.1	0.2	0.4	0.1	0.1
SrO	0.1	0.1	0.1	0.1	0.0	0.1
BaO	0.0	0.0	0.0	0.0	0.0	0.0
Cl	**12.9**	**11.7**	**13.6**	**13.6**	**24.8**	**13.0**

Limited correlation between applied treatment and compositional variation was noted with the exception of treatments with higher nitrogen application which appeared to contain higher sodium and lower potassium levels. In fact very low levels of SiO_2 were noted irrespective of treatment applied thus rendering oilseed rape very poor for biosilicate extraction. Interestingly, ashes from oilseed rape have a low melting point in comparison to other straws due to high levels of alkaline metal, chlorine and sulphur content which could also cause problems during combustion, however; the low levels of silica are beneficial for preventing silicate formation in incinerators.

A large scale dewaxing process was developed in Bangor in order to prepare straw for subsequent particleboard trials. A 50 litre reactor was 2/3 filled with straw (approx 5 kg), and 40 litres of ethanol (IMS) was added (Figure 17). The reactor was closed under reflux for 2 h, cooled, partially drained to draw off a significant portion of the ethanol soluble waxes. A further 25 litres of ethanol was then added to the system, to further wash the straw, and the system brought back up to reflux for a 2 h. The solvent was drained while hot to minimise the opportunity for redeposition of wax on the straw particles during cooling.

Figure 17. 50 litre dewaxing of wheat straw. At the start of the reaction the straw bulk floats above the ethanol with only partial mixing (shown), but as dewaxing proceeds the straw becomes better wetted with ethanol.

The ethanol-damp straw was cooled, isolated and allowed to dry in trays within a large fume hood to control any further ethanol vapour safely. The trays were then oven-dried (40 °C) for complete removal of residual ethanol. The ethanol was reclaimed from the wax-rich solution by crude distillation, to allow re-use in the first wash process of the next extraction. The success of this dewaxing treatment was compared with traditional laboratory Soxhlet extraction of wheat straw; the wax content before and after large scale dewaxing was 4.96% and 2.31%, so a large improvement in wheat straw bonding performance was expected. This straw was used later for board manufacturing trials.

4.2.1. OSR wax characteristics

Gas chromatography-mass spectrometry (GCMS) analysis of the extracted wax (Figure 18) showed the presence of nonacosane (C29 at 38.66 min), 15-nonacosanone (40.66 min), triacontanol (40.89 min) and various phytosterols, e.g. β-sitosterol (43.66 min), stigmasterol (42.82 min) and campesterol (42.49 min).

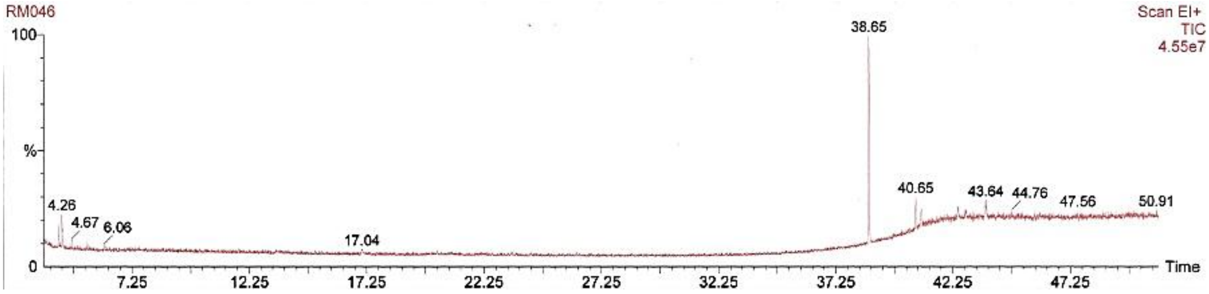

Figure 18. GCMS chromatogram for extract from oilseed rape (Treatment 1)

In 2011, material from field trials with four different varieties of wheat straw, and four different varieties of oilseed rape straw were available, however these were used primarily for wax extraction studies.

4.2.2. Dewaxing OSR from 2011 field trials

The samples from the 2011 harvest were dewaxed and trends in the four different varieties (Cabernet, Castille, Dimension and Vision) are represented in Figure 19. There were some samples missing from the matrix due to degradation during storage. The greatest losses occurred in the samples from the low PGR and high nitrogen treatments. The three samples which it was possible to run from this group had the lowest wax content (all below 1%) of all samples tested, which may have contributed to the ready onset of rot in this material. Many of the most rotten samples were very leggy, a likely result for this combination of high nitrogen and low plant growth regulator (and low fungicide).

The samples with lower nitrogen and low plant growth regulator did not show this trend as significantly, with some recording high wax contents (around 4%) on either the low or the high seed rate, however, the Vision variety had less wax in this low PGR treatment, giving results of 1.53% at high seed rate and 1.76% at low seed rate.

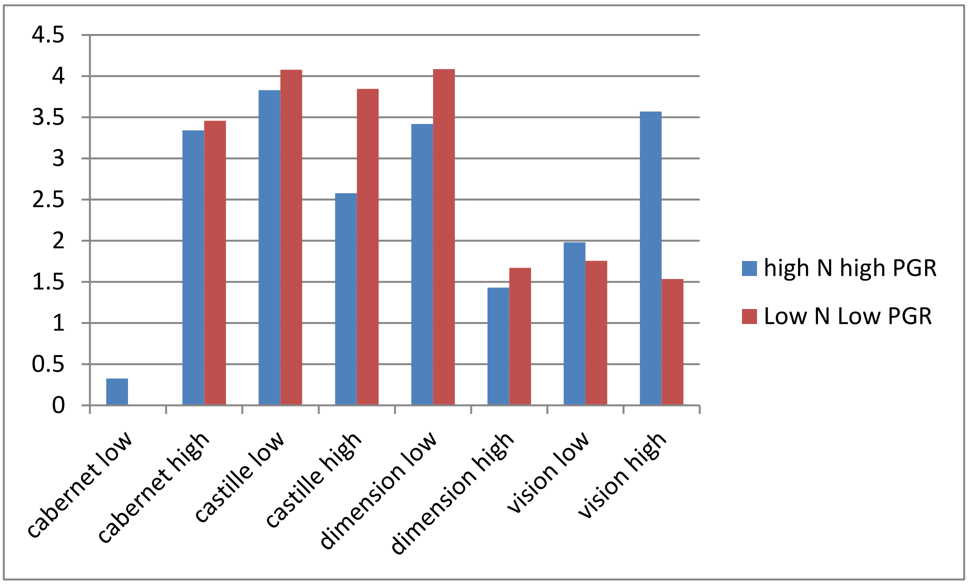

Figure 19. Comparison of wax content (%) for the high N and PGR and the low N and PGR samples, only Cabernet with low seed rate has a missing value (for low N and low PGR)

All four samples of Castille which were available for testing showed high wax levels, 2.58% for high seed at high N and high PGR being the lowest, and 4.08% for low seed rate at low N and low PGR. Castille was not the only variety where low seed rate gave higher wax than high seed rate (Figure 20). In Dimension, this was also the case for the High PGR – high N combination and the Low PGR Low N combination. For Cabernet and Vision however the pattern appeared either less clear, or difficult to prove due to missing samples.

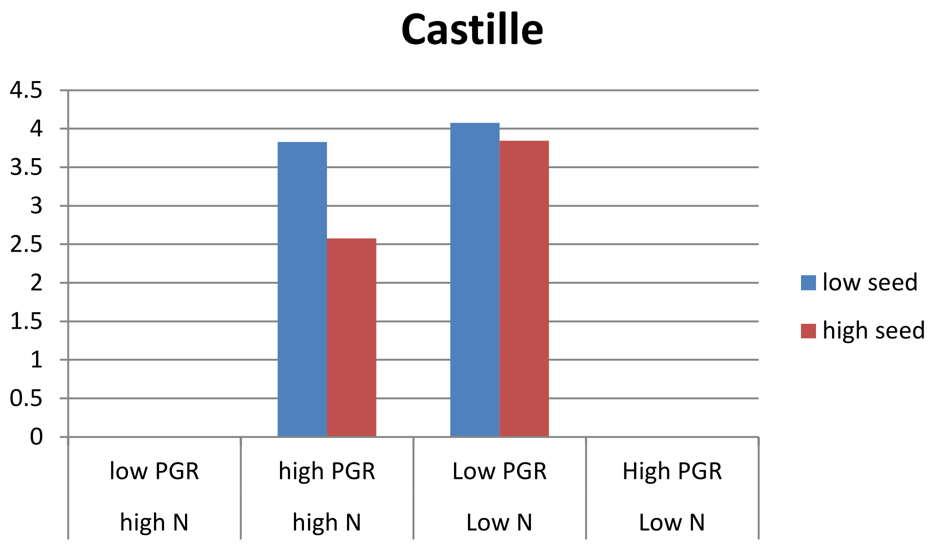

Figure 20. Wax content of four samples of OSR variety Castille, note that no low PGR high N and the High PGR low N samples were available.

Dimension had a greater number of samples available for testing (Figure 21), and the reverse trend was seen here compared to Castile and Vision. The lower seed rate appeared to have a greater wax content than the high, except where high PGR and low N were used. There was no data for the low PGR, high N, high seed rate scenario.

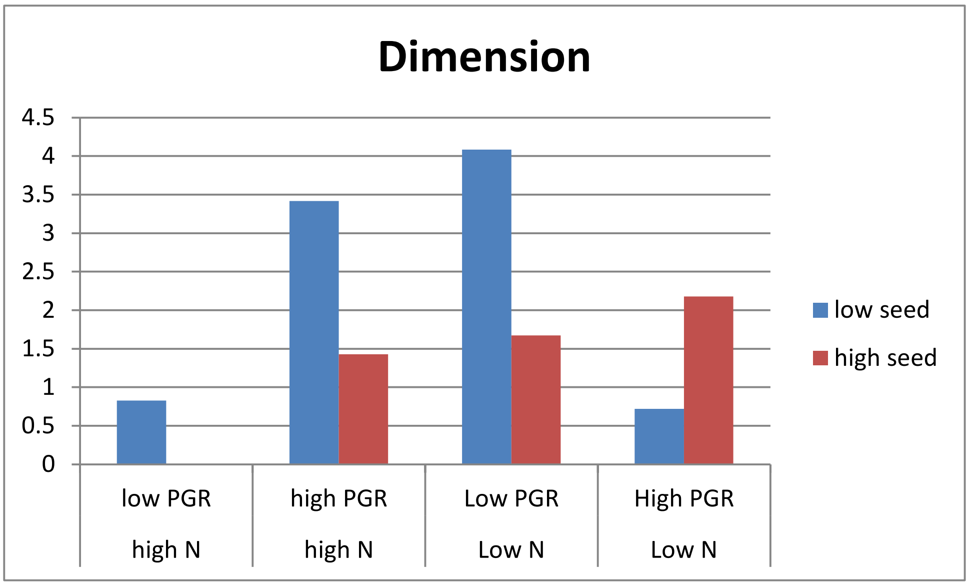

Figure 21. Wax content of seven samples of OSR variety Dimension.

A dewaxing experiment was conducted, to compare the quantity of wax removed by cold ethanol soak (industrial methylated spirits) with the quantity removed by Soxhlet extraction using hot ethanol (Soxhlet). Oilseed rape straw (10 g) treatment 2 and 3 from the 2010 harvest were soaked in ethanol. No samples showed a weight loss after the six hour period. The ethanol which was drained from the OSR straw had however changed colour, indicating that some material may have been removed, but nothing too significant.

In the Soxhlet extraction using hot ethanol only, a significant quantity of wax was removed, 2.65% (treatment 2) and 3.46% (treatment 3). These values were relatively close to the values seen when toluene:ethanol 2:1 (v/v) solution had been used for direct dewaxing of the wheat straw in composition analysis (3.00% and 3.35%).

To investigate the completeness of the removal of wax by the cold ethanol method, a subsample of the cold dewaxed material was extracted using toluene:ethanol solution in a Soxhlet. Approximately, 1.45% wax was removed for treatment 2 and 0.87% for treatment 3, confirming that only a proportion of the initial quantity of wax had been removed during cold soaking.

5. BIOSILICATE GENERATION AND BINDER FORMULATION

5.1. Laboratory scale biosilicate formation (York)

Considerable work was undertaken to understand the changes occurring in the inorganic species in wheat straw during the combustion and extraction of wheat straw ashes and chars on a laboratory scale. This work has been published and the salient features are reported herein.

i. A large proportion of silica can be extracted utilising the inherent alkalinity of the ashes formed. The required additional alkali required can be calculated from the initial inorganic content of the straw. However, less than 100% of the silica is completely solubilised.
ii. Extraction of silica increases with increased extraction temperature up to 100 °C and at lower combustion temperatures.
iii. Lower combustion temperatures are required to prevent crystallisation of silica, prevent alkali silicate formation and reduce evaporation of alkaline species.
iv. Pre-treatment of wheat straw can have a large impact on the mineralogical changes occurring during combustion and the resulting extraction of silica. Acid washing removes salts and calcium and results in silica with a greater amorphous character but a less alkaline solution following combustion and extraction. Water washing and ethanol Soxhlet extraction both remove salts (particularly KCl). However, ethanol extraction does not affect the alkalinity of the extraction solution formed after combustion with similar levels of silica extracted.

Ashes were collected from two commercial biomass combustion facilities burning miscanthus (Ely) and wood chips/green biomass (Eccleshall). The starting materials from these facilities were analysed on a lab-scale to compare their combustion and extraction characteristics. The combustion ashes were further characterised and the extraction of silica from the miscanthus bottom ash was studied using both potassium hydroxide and concentrated fly ash solutions. The alkali silicate solutions formed were tested as binders for wheat straw particleboards.

5.2. Power station ashes

To scale-up the extraction and utilisation of inorganic species from combustion residues, and transfer knowledge gained at a lab-scale, several ashes were collected from two biomass power stations.

Ely Power Station, at 38 MW, is the largest straw burning power station in the world, with a total fuel demand of 200,000 tonnes per annum. The main fuel is wheat straw with additional utilisation of miscanthus and oilseed rape as required. At the time of collection Ely Power Station was burning miscanthus straw. Around 3000 tonnes pa of fly ash is produced, which is currently sold as a fertiliser and soil enhancer. Approximately 10,000 tonnes pa of bottom ash is formed, for which there is no current market. The materials collected were (Figure 22):

a. Bottom ash, quenched in water (Ely-BA1)
b. Fly ash (Ely-FA1)

Eccleshall is a 2 MW power station mainly using clean wood chip from forestry and aboricultural arisings along with an additional feed of miscanthus. 5 tonnes of bottom ash is produced a day and 300 kg of fly ash, with an annual production of 500-700 tonnes and 100 tonnes respectively. The fly ash is currently sold for the production of concrete blocks. The materials collected were (Figure 22):

a. Bottom ash, quenched in water (Ecc-BA1)
b. Fly ash (Ecc-FA1)
c. Starting materials of Wood Chip (WC) and Miscanthus (Mis)

The starting fuels were initially analysed to compare their extraction trends to those of the wheat straw previously studied. The ashes were then tested to study their suitability for the formation of biosilicate solutions as binders for inorganic composite boards.

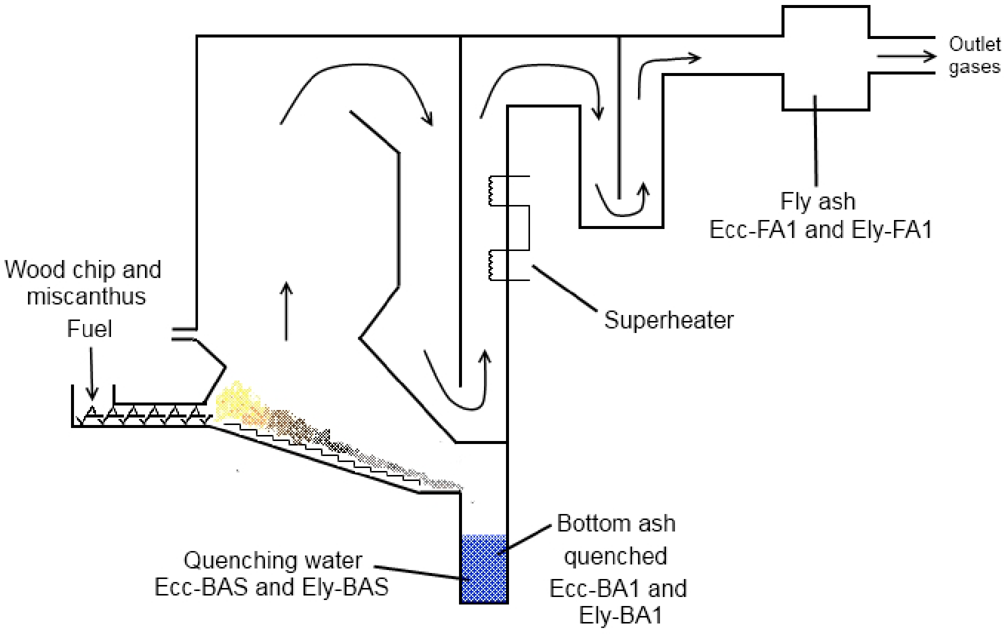

Figure 22. Basic layout and collection points of material from power stations burning wood chip and miscanthus biomass (Originally in colour)

5.2.1. Fuel analysis

The wood chip and miscanthus fuels that were collected from Eccleshall power station had a high moisture content and were therefore air dried before a full analysis was undertaken. The proximate and ultimate analyses of the fuels are shown in Table 14. Where the analysis was undertaken in duplicate or triplicates the average is shown, along with the standard deviation.

Table 14. Fuel analysis of wood chip and miscanthus fuels

	Wood Chips	Miscanthus
Moisture (%) [a]	33.2 ± 0.9	22.6 ± 2.0
Moisture (%) [b]	9.8 ± 0.2	7.4 ± 0.1
Volatile matter (%) [db]	80.0	67.0
Fixed carbon (%) [db]	15.3	28.5
Ash (%) [db]	4.7 ± 0.1	4.5 ± 0.5
C (%) [db]	50.0 ± 0.3	48.8 ± 0.2
H (%) [db]	5.14 ± 0.1	5.28 ± 0.2
N (%) [db]	0.26 ± 0.1	0.56 ± 0.1
O (%) [db]	39.8 ± 0.7	40.9 ± 0.3
HHV (MJ/kg) [db]	19.5 ± 0.2	17.1 ± 0.1
Ash (%)		
Na_2O	1.22	0.98
MgO	2.79	3.14
Al_2O_3	3.98	0.82
SiO_2	28.0	45.4
P_2O_5	3.74	3.52
SO_3	0.42	0.50
K_2O	9.61	24.9
CaO	31.39	8.28
TiO_2	0.24	0.06
V_2O_5	0.01	0.00
Cr_2O_3	0.02	0.08
Mn_3O_4	0.16	0.28
Fe_2O_3	4.25	1.44
ZnO	0.09	0.08
SrO	0.09	0.02
Y_2O_3	0.00	0.00
ZrO_2	0.00	0.00
BaO	0.06	0.04
Cl	3.1	6.3
Loss on Ignition	10.8	4.2

a = as received; b = air dried; db = dry basis

The ash (dry basis) content is similar for both fuels. Generally, wood is observed to have a lower ash content than herbaceous biomass (Pettersson *et al.*, 2009; Thy *et al.,*2006; Rajamma *et al.,*2009), however, a large percentage of the woody material combusted at the Eccleshall plant consists of aboricultural arisings. These are the clippings from the management of municipal parks and verges and therefore contain a high content of fast growing biomass, particularly leaves, which generally have a higher concentration of nutrients (Biomass Energy Centre, 2011; Salisbury and Ross, 1992; Bryers, 1999, Monti *et al.,* 2008).

The carbon content and calorific value of the wood chips are slightly higher than miscanthus, whilst the oxygen content is slightly lower. Generally woody biomass contains more lignin and less hemicellulose than grasses (Barneto *et al.,*2009), which could therefore account for the observed differences in the C and O content. A higher heating value is directly correlated to lower O/C ratios (Jones *et al.,* 2006).

The inorganic composition of the ash varies significantly between the two materials. The miscanthus ash has a similar distribution to that of wheat straw with higher K_2O (24.9%), SiO_2 (45.4%) and Cl (6.3%) contents and lower amounts of CaO (8.9%) and other elements, based on their oxide content. In contrast, the species with the highest concentration in the wood chip ash is CaO (31.4%), followed by SiO_2 (28.0%) and then K_2O (9.6%). The chlorine content is low (3.1%), although not insignificant. The aluminium and iron content in the wood chip ash is also high. This may be due to contamination of the fuel during its collection from homes and businesses (Miles *et al.,* 1996). Indeed, a magnetic portion was found within the ashes. Similar variations of C, H, N content and ash composition have been noticed previously between wood pellets and straw (Pettersson *et al.,*2009; Thy *et al.,*2006; Miles *et al.,* 1996). The variation in the inorganic species between the fuels could significantly impact on the formation of ashes under combustion conditions and consequently their use.

5.2.2. Combustion-extraction trends

The miscanthus (Mis) and wood chip (WC) fuels were combusted at temperatures between 400 – 800 °C for 2 h to ensure complete combustion. The ashes were then quenched in water, leached for 24 h at room temperature and the filtrates were analysed for dissolved species (Table 15, Figure 23, Figure 24).

Table 15. Levels of extraction of Si, K, Ca and Cl from miscanthus and wood chip ash

Name	Combustion	Initial	Final	Si (%)	K (%)	Ca (%)	Cl
Mis-400-2	400	12.2	11.3	38.3± 1.3	72.5± 3.5	0.0	37.0
Mis-500-2	500	12.1	11.3	26.6± 1.7	63.5± 3.7		
Mis-600-2	600	12.2	12.3	10.4± 1.2	55.5± 3.4	0.0	40.9
Mis-700-2	700	12.0	12.2	0.3 ± 0.3	19.0± 1.3		
Mis-800-2	800	11.8	11.9	0.9 ± 0.1	10.2± 0.7	2.0 ± 0.1	40.7
WC-400-2	400	11.9	12.2	1.9± 0.03	96.3± 6.3	0.0	5.8
WC-500-2	500	11.5	11.9	1.4 ± 0.1	78.4± 4.0		
WC-600-2	600	12.7	12.8	0.5 ± 0.3	59.8± 3.9	13.2 ± 1.0	5.7
WC-700-2	700	12.4	12.5	0.2 ± 0.3	29.1± 2.7		
WC-800-2	800	12.7	12.7	0.5 ± 0.2	9.3 ± 1.1	15.7 ± 0.5	5.7

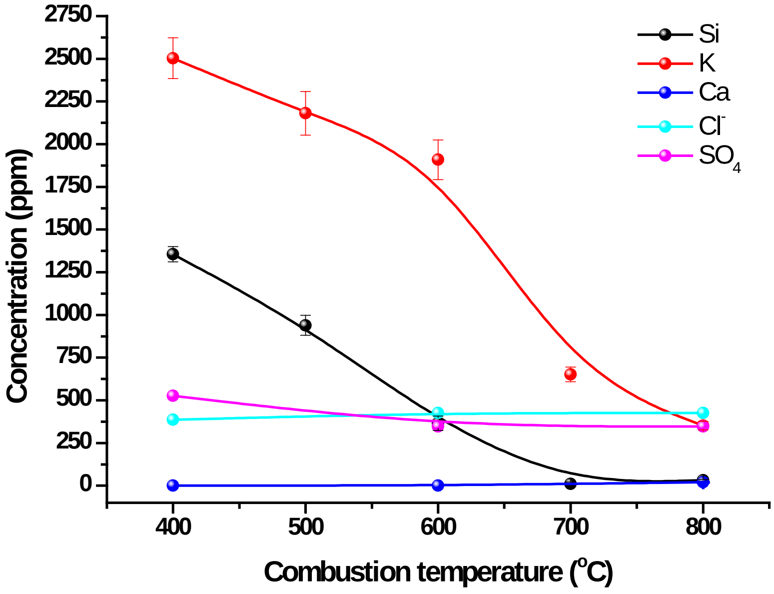

Figure 23. Concentration of various elements in extracts of miscanthus ash formed at different combustion temperatures (Originally in colour)

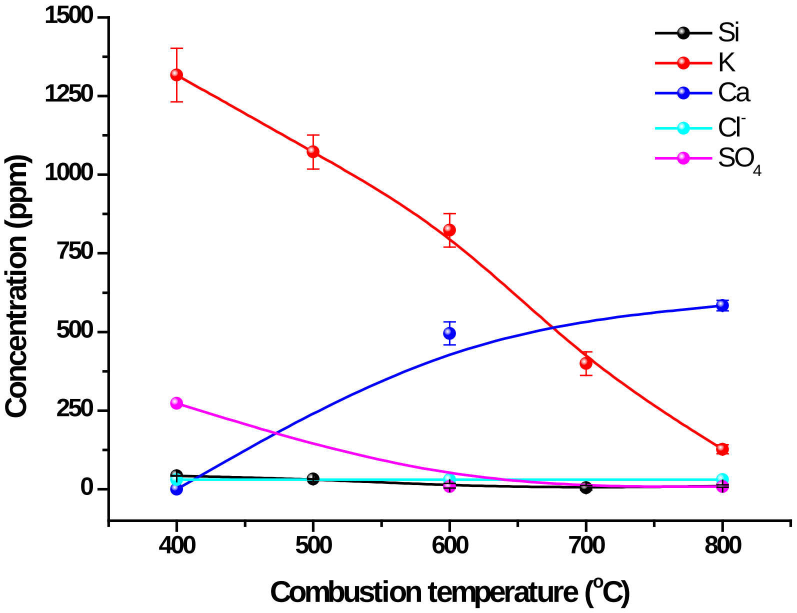

Figure 24. Concentration of various elements in extracts of wood chip ash formed at different combustion temperatures (Originally in colour)

There is a stark contrast in the extraction trends for the main inorganic species from miscanthus (Figure 23) and wood chip (Figure 24) ashes. At 400 °C both ashes display initial high levels of dissolution of potassium (Table 15), with that of the wood chips nearing 100%. The potassium extraction of the wood chips decreases almost linearly with increasing combustion temperature, whilst the potassium extraction only reduces significantly above 600 °C for the miscanthus ash. Chloride and sulphate extraction levels remain consistent at all combustion temperatures from the miscanthus ash. Chloride extraction is very low from the wood chips, whilst sulphate extraction decreases above 400 °C. The silica and calcium extraction trends display the most obvious contrast between the two biomass materials. The maximum silica extraction from the miscanthus ashes is 38% at 400 °C and decreases with increasing combustion temperature, following the same trend observed for wheat straw ashes. Minor calcium concentrations in the filtrate only become apparent at a combustion temperature of 800 °C. In contrast, the maximum silica extraction from the wood chip ashes is only 1.9%, remaining low at all combustion temperatures, whilst the calcium concentration is significant at 600 °C (13.2%) and increases with increasing combustion temperature.

These extraction trends demonstrate that the inorganic material within miscanthus and wood chips behave very differently during combustion. Very low levels of silica are solubilised, even at low temperatures of combustion, from the wood chip ash despite a sufficiently high alkalinity within the solutions formed. This is highlighted by the difference in solution pH at the beginning and end of the extractions for the two materials at 400 °C (Table 15). The decrease in pH following extraction for miscanthus is compatible with the results obtained for wheat straw, where the dissolution of silica causes a lowering of the pH. In comparison, for wood chip ash, the pH increases during extraction and with higher combustion temperatures, which correlated with the increasing levels of calcium dissolved.

XRD analysis of the species present within the ashes further emphasises the differences between the materials (Figure 25, Figure 26). Miscanthus ashes have a similar speciation to wheat straw ashes. The main species present at 400 °C are KCl and $CaCO_3$. A decrease in $CaCO_3$ content occurs at 600 °C coinciding with a reduction in silica extraction. The KCl content reduces at 800 °C suggesting that devolatilisation is occurring, although this is in contrast to the constant levels of chloride detected in the solutions formed at all combustion temperatures. K_2SO_4 is observed at all combustion temperatures. The wood chip ash formed at 400 °C contains a much lower level of KCl, a higher proportion of $CaCO_3$ and quartz and a high content of fairchildite ($K_2Ca(CO_3)_2$). The high level of quartz observed in all of the ashes could be due to contamination of the fuel. As the combustion temperature increases a decrease in the concentration of quartz and $CaCO_3$ occurs, combined with the formation of calcium silicate and portlandite ($Ca(OH)_2$), which was not detected in either the wheat straw or miscanthus ashes. In addition, the diffractograms of the wood chip ashes have a much flatter baseline. The content of amorphous material in a sample can be semi-quantitatively calculated from the area of the amorphous halo in an XRD pattern (Tianinen *et al.,* 1999). This therefore indicates that the wood ash is much more crystalline than the miscanthus and wheat straw ashes. The solubility of silica from wood chip ashes is therefore suggested to be due to the lack of amorphous silica and the formation of insoluble calcium silicate at higher combustion temperatures.

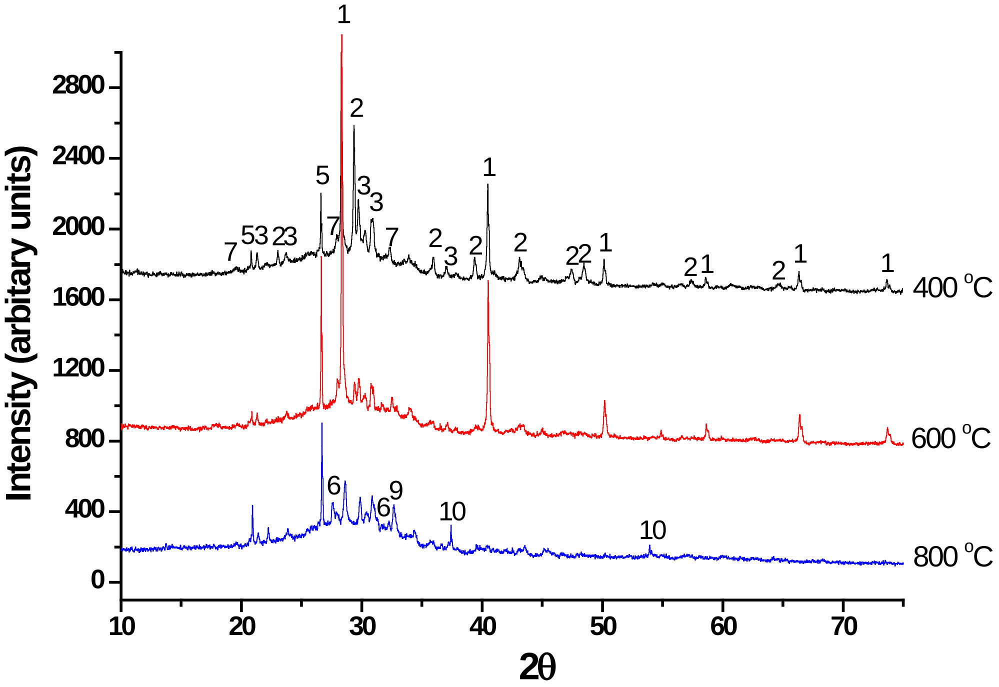

Figure 25. Diffractograms of miscanthus ashes formed at different combustion temperatures: 1 = Sylvite (KCl); 2 = Calcite ($CaCO_3$); 3 = Arcanite (K_2SO_4); 5 = Quartz (SiO_2); 6 = Calcium silicate ($CaSiO_2$); 7 = Fairchildite ($K_2Ca(CO_3)_2$); 9 = Calcium silicate ($Ca_2(SiO_4)$); 10 = Calcium oxide (CaO) (Originally in colour)

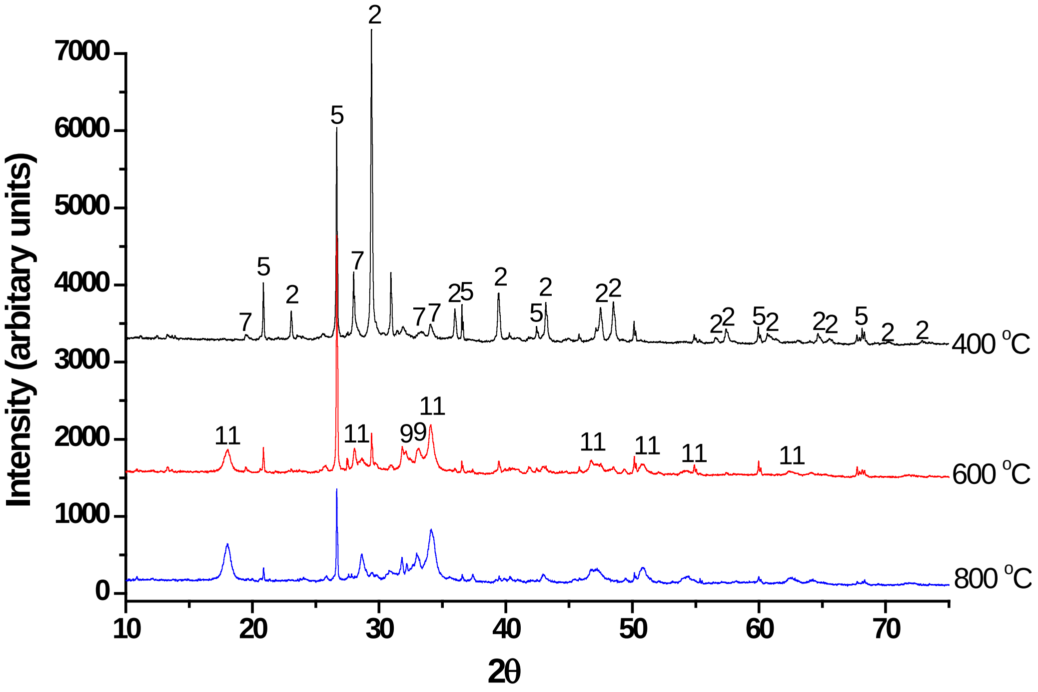

Figure 26. Diffractograms of wood chip ashes formed at different combustion temperatures: 2 = Calcite ($CaCO_3$); 5 = Quartz (SiO_2); 7 = Fairchildite ($K_2Ca(CO_3)_2$); 9 = Calcium silicate ($Ca_2(SiO_4)$); 11 = Portlandite ($Ca(OH)_2$) (Orginally in colour)

The data described above intimates that the bottom ashes collected from the two power stations will behave differently, particularly with respect to the extractability of the silica present within them. However, since the ashes obtained from both power stations had been formed under different conditions to those obtainable under laboratory conditions, and particularly since a separate fly ash fraction was acquired, all of the ashes collected were analysed further to gain information about their composition.

5.2.3. Mineral analysis of ashes

Both the fly ash and bottom ash from each power plant were analysed by XRF to determine their elemental composition (Table 16). As collected, the bottom ashes were wet from direct quenching in water. Before analysis, the bottom ashes were dried and ground to <125 μm to ensure that a homogeneous sample was selected. The powder formed was dark grey in the case of Ely-BA1 and creamy-white for Ecc-BA1. The fly ashes were low in density, fine and dark.

The main inorganic elements present in the power station ashes are silica, potassium, calcium and chlorine, as observed for the initial fuels. The data indicates that there is a fractionation of the elements between the fly ash and the bottom ash, dependent on the volatility of the elements. Potassium, chlorine, sulphur, sodium and phosphorous are enriched in the fly ash, whilst the majority of the silica is captured in the bottom ash.

Calcium is distributed between both ashes. A similar distribution of elements between fly ashes and bottom ashes has been detected in a power plant burning straw previously (Miles *et al.,* 1996).

XRD analyses of the mineral species present in each of the ashes show that both fly ashes are mainly composed of sylvite (KCl) (Figure 27, Figure 28). This has frequently been found to be the major phase in fly ashes from other power plants combusting both woody and herbaceous biofuels (Pettersson *et al.,* 2009), however, other researchers have also observed fly ashes to contain quartz (Rajamma *et al.,* 2009).

Table 16. a) Elemental composition of fly ash and bottom ashes from two biomass power plants analysed by XRF, all in wt%. b) Elemental composition of solutions formed from the water leaching of power station ashes. All concentrations in ppm.

a)

Compound	Ely-FA1	Ely-BA1	Ecc-FA1	Ecc-BA3
Na_2O	2.45	0.16	2.24	1.18
MgO	1.02	2.82	2.55	2.69
Al_2O_3	0.19	0.76	3.13	6.54
SiO_2	6.59	63.0	18.2	51.9
SO_3	3.02	2.74	2.78	2.28
P_2O_5	18.3	4.37	7.80	1.45
K_2O	32.0	14.6	23.3	8.70
CaO	16.8	8.28	17.7	18.7
TiO_2	0.01	0.06	0.30	0.47
V_2O_5	0.00	0.00	0.01	0.01
Cr_2O_3	0.00	0.01	0.03	0.04
Mn_3O_4	0.05	0.14	0.26	0.30
Fe_2O_3	0.12	0.50	1.98	4.72
ZnO	0.08	0.02	1.17	0.04
SrO	0.03	0.02	0.06	0.13
Y_2O_3	0.00	0.00	0.00	0.00
ZrO_2	0.00	0.00	0.01	0.01
BaO	0.02	0.06	0.08	0.34
CuO	0.01	0.02	0.05	0.15
SnO_2		0.09	0.06	0.03
Cl	19.1	0.05	17.7	0.28
NiO	0.00			0.012
Br	0.53		0.12	
PbO	0.006		0.27	0.03
Rb_2O	0.023		0.03	0.02
Nb_2O_5		0.038		
In_2O_3		0.031		
Sb_2O_3			0.03	
CdO			0.02	
Cr_2O_3			0.02	0.060
ZrO_2			0.01	0.060
WO_3				0.011
Co_3O_4				0.008
Sum	100.4	97.8	99.9	100.1

b)

Element	**Ely-FA1**	**Ely-BA1**	**Ecc-FA1**	**Ecc-BA3**
Al	0.2	0.5	0.3	64.4
As	0.7	0.2	0.6	2.4
B	2.9	0.2	1.7	1.0
Ba	0.0	0.0	0.1	Nd
Ca	6.4	1.8	52.9	5.2
Cd	nd	nd	nd	0.0
Co	0.0	nd	nd	Nd
Cr	0.2	nd	0.1	0.1
Cu	0.1	nd	0.1	0.4
Fe	nd	nd	nd	Nd
Hg	0.4	nd	0.0	1.3
K	12873	988	9922	560
La	0.0	nd	0.1	0.0
Li	0.2	nd	0.1	Nd
Mg	0.1	1.0	nd	1.0
Mo	1.6	0.2	0.9	0.4
Na	1345	20.4	861	91.4
Ni	nd	nd	nd	0.2
P	0.5	6.8	0.1	0.8
Pb	nd	nd	0.1	Nd
Pd	0.1	0.5	0.2	0.4
Rb	24.7	1.2	14.3	1.6
S	2757	248	2220	82
Sb	0.5	nd	nd	0.5
Si	2.8	273.3	1.6	12.3
Si (AAS)	4.0	462.7	6.3	10.4
Sn	0.2	nd	0.2	2.4
Sr	0.1	0.0	0.2	0.1
Tl	0.7	1.0	0.5	2.4
V	0.1	0.4	0.1	0.4
W	0.3	15.1	0.1	1.1
Zn	0.1	0.2	0.1	0.2
Cl	12038	80.8	7895	38.3
NO_3	88.8	73.3	68.0	50.0

Ely-BA1 (mainly miscanthus) (Figure 27) is primarily composed of cristobalite, whilst Ecc-BA1 (mainly wood chips) (Figure 28) is principally composed of quartz. The presence of these crystalline phases is consistent with the main elemental composition of each ash but is in contrast to the ashes formed from each starting material under lab-scale conditions up to 800 °C. In particular, purer silica phases are observed in each of the bottom ashes, similar to those observed for wheat straw ashes with low concentrations of alkali metals in the initial straw. This suggests that both potassium and calcium are more easily volatilised and less likely to be captured in the bottom ashes under the power plant operating conditions. However, the highly crystalline silica content may affect its ease of solubilisation (Iler, 1979).

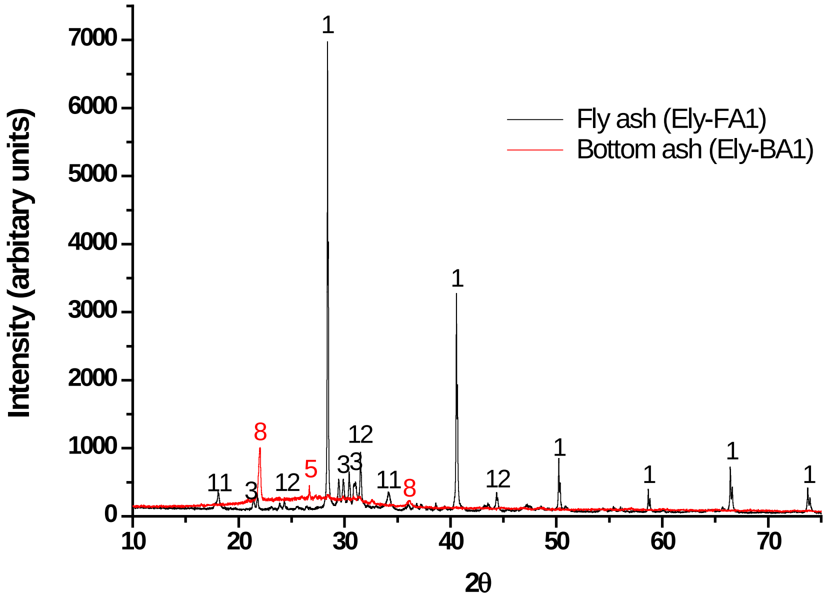

Figure 27. XRD of Ely-BA1 and Ely-FA1 - fly ash and bottom ash from a combustion facility primarily using miscanthus: 1 = Sylvite (KCl); 3 = Arcanite (K_2SO_4); 8 = Cristobalite (SiO_2); 11 = Portlandite ($Ca(OH)_2$); 12 = Aphthitalite ($K_3Na(SO_4)_2$) (Originally in colour)

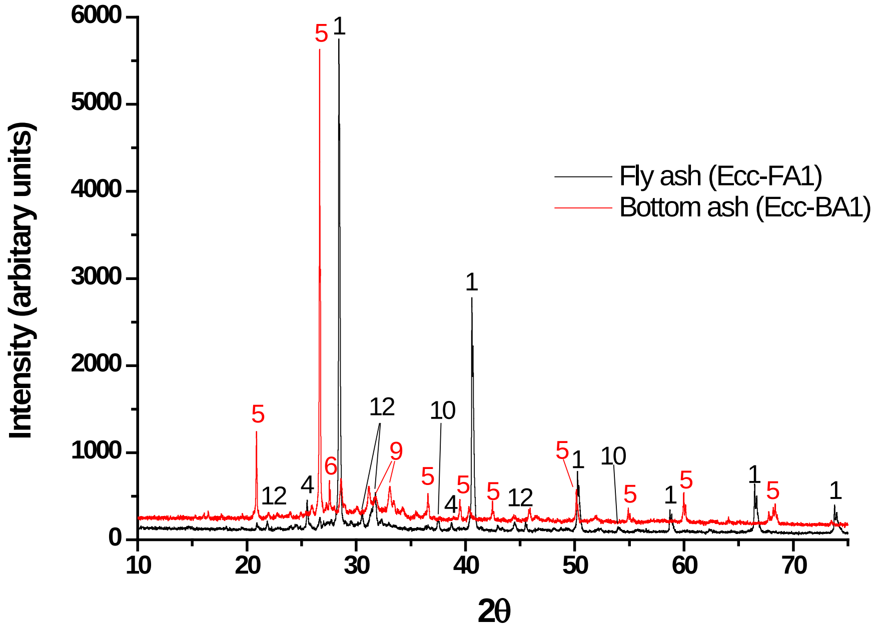

Figure 28. XRD of Ecc-BA1 and Ecc-FA1 - fly ash and bottom ash from a primarily wood chip combustion facility: 1 = Sylvite (KCl); 4 = Anhydrite ($CaSO_4$); 5 = Quartz (SiO_2); 9 = Calcium silicate ($Ca_2(SiO_4)$); 10 = Calcium oxide (CaO); 12 = Aphthitalite ($K_3Na(SO_4)_2$) (Originally in colour)

5.2.4. Chemical analysis of ashes

In order to study the potential alkalinity of the different ashes, the ashes were leached in water at a liquid:solid ratio of 3 over 24 h and the pH of the solution formed over time was measured (Figure 29). This illustrates a sizeable difference between both the fly ashes and bottom ashes from the two power stations burning different fuels. The elemental content of the solutions formed were also analysed by inductively coupled plasma atomic emission spectroscopy (ICP-AES) (Table 17). Analysis of potassium, silicon and sodium by atomic absorption spectroscopy (AAS) highlighted the same trends in concentrations, although gave slightly higher absolute values.

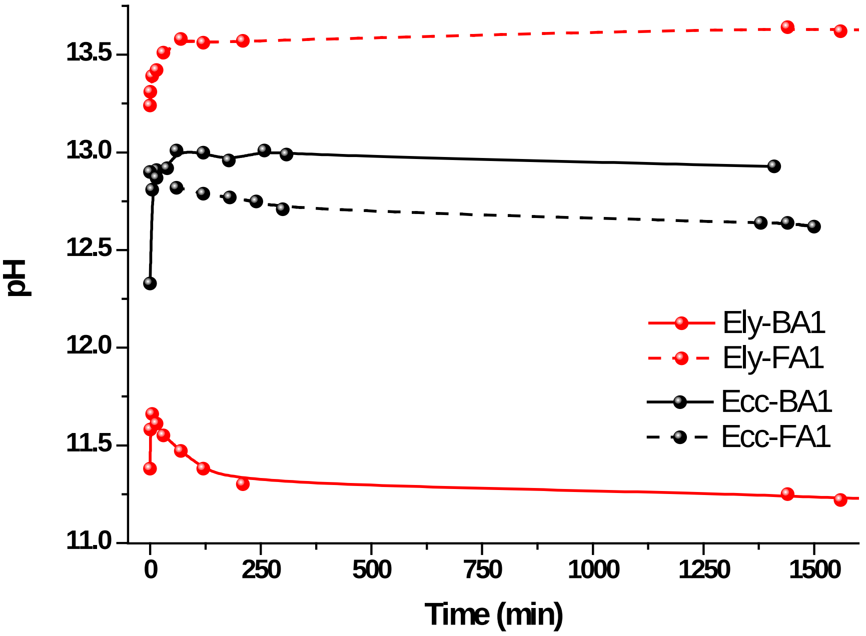

Figure 29: pH of solutions during the leaching of power station bottom ashes and fly ashes with time (Originally in colour)

All of the ashes display an instantaneously high pH upon addition of the ashes to water (13.2 for Ely-FA1 and 11.4 for Ely-BA1 within 30 s). Ely-FA1 has the highest initial pH which is followed by a slower increase up to a constant level of pH 13.6 after 70 min. This suggests an initial fast release of alkali species deposited on the surface of the ashes followed by a diffusion controlled release of species through the solid matrix as proposed for straw char (Jensen *et al.,*2001). The main element contributing to the alkalinity of the solution appears to be potassium with a minor input from sodium. Ely-BA1 has a much lower initial and final pH. It increases sharply within the first few minutes followed by a slow decrease indicating the neutralisation of some of the alkalinity. The presence of silica in the final solution indicates that this may be causing the gradual reduction as observed for lab-scale ashes. However, this dissolution only represents 0.7% of the silica present within the ash.

In comparison, the Ecc-BA1 shows a much slower increase in the pH of the solution with no decrease in the pH over time, whilst Ecc-FA1 reaches the maximum pH within the first minute followed by a slight decline over the following 24 h. Only a minute quantity of silica is dissolved from Ecc-BA1 in water. The minor amount of aluminium that is dissolved could be expected to neutralise some of the alkalinity, however, this does not appear to be the case. The reason for the slight decrease in alkalinity of the Ecc-FA1 with time is unknown. It could be due to some CO_2 from the atmosphere dissolving into the solution; however, this does not appear to have occurred for the other ashes studied under the same conditions.

The concentrations of the elements in the water solutions echo the concentrations in the starting ashes. Higher concentrations of potassium, chlorine, sulphur and sodium are found in the fly ash solutions compared to the bottom ash solutions. The low concentration of potassium in the bottom ash extracts suggests that it is more tightly bound within these ashes. Detectable levels of calcium are only found in the Ecc-FA1 solution indicating that the calcium species present in the ashes are also insoluble. The elemental analysis of the ashes indicated that the fly ashes were more suitable as fertilisers, having higher P and K levels. The water solubility analyses show that they do have a higher content of available potassium, however, the soluble phosphate levels are low. Chemical fractionation using ammonium acetate would show whether these are, however, available via ion exchange (Pettersson *et al.,* 2009).

Very low levels of other elements are observed in solution, many of them at or near the limit of detection. In particular, a major element of concern, cadmium is not detected in the solutions. Concentrations of other heavy metals including Cr, Zn, Ni, Pb and Cu are very low or were not detected.

This data indicates that the silica within the ashes is not solubilised directly using the inherent alkalinity of the ashes in water at room temperature. However, utilising the alkalinity of the fly ashes, particularly for the miscanthus ashes (Ely-FA1), could be a method to solubilise the greater content of silica in the bottom ashes.

5.3. Silicate analysis development

Within this study there was a desire to produce a silicate solution similar in SiO_2 and wt% to commercial silicate solutions from combustion residues. Commercial silicate solutions are normally analysed for solids content and SiO_2:M_2O content by measuring their density and alkali content by titration. However, this is also a time-consuming process and requires a large amount of solution. An alternative method was required that was quick and needed only a small quantity of solution to analyse the silica content.

It was noticed during some early work that the IR absorbance of the silicate bands (1250 - 650 cm^{-1}) increased in intensity with increasing concentration of the solution. This also gave further information about the nature of the silicate species within the solution and could be used with only a small drop on an attenuated total reflectance infrared spectrometer (ATR-IR), with analysis taking under a minute. It was therefore decided to test the hypothesis that the silica concentration could be analysed by studying the changing area of the silicate IR band. Several commercial silicate solutions were diluted to different concentrations (4, 8, 12, 16 and 32% of the original concentration) and analysed by ATR-IR. Solutions with both sodium and potassium counter-ions and of various molar ratios were chosen. Details of the solutions used based on the product information sheets are shown in Table 17.

Infrared spectra of the K120 solution at all dilutions, following subtraction of the water background, are shown in Figure 30, whilst IR spectra of all of the 32% silicate solutions are displayed in Figure 31. Figure 30 demonstrates that the general shape of the observed spectra remains constant at all of the dilutions used, whilst the overall intensity of the absorbance increases with increasing concentration of the solution. The peak maxima do shift slightly from 1017 to 1009 cm^{-1} as the concentration of the silicate solution increases. This was also observed by Bass and Turner (1997) and Halasz *et al.*(2007), but ascribed to different causes

Table 17. Details of commercial silicate solutions used for silicate analysis development

Name (Counter-ion)	**Mean specific gravity (g cm^{-3} @ 20 °C)**	**Mean wt ratio (SiO_2: M_2O)**	**Mean molar ratio (SiO_2: M_2O)**	**Mean M_2O (wt%)**	**Mean SiO_2 (wt%)**	**Mean total solids (wt%)**
C501 (Na)	1.6	1.6	1.65	18.0	28.8	46.7
C503 (Na)	1.5	2.5	2.58	12.5	31.1	43.6
C75 (Na)	1.38	3.2	3.3	8.6	27.6	36.2
K120 (K)	1.6	1.43	2.24	21.6	20.8	52.4
K78 (K)	1.39	2.09	3.27	13.0	27.1	40.1
K53 (K)	1.26	2.48	3.89	8.6	21.3	29.9

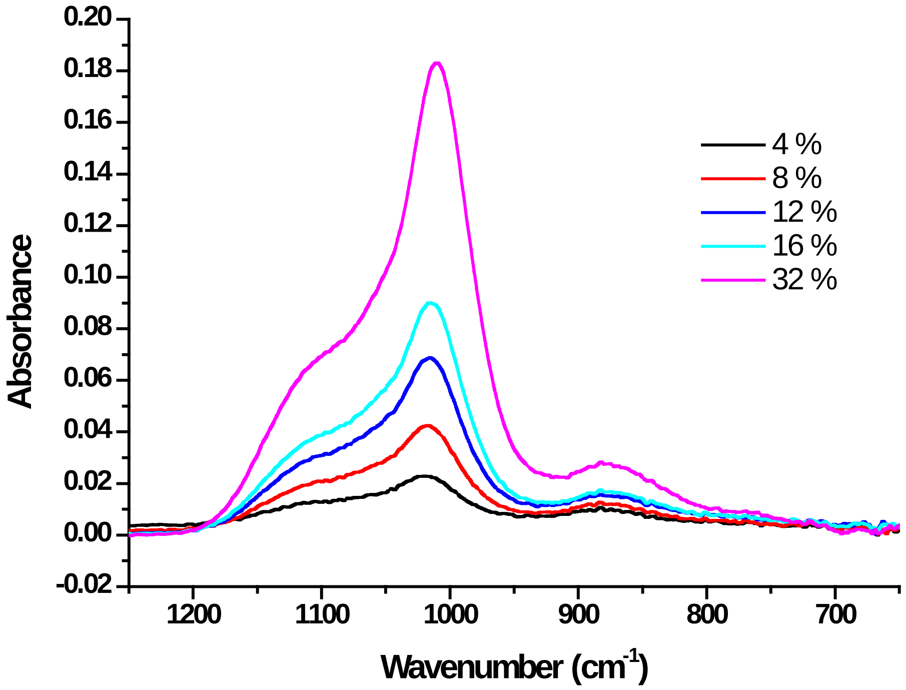

Figure 30: Infrared spectra of K120 solution at various concentrations relative to the original solution (Originally in colour)

Figure 31 exemplifies how the shape of the observed absorbance spectra alters with changing silicate speciation. The higher ratio silicate solutions (C75, K78 and K73) display a shift in the frequency of the main peak (1018 cm-1) to higher wavenumbers and greater development of a high frequency shoulder (1225-1064 cm-1). The lowest ratio silicate solution (C501) shows the reverse behaviour.

The area of the silicate band between 1250-650 cm^{-1} was correlated to the silicon concentration of the initial solution analysed by AAS. The concentration was not taken from the data sheets due to the variation in silica concentration between each batch. The correlations for the dilutions of each individual solution are shown in Figures 32 and 33 whilst the correlation for all of the solutions combined is shown in Figure 34. These reveal a very strong linear correlation between the Si concentration as measured by AAS and the area of the silicate peak, with R2 values for each of the silicate solutions of 0.99.

The inset diagram in Figure 33 demonstrates that this correlation continues at concentrations up to those of the initial commercial silicate concentrations.

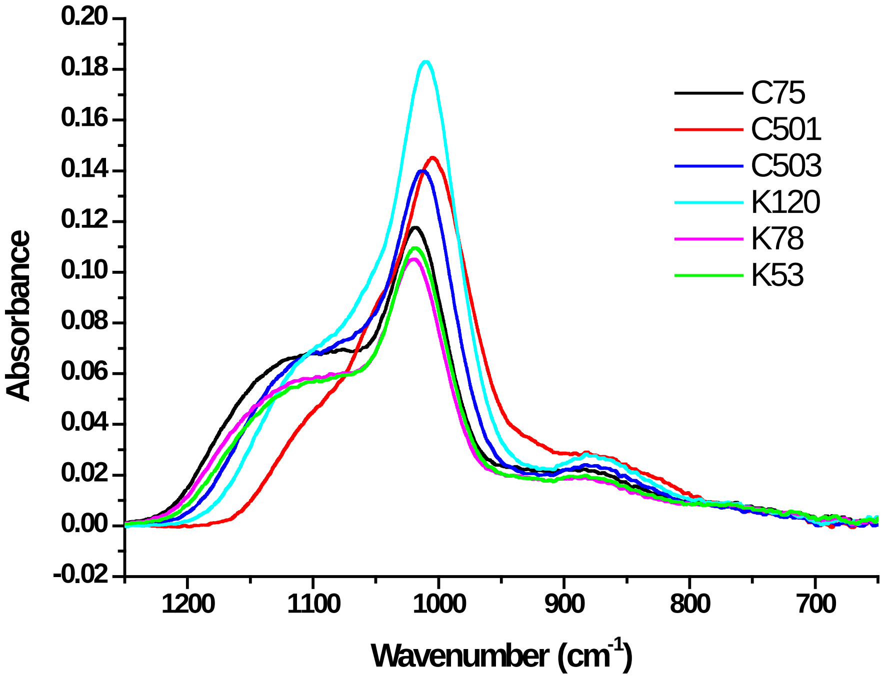

Figure 31. Infrared spectra of various commercial silicate solutions diluted to 32% of the original concentration (Originally in colour)

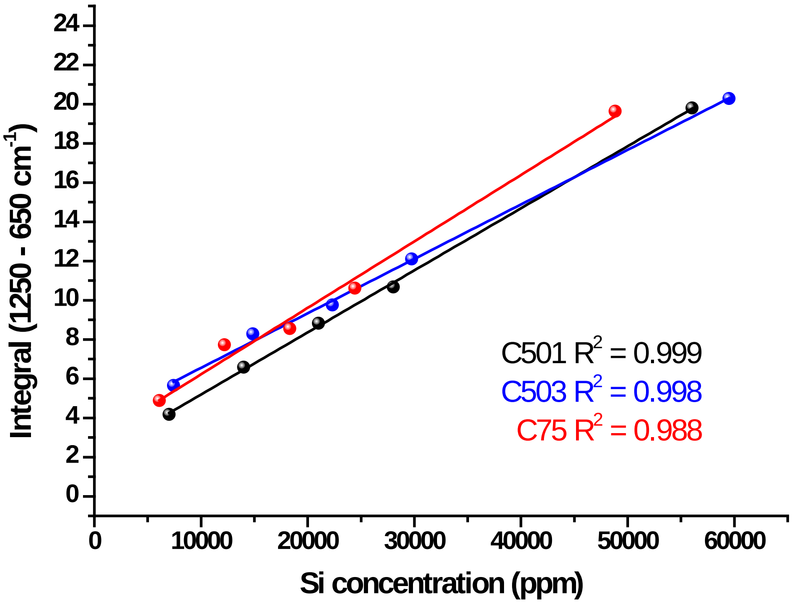

Figure 32. Correlation between the Si concentration of three sodium silicate solutions analysed by AAS and the area of the silicate band in their IR spectra (Originally in colour)

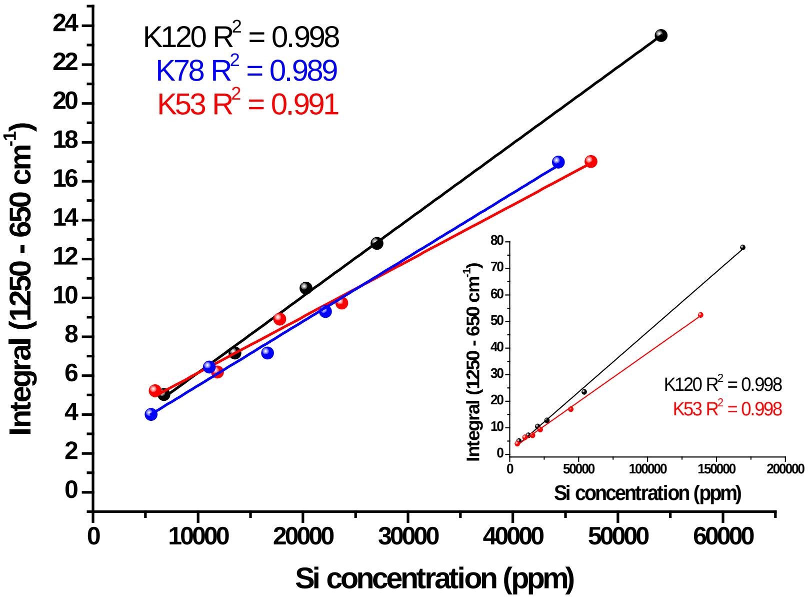

Figure 33. Correlation between the Si concentration of three potassium silicate solutions analysed by AAS and the area of the silicate band in their IR spectra (Originally in colour)

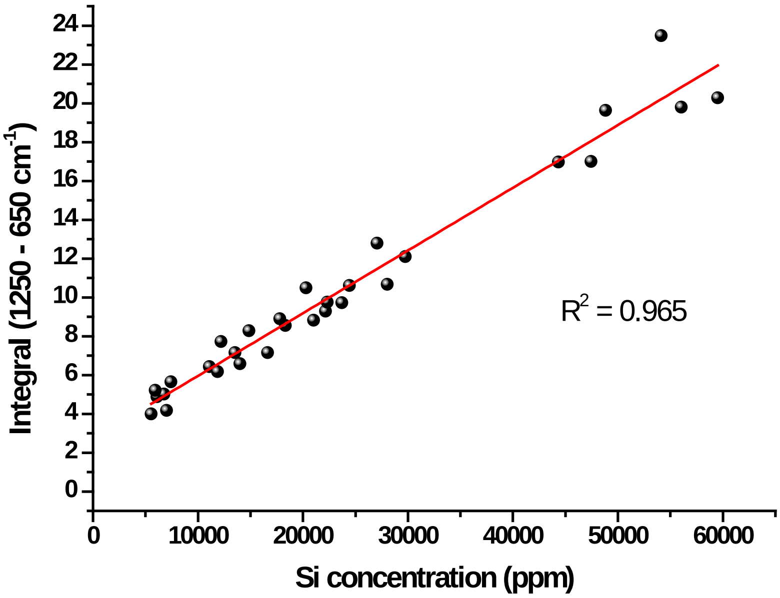

Figure 34. Correlation between the Si concentration of several potassium and sodium silicate solutions analysed by AAS and the area of the silicate band in their IR spectra (Originally in colour)

Table 18. Slope, intercept and R^2 values for the correlation between Si concentration analysed by AAS and silicate IR band area for different silicate solutions

Name (Counter-ion)	**Mean molar ratio (SiO_2: M_2O)**	**Slope (x10^{-4})**	**Intercept**	**R^2**
Crystal 501 (Na)	1.65	3.17	2.02	0.999
Crystal 503 (Na)	2.58	2.78	3.77	0.998
Crystal 75 (Na)	3.3	3.39	2.83	0.998
K120 (K)	2.24	3.93	2.21	0.998
K78 (K)	3.27	2.88	3.24	0.989
K53 (K)	3.89	3.30	2.18	0.991
Combined		3.23	2.72	0.965

When the data points for all of the solutions are combined (Figure 34) a strong linear correlation is still observed, although it is slightly weaker and appears to show greater disparity as the concentrations of the solutions increase. This appears to be due to variations in the slopes of the linear trends for each individual silicate solution (Table 18). K120, in particular, seems to show a greater increase in peak area with increasing concentration than the other solutions. However, there does not appear to be any connection between the changing linear relationship on dilution and the molar ratio of the solution.

This data indicates that using the IR integral is a valid and valuable method for the analysis of the silica concentration of both sodium and potassium silicate solutions of different molar ratios. The method appears to be best utilised for dilutions of solutions of one molar ratio, however, the linear relationship still remains robust when samples with a wide range of solids concentrations and molar ratios are used, particularly at lower concentrations.

Shortly following the development of this method, Falcone *et al.*(2010) published details of a method using the position of the maximum band (~1000 cm^{-1}) and the area of the silicate peak (1250-715 cm^{-1}) to determine the concentration and ratio of a silicate solution. However, these researchers only studied sodium silicate solutions and the correlation between the area of the band and the concentration of the solution was only demonstrated for a solution of a single molar ratio. This study, therefore, expands on this work and establishes the validity of this method for a wider range of solutions. Consequently, this method was utilised and tested further for the analysis of silicate solutions formed from the extraction of biomass ashes.

5.4. Biosilicate solution

5.4.1. Effect of alkali concentration

The extraction of Ely-BA1 was initially tested, since the data had indicated that silica was more easily solubilised from miscanthus ash during the lab-scale tests and from the miscanthus bottom ash by water extraction. The effect of several concentrations of potassium hydroxide solution were tested on ash ground to <125 μm, under reflux for 24 h (Table 19 and Figure 35). This highlights that the majority of the silica present in the ash can be extracted under these conditions, forming solutions of varying molar ratios and with the solids content slightly lower or similar to those of commercial silicate solutions. The data from both the Si AAS analysis and IR integral analysis of the solution indicates the same extraction trend with increasing alkali concentration, although there is a discrepancy between the two methods of analysis for the 3 M concentration solution. Overall, this implies a KOH concentration of 7.5 M or above is necessary to reach the maximum silica extraction of 80%. Studies of the formation of geopolymers from aluminosilicate mineral wastes have shown that the dissolution of Si and Al increases exponentially with increasing pH (Phair and Van Deventer, 2002).

Table 19. Results of silica extraction from Ely-BA1 using KOH solutions of different concentrations (based on AAS analysis)

[KOH] (M)	[Si] (ppm)	Si extraction (%)	Density (g/cm^3)	SiO_2 (wt%)	K_2O (wt%)	Weight ratio (SiO_2:K_2O)	Solids content (%)
1	24771	42.1	1.09	4.8	4.3	1.13	9.14
3	48572	82.5	1.22	8.5	11.6	0.74	20.0
5	43112	73.5	1.27	7.2	18.5	0.39	25.7
7.5	48095	81.7	1.37	7.5	25.7	0.29	33.1
10	47631	80.9	1.46	7.0	32.3	0.22	39.3

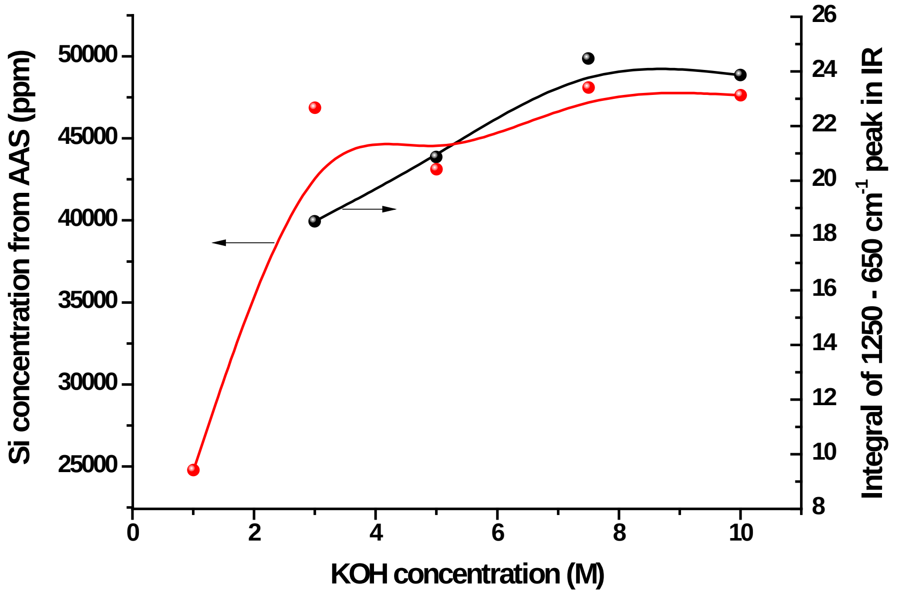

Figure 35. Comparison of Si concentration analysed by AAS and using the IR integral for Ely-BA1 extraction solutions formed with different KOH solution concentrations (Originally in colour)

Variations in the silicate solutions formed with different KOH concentrations can be observed by studying the IR spectra (Figure 36). These display a reduction in the high frequency shoulder, shift of the frequency of the main silicate peak to lower wavenumbers and development of peaks at lower frequencies with an increase in the KOH solution concentration and a reduction in the SiO_2:K_2O molar ratio. These changes were also observed by Bass and Turner (1997) for commercial sodium silicate solutions on going from SiO_2:Na_2O ratios of 3.3 to 0.2 and by Halasz *et al.* (2007a) on the dilution of aqueous solutions of crystalline Na_2SiO_3.

The connection of IR peaks to specific silicate species or sites is still contentious; however, some conclusions can be drawn, with the starting point for most analyses of silicate solutions by FTIR being a comparison with solid silica glasses and gels, for which a much greater body of research exists. In solid silica three main bands are observed centred around 1070 (with a high frequency shoulder at 1200 cm^{-1}), 810 and 457 cm^{-1} (Kirk, 1988) The latter is assigned to rocking or bending of the bridging O-atom (Greiner- Wronowa *et al.,* 1999; Perry *et al.,* 1991) whilst the peak at 810 cm^{-1} is characterised as symmetrical stretching or bending of the Si-O-Si bond (Kirk, 1988; Greiner- Wronowa *et al.,* 1999; Perry *et al.,* 1991; Martinez *et al.,*1998).The most intense mode, centred at 1076 cm^{-1}, is correlated to the asymmetrical stretching of the Si-O-Si bond (Galeener, 1979), with its high frequency shoulder potentially due to coupling of vibrational modes in the silica skeleton or when the stretching is 180° out of phase (Kirk, 1988). A band is also sometimes observed around 960 cm^{-1}, which is frequently assigned to silanol (Si-OH) or Si-O$^-$ stretching on the surface of the amorphous silica (Perry *et al.,* 1991; Martinez *et al.,*1998), or to the localised vibrations of cations against the silica framework in sodium and potassium silicate glasses (Gervais *et al.,* 1987). This peak is observed to decrease on annealing of silica at high temperatures and to shift to lower frequency where the counter-ion is K$^+$ as opposed to Na$^+$(Martinez *et al.,*1998; Gervais *et al.,* 1987).In addition, when silica is heated to higher temperatures the most intense band shifts to higher frequency (~1120cm^{-1}) and the shoulder increases in relative intensity, suggested to be due to bond shortening and a reduction in the mean bond angle as densification of the silica structure occurs (Perry *et al.,* 1991).

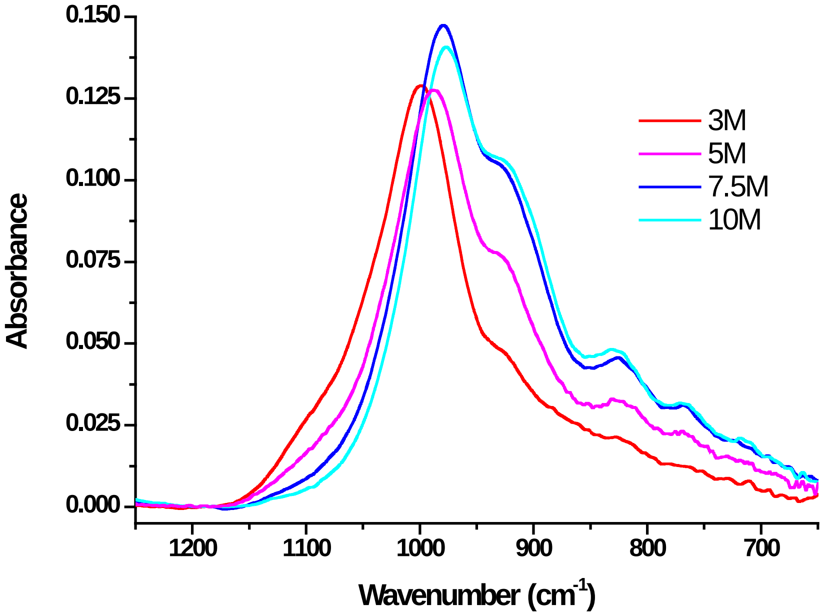

Figure 36. IR spectra of silicate solutions formed by the extraction of Ely-BA1 using different KOH concentrations (Originally in colour)

In contrast to solid silica, the main peak present in the silicate solutions is found at lower wavenumbers, 1010 – 977 cm^{-1}, with several peaks present at even lower wavenumbers. Different authors have associated these peaks with different species (Table 20). Bass and Turner (1997) attributed the position and presence of different peaks in the IR spectra of silicate solutions to different Q^n species (Bass *et al.,*1999) In contrast, Halasz *et al.* (2007a; 2010) connected them to a change in the degree of dissociation dependent on both the concentration and ratio of the silicate solution, whilst Osswald and Fehr (2006) identified changes due to the alteration in the ratio of surface silanol groups to internal siloxane groups as particle sizes decreased. Water solvation was also found to be important for better fitting of calculated IR spectra to the experimental data (Halasz and Derecskei-Kovacs, 2008).

Table 20. Absorption band frequencies and identification in the ATR-IR spectra of Ely-BA1 silicate solutions

	Concentration of KOH extraction solution (M)				**Assignment**		
	3	**5**	**7.5**	**10**	**Bass and Turner (1997)**	**Osswald and Fehr (2006)**	**Halasz *et al.* (2007a; 2010)**
Band positions observed (cm^{-1})				714			δ_{as} (H)O-Si$^-$O(Na)
		768	769	764			δ_{as} (H)O-Si-O(H)
	824	825	826	828			υ_s (Na)O-Si$^-$O(Na)
					SiO$^-$ small anions	δ Si-OH	δ_{as} $^-$O-Si-O$^-$
	923	926	924	921	Monomer and dimer	υ Si-OH	υ_s (H)O-Si-O(Na)
	999	989	979	977	Linear Q1 and monomer	υ_{as} Si-O-Si (surface)	υ_{as} (X)O-Si-O(X) where X = Na, H in $Na_2H_2SiO_4$
	1097	1096			Q^3 and Q^2 species	υ_{as} Si-O-Si (internal)	

Overall, the literature data indicates that the shoulder at 1080-1097 cm^{-1}, only observed in the solutions using the lower concentration KOH extraction solution, is due to asymmetric Si-O-Si stretching (υ_{as}). Most data indicates that silicate anions adopt formations that are as condensed as possible such as cyclic- and cage-like- species (Bass and Turner, 1997; Gomes *et al.,* 2008) The reduction in this absorption band with decreasing SiO_2:M_2O ratio suggests a reduction in Si-O-Si bridging bonds and a shift to smaller anionic species. The absence of absorption bands at higher wavenumbers in this study (~1200 cm^{-1}) indicates a lack of colloidal silica (Q^4) (Falcone *et al.,* 2010).

The main band shifts to lower wavenumber, from 999 – 977 cm^{-1}, with increasing alkali content. Overall, all three authors correlate this absorption band to surface υ_{as} (Y)O-Si-O(X) where Y = Si or H, and X = - charge or H with the absorption band shifting as the attached functional groups vary (Osswalk and Fehr, 2006). Bass and Turner (1997) suggested that the position of the IR absorption band could be correlated to individual Q^n species. However, more recently Falcone *et al.* (2010) have suggested that assignment of absorption bands to specific species is not supported and instead, that the large variation in the shift in the absorption band around 980 cm^{-1} may be due to changes in hydrogen bonding affecting $Si-O^-$ stretching. These suppositions are supported by computational studies of the changing molecular structure of silicate species (Gomes *et al.,* 2008; Gibbs *et al.,* 1998) With a decreasing SiO_2:M_2O ratio NMR studies show the main species formed to be Q^0 monomer as an increasing number of repulsive anions are formed (Bass and turner, 1997). Where a silicon atom is bonded to a charged oxygen atom, computational studies indicate that the SiO^- bond is shortened, whilst silanol and siloxane bonds on the same atom are lengthened. The longest bond in the latter is the one attaching the bridging oxygen to the $Si-O^-$ species and therefore makes it more susceptible to hydrolysis. Bond strength is negatively correlated to bond length and therefore if the bond length increases, a shift in the IR spectra to lower wavenumbers would be expected (Brown and Shannon, 1973). The studies by Halasz *et al.*(2007a; 2010) on sodium silicate solutions indicated that the shift to lower wavenumbers for the main absorption band may also be associated to the increased surface adsorption or ion pairing of sodium metal cations at anionic sites at higher solution concentrations and higher alkali ratios as dissociation decreases (Halasz *et al*., 2007a; Halasz *et al.,*2010; Osswald and Fehr, 2006) Electrical conductivity measurements and sodium selective electrode measurements showed a decreasing proportion of free Na^+ in solution at higher concentrations and a decreasing number of totally dissociated anions with higher Na/Si ratios (Halasz *et al*., 2007a; Halasz *et al.,*2010) This could decrease the frequency of absorption by decreasing the force constant. Silicate anion pairing with alkali metal cations has been identified by NMR and computational methods indicate that ion-pairing is energetically favourable for monomeric, dimeric and higher anionic species (McCormick *et al*., 1989; Mora-Fonz *et al*., 2007). ^{29}Si NMR measurements indicate that ion pairing is favoured by a rising OH^-:Si ratio (Kinrade and Pole, 1992). Upon the addition of base, the level of negative charges on silicate anions will increase either by deprotonation or depolymerisation, such as:

$(Si_nO_xH_y)^- + OH^- \rightarrow (Si_nO_xH_{y-1})^{2-} + H_2O$

Or $(Si_{2n}O_{2x}H_{2y})^- + OH^- \rightarrow (Si_nO_xH_y)^- + (Si_nO_{x+1}H_{y+1})^-$

This will eventually reach a maximum when all of the anions are depolymerised to monomer anions. At this point, the addition of further base results in the increasing formation of anion-cation pairs (McCormick *et al.,*1989; Rees *et al.*,2007). This can stabilise silicate anions, reducing the likelihood of condensation reactions but can also reduce electrostatic repulsions thereby mediating silicate condensation (Kinrade and Pole, 1992). Whichever is the dominating factor will depend on the strength of the cation-anion interaction, with evidence suggesting that this depends on the cation in the order $Li^+>Na^+>K^+>Rb^+>Cs^+$ from ^{29}Si NMR (Kinrade and Pole, 1992), or in the order $Li^+<Na^+<Cs^+<Rb^+<K^+$ based on the preferential formation of $M^+–^-O$-Si pairs from NMR of the alkali metal (Sanchez and McCormick, 1991). The latter assignments were supported by theoretical calculations of the energy change associated with the replacement of a water molecule with a silicate anion within the hydration sphere of the alkali metal cation. Moreover, at high solids concentrations and low SiO_2:K_2O ratios, where insufficient water may be present for hydration of the alkali cation, the replacement of a water molecule of solvation by Si-O^- may be even more favourable (Provis *et al*., 2005). All of this data, along with observations for the shift of IR frequencies due to the alkali metal cation in silicate glasses (Gervais *et al.,* 1987), suggest that the assignments by Halasz *et al.* may most accurately correlate with the results observed in this study (Halasz *et al.,*2007a;Halasz *et al.,*2010). That is, that the shift of the main absorption band at 1010 – 977 cm^{-1} is due to υ_{as} (Y)O-Si-O(X) where Y = Si or H and X = $^-$, H or K^+ and is dependent on the degree of anion-cation pairing in solution. The increasing relative intensity of the 970–1010 cm^{-1} absorption band can overall be associated with the increasing concentration of surface species with respect to siloxane bonds and therefore the formation of more Q^0, Q^1 and Q^2 species with increasing alkali concentration as observed by NMR.

Bands at 934 cm^{-1} have been linked to υ_s of (Na)O-Si-OH species and those at 830 cm^{-1} with υ_s of (Na)O-Si-O(Na) (Halasz *et al.,* 2010). These would be expected to be observed at a lower frequency in the presence of a heavier potassium cation, which is indeed the case, and so further supports these assignments. The absorption band at 776 cm^{-1} has been ascribed to the HO-Si-OH bending vibration (δ_{as}) (Halasz and Derecskei- Kovacs, 2008). The decrease in all of these absorption bands with decreasing concentration and increasing SiO_2:K_2O molar ratio supports the theory of the formation of more dissociated and condensed species.

5.4.2. Reproducibility

Using the data from the study above, the required ratio of Ely-BA1 and KOH was calculated for the formation of a solution with an equivalent ratio to the commercial K120 solution. K120 was chosen as the solution to simulate as initial testing had shown that this was a promising silicate binder for board formation. The extraction calculation was based on an assumption that 80% of the silica present in the bottom ash could be solubilised. The maximum total solids content of the solution formed was lower than that of the K120 solution due to the difficulty of efficient stirring of the solution at higher solid:liquid ratios. It was noticed that the ash was hydrated during the reaction with a large amount of solid black sludge formed as the reaction progressed. The results of the extraction are shown in Table 21.

The results demonstrate quite a varied degree of reproducibility based on Si AAS analysis of the solutions formed (65.9 ± 7.3%). The much lower Si concentration for experiement 17 and the generally low extractions compared to those described earlier are probably caused by poor stirring, specifically due to the higher initial solid:liquid ratio used. Overall, analysis using the IR integral and the linear correlation equation found for the commercial solutions discussed earlier, reasonably accurately determines the silica concentration. The concentrations are always slightly lower than those found by Si AAS, for experiment 9 and 15 significantly so. However, this may imply a greater degree of error in the dilutions of the highly concentrated solutions during AAS analysis than within the IR data.

The densities, weight ratios and solid contents are similar for all of the solutions. They are lower in all cases than the commercial K120 solution, due to the low solid:liquid ratio used and the lower than predicted extraction of silica.

The silica concentrations of the solutions from experiments 18–21 were calculated using the IR method based on the correlation between the Si AAS and IR integrals for experiments 9 – 17 (Figure 37). The linear relationship and fit are similar to that found for the combined commercial silicate solutions (Figure 34), despite the concentrations of the solutions being higher.

Table 21. Analysis of biosilicate solutions from Ely-BA1 ash using constant KOH solution concentrations and ash:liquid ratios with extraction occurring under reflux over 24 h

Expt No.	Si conc AAS (ppm)	Integral	Si conc IR (ppm)	Si extraction (%)	Density (gcm^{-3})	SiO_2 (wt%)	K_2O (wt%)	Wt ratio (SiO_2: K_2O)	Solids content (%)
9	131630	40.9	115107	74.5					
12	114124	37.3	104335	64.6	1.35	18.0	18.6	1.0	36.6
13	107583	36.0	100346	60.9	1.34	17.2	18.8	0.9	36.1
14	117747	39.4	110436	66.7	1.35	18.7	18.6	1.0	37.3
15	124978	41.1	115694	70.8	1.36	19.6	18.4	1.1	38.1
17	95150	33.4	92614	53.9	1.32	15.4	19.1	0.8	34.5
18		43.1	135701	76.8	1.38	21.0	18.2	1.2	39.2
20		36.6	109247	61.8	1.35	17.4	18.7	0.9	36.0
21		36.8	110044	62.3	1.35	17.4	18.6	0.9	36.1

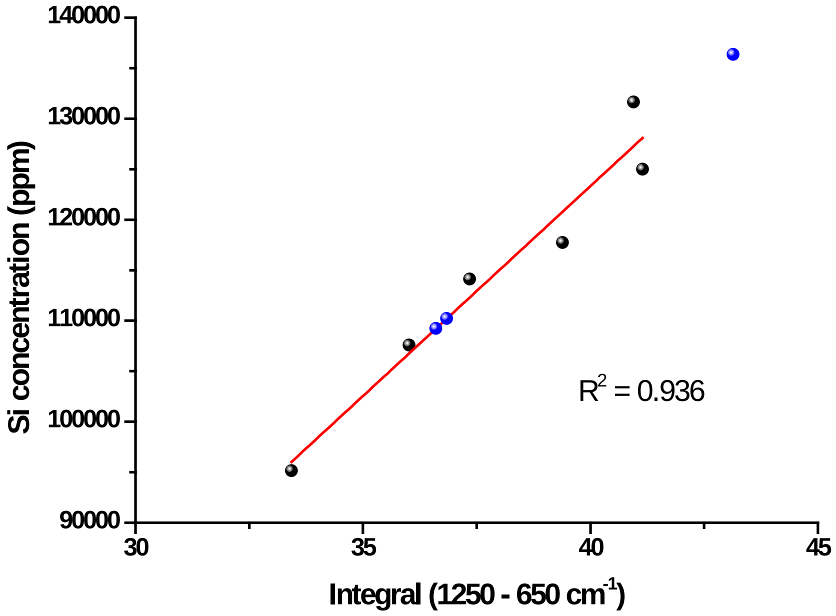

Figure 37. Correlation between the IR integral and Si AAS analysis for several silicate solutions formed from the extraction of Ely-BA1. The points in blue indicate solutions calculated from the linear fitting. (Originally in colour)

Two of the solutions formed from Ely-BA1 were analysed by ICP-AES to study their elemental content, the results of which are shown in Table 22. The elemental composition of the solutions is highly reproducible. The data illustrates the predominance of potassium and silicon. The levels of silicon detected are lower than those found by AAS, however, previous measurements indicated that ICP-AES was not as accurate for analysing the amount of silicon and potassium present at very high concentrations. The other elements present are the same as those observed in the water extracted solutions (see earlier), but are generally found at a slightly higher concentration.

Table 22. Elemental analysis of two potassium silicate solutions formed from Ely-BA1

	BA1-12		**BA1-13**	
Element	**Concentration (ppm)**	**Percentage (wt%)**	**Concentration (ppm)**	**Percentage (wt%)**
Al	198	0.09	179	0.08
As	1.2	0.00	Nd	
B	15.0	0.01	14.0	0.01
Ba	16.0	0.01	1.2	0.00
Bi	Nd		0.5	0.00
Ca	14.0	0.01	27.0	0.01
Co	Nd		0.3	0.00
Cr	0.1	0.00	0.2	0.00
Cu	Nd		1.0	0.00
Fe	4.0	0.00	5.0	0.00
K	140440	62.0	133780	62.4
La	0.1	0.00	0.1	0.00
Mg	13.0	0.01	14.0	0.01
Mn	2.0	0.00	2.0	0.00
Mo	5.0	0.00	5.0	0.00
Na	725	0.32	710	0.33
P	5005	2.21	4651	2.17
Pb	1.1	0.00	1.3	0.00
Pd	2.0	0.00	1.9	0.00
Rb	54.8	0.02	51.8	0.02
S	1578	0.70	1463	0.68
Si	78471	34.6	73262	34.2
Sn	0.3	0.00	Nd	
Sr	0.4	0.00	0.3	0.00
Ti	0.7	0.00	0.7	0.00
Tl	4.2	0.00	0.6	0.00
V	4.9	0.00	4.6	0.00
W	89.5	0.04	85.1	0.04
Zn	Nd		2.0	0.00
Zr	1.4	0.00	1.2	0.00
Sum	226646		214265	

Sulphur and phosphorous both display a higher level of dissolution than by water extraction and both were also major components in the initial ash. This could indicate that they were either trapped in silica melts or forms that were more easily dissolved under the highly alkaline and hot conditions used for the extraction of silica. The low levels of magnesium and calcium suggests that any that has dissolved has co-precipitated some silica from solution, which may account for the incomplete dissolution of the silica present in the ash. Alumina is soluble in alkaline solutions which accounts for its increased concentration in comparison to the water extraction of Ely-BA1. Aluminium is known to flocculate colloidal silica, although this is unlikely to occur for the highly concentrated and charged silicate anions in the solution formed, although aluminosilicate species might form (Iler, 1979). Very minor quantities of other elements are present, however these should not pose challenges for the utilisation of the silicate solution for a variety of applications.

5.4.3. Effect of time

A kinetic study on the extraction of Ely-BA1 ash was carried out using the same experimental conditions as for experiments 9–21, to ensure that equilibrium was reached over the reaction period and to obtain a greater understanding of the extraction process (Figure 38a). The experimental work was carried out by an undergraduate student, Anna Schaub, in collaboration with and under the supervision of Ms Jennie Dodson. Due to the high temperature of extraction, large inaccuracies occurred if samples were taken from the reaction vessel and directly analysed by IR. Therefore, each measurement corresponds to a separate sample, rapidly cooled before analysis.

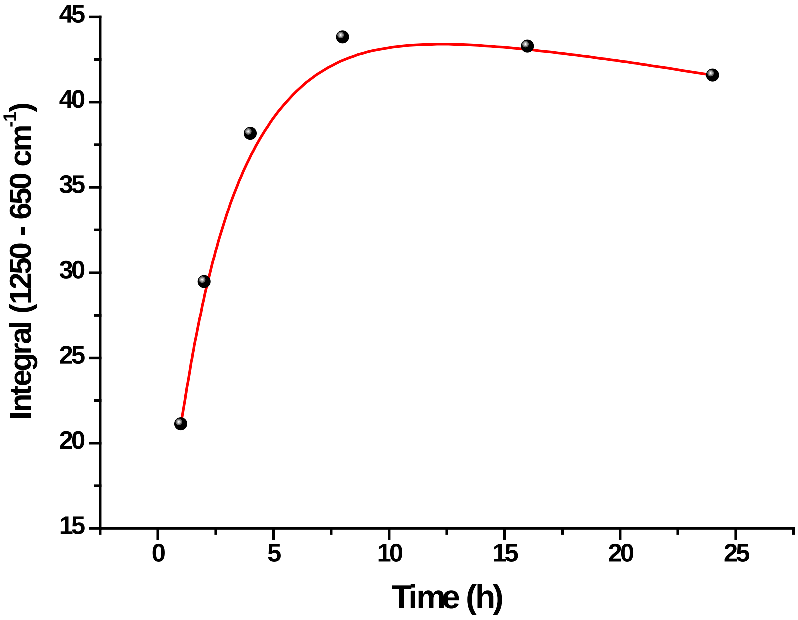

Figure 38a. Area of silicate absorption band vs time during the extraction of Ely-BA1 ash (Originally in colour)

This data shows a rapid rise in silica dissolution over the first few hours, with a maximum extraction after 8 h. Following this there is a slight decrease in the area of the silicate absorption band, from the IR analysis, with increasing time. This could be due to variations in the extraction between different samples or some concentration of the solution before analysis, however, it could also indicate a re-precipitation or polymerisation of silica out of the solution beyond this point. Consequently, there could be an optimum extraction time.

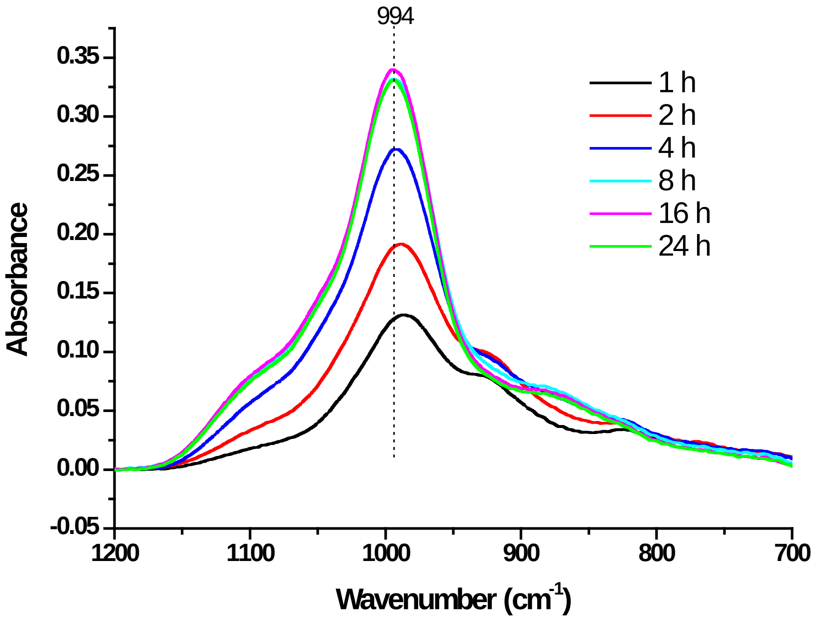

Figure 38b. IR spectra of silicate solutions formed during the extraction of Ely-BA1 for different lengths of time (Originally in colour)

The changes occurring in the silicate IR band during extraction are shown in Figure 38b. This clearly highlights differences in the silicate bands and silicate species present as dissolution progresses. These appear to be similar to those observed on extraction of Ely-BA1 with different concentrations of KOH. At the lowest SiO_2:K_2O ratio (1 h) the main bands in the IR spectra are found at 986, 927 and 822 cm^{-1}, similar to those detected using a 5, 7.5 or 10 M KOH solution described earlier. As the extraction progresses, and the SiO_2:K_2O ratio increases, the overall silicate band increases in intensity, a high frequency shoulder at 1100 cm^{-1} develops, the main absorption band shifts to higher wavenumber (994 cm^{-1}, 24 h), the bands at 927 and 822 cm^{-1} reduce in intensity, whilst a new band at 880 cm^{-1} appears. This process appears to be gradual with the spectra of the solution formed after 4 h displaying all of these absorption bands. Overall, according to the IR assignments described earlier, initially monomeric anions with a low dissociation of the K^+ counter-ion are extracted into solution. As the extraction progresses, increasing dissociation of the anion occurs as the ratio of SiO_2:K_2O increases, eventually leading to the formation of larger anionic species evidenced by the shoulder around 1100 cm^{-1}.

5.4.4. Using fly ash solution for extraction

The experiments above show that a concentrated potassium silicate solution can be controllably formed from biomass bottom ashes. However, a highly concentrated hydroxide solution was required. The overall aim of this study was utilise the inherent alkalinity of the combustion residues. Earlier tests had shown that, following combustion in a large-scale system, this mainly resided in the fly ashes. Therefore a test was undertaken to observe whether a sufficiently concentrated alkaline solution could be formed from the fly ashes to extract silica from the bottom ashes and form a potassium silicate solution, similar to those achieved using synthetic potassium hydroxide. Ely-FA1 was leached with water at a liquid:solid ratio of 5:1. The filtered solution was reduced to a volume 1/16th of the original, at which point salt was beginning to crystallise out of solution. The alkalinity of this solution was tested by titrating against a 0.1M HCl solution. This gave a solution concentration of 1.4 M. Based on the analysis of the concentration of the alkaline solution, the amount of bottom ash required to produce an approximately 1.2 weight ratio potassium silicate solution was calculated. The resultant mixture extracted under reflux.

The IR spectra of the solution formed are shown in Figure 39. This is different in shape to the silicate solutions formed using potassium hydroxide solutions of higher concentrations, however, a solution formed using a 1M KOH solution and the same liquid:solid ratio, displays a similar IR spectra, both of which more closely resemble the higher molar ratio commercial silicate solutions. The developed high frequency shoulder around 1105 cm^{-1} is usually attributed to υ_{as} Si-O-Si and indicative of the presence of more highly polymerised silicate species and high SiO_2:M_2O ratio solutions (Bass and Turner, 1997; Falcone *et al.,* 2010) However, based on the IR absorption band areas, silica extraction from the bottom ash using the fly ash solution only reached 27%, producing a solution with a lower ratio than the majority of the Ely-BA1 solutions.

This demonstrates, in principle, that it is possible to form a sufficiently alkaline solution using the collected fly ashes to extract a proportion of the silica from the bottom ashes. Unfortunately, it was not possible to form a solution of higher alkalinity due to the precipitation of salts from the fly ash solution on concentrating it. Further analysis of the salts precipitating might, however, provide information about further possible uses of the fly ashes.

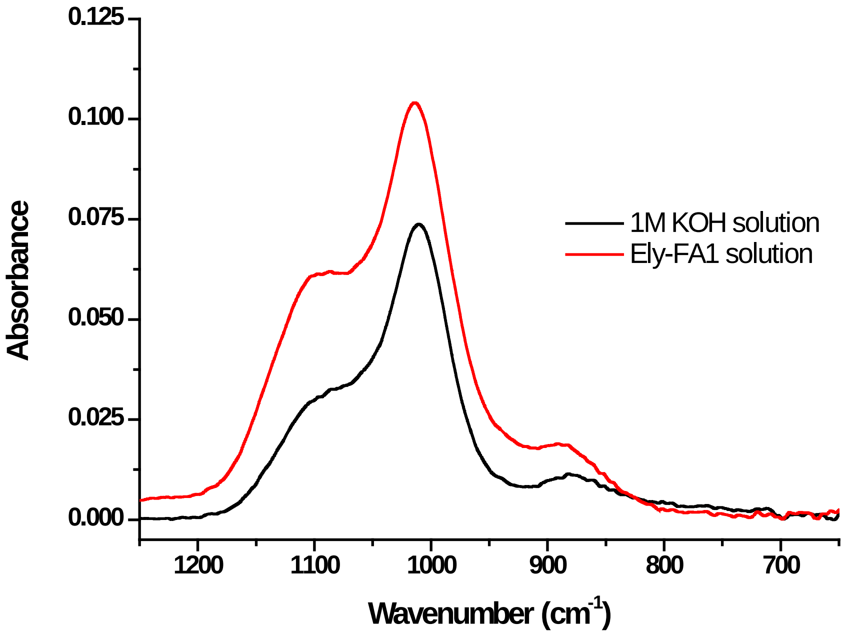

Figure 39. IR spectra of silicate solutions formed during the extraction of Ely-BA1 using a 1M KOH solution and a concentrated solution from the extraction of Ely-FA1 (Originally in colour)

5.5. Preliminary Board formation

5.5.1. Biosilicate

The silicate solutions formed above had lower silica content than commercial K120. Therefore, in order to compare the results using both the bottom ash and commercial silicate solutions, the biosilicate solutions were concentrated further. Two solutions were formed; one with a SiO_2 concentration similar to K120 and the other with a higher concentration, to observe if this improved the binder efficacy. Comparisons of the solutions are shown in Table 23. The differences in the weight ratios between K120 and the biosilicate solutions are due to a lower than expected extraction of SiO_2 from the Ely-BA1 ash, resulting in a higher total solids content for the same SiO_2 wt% for Biosilicate 1 compared to K120, and therefore a higher density.

Table 23. Characterisation of silicate solutions used for binder tests

Name	Silicate absorption band area (IR)	SiO_2 (wt%)	K_2O (wt%)	Solids content (wt%)	SiO_2:M_2O wt ratio	Density (gcm^{-3})
K120	77.9	31.8	21.6	53.4	1.47	1.52
Biosilicate 1	75.8	29.4	31.4	60.7	0.94	1.64
Biosilicate 2	103.8	36.7	39.2	75.9	0.94	1.85

The effect of these variations on the silicate anion speciation can be observed from the IR spectra of all three solutions (Figure 40). Although the area of the silicate absorption band is almost identical for K120 and Biosilicate 1, representing the slight difference in silica content, the K120 solution has a more developed high frequency shoulder and absorption band at 880 cm^{-1} with the main absorption band shifted to a slightly higher wavenumber. This follows the trend observed for increased SiO_2:K_2O ratio solutions, as larger or more dissociated anions form. Biosilicate 2 generally has a similar shape, but with greater intensity, than that of Biosilicate 1. However, the main absorption band is shifted to even lower frequency (963 cm^{-1}), with the band at 884 cm^{-1} increasing in relative intensity. A similar effect was observed by Halasz *et al.* (2007a) as a monomeric solution was concentrated.

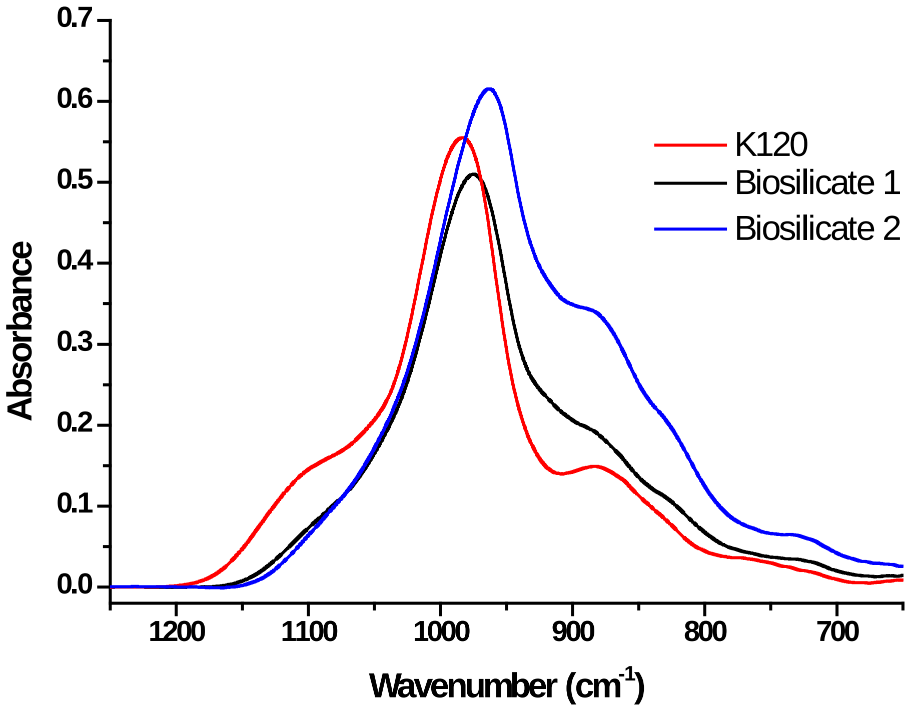

Figure 40. IR spectra of K120 and Ely-BA1 biosilicate solutions used as binders for board formation testing (Originally in colour)

5.6. Conclusions and Further Work

This work has shown that different biomass materials, specifically miscanthus and wood chips, show varying elemental solubility trends with combustion temperature dependent on their initial inorganic composition. The low solubility of silica from wood chip ashes could be attributed to the formation of insoluble calcium silicate. The trends for miscanthus were comparable to wheat straw, highlighting their similarities as herbaceous grasses, with significant levels of silica extracted by the inherent alkali content but reducing at combustion temperatures above 500 °C.

The fly ashes and bottom ashes obtained from the large-scale combustion of miscanthus straw and wood chips displayed greater similarities with comparable partitioning of elements between the two ash deposits. Greater potassium, chlorine and sulphur levels were found in the fly ash, mainly as sylvite, whilst chiefly crystalline silica remained in the bottom ashes.

The extraction of silica from the miscanthus straw-based bottom ashes was achieved utilising a highly alkaline potassium hydroxide solution. The extraction could be controlled to produce a solution of similar concentration and ratio to the commercially available silicate solutions. Initial tests also suggested that a concentrated alkaline solution could be formed from the fly ash. This could dissolve some of the silica within the bottom ash, however, it was not sufficiently alkaline to dissolve the majority.

The solutions produced using potassium hydroxide extractants were tested as binders for the formation of inorganic composite boards with a wheat straw substrate. The results for both the internal bond strengths were promising, however, further work is necessary to study the production of solutions with varying concentrations and weight ratios and to improve the water swelling of the boards. In addition, it would be interesting to study the use of CO_2 as a hardener to set the binder, which could be obtained from the combustion facility in an integrated system. Furthermore, this work suggests that using a substrate with a higher silica content, such as rice hulls, rice straw or sugarcane, could potentially enable the production of boards directly using the *in situ* silica content within the biomass as part of the binder.

A new IR method for the analysis of the silica concentration in the solutions was developed enabling the fast, rapid and accurate assessment of the concentration of the solution formed. However, the data obtained indicated that the relationship between the peak area and silica concentration varied with the silicate solution molar ratio. Further exploration of this relationship and the association of spectral peaks with silicate solution structures are needed to extend the applicability of IR spectroscopy in the study of silicate solutions.

6. BINDER FORMULATION AND BOARD MAKING TRIALS

In using silicates as the binder system, the presence of a suitable hardener in the formulation was imperative. In a first approach, the direct addition of acids e.g. acetic acid was tried. This led, however, to very fragile boards which most likely related to the very fast hardening of the silicate under the direct influence of the present acid. In view of PQ’s experience with silicates, the effectiveness of one of their commercial hardeners (R100) was evaluated. R100 is a mixture of diesters, the exact composition of which cannot be disclosed. The hardening power of such a mix of diesters relates to a gradual hydrolysis of the ester functions to carboxylic acids. More specifically, upon hydrolysis of the different diesters a gradual decrease of the pH is achieved therewith, assuring a controlled hardening of the silicate. Quite surprisingly, this approach led equally to fairly weak boards (see later). In a parallel route, the use of proteins was investigated. Similarly to the ester groups in the R100 mixture, proteins contain amide (peptide) bonds which can also hydrolyze.

6.1. Biomass

Soft wheat straw varieties *e.g.* Viscount were found more performing than hard wheat straw varieties *e.g.* Humber. Initial experiments used the hammer milled wheat straw as produced. However, after initial boards had been produced for the R100 hardener study, it was decided that the wheat straw should be sieved to remove fine particles and reduce issues of resin clumps, or resin being wasted adhering small non-structural particles into the panel. An industrial sieve shaker was used with a 4 mm screen above and 0.25 mm screen below. Only the middle fraction was used. Experiments were conducted on air separation, to remove dense particles such as nodes and rachis, and leave the stem and leaf pieces for manufacture. This was successful on the laboratory scale, however, the throughput of the machine was not sufficient to produce material for 300 x 300 mm panels.

The generalised procedure for making 5 x 5 cm boards in the laboratory (York) is represented photographically in Figure 41. The straw was mixed in a bowl with a common hand mixer. In the first step, one half of the protein solution was dropped onto the straw with a pipette. Secondly, the silica solution was added and finally, the other half of the protein solution was intermixed. The boards ware pressed at 120 °C. Non adhesive paper was used to prevent the biomass sticking to the surface. After a 1 min pre-press within a rectangular aluminium form, which gives the board the approximate dimensions, the boards were pressed for 8 minutes. Spring-back is prevented by putting a weight on top of the freshly pressed board for approximately 1 h. Pieces of 5 cm x 5 cm were cut from the original board to test the internal bond strength at the laboratory of the project partners at Bangor University. The samples were conditioned for one week at 20 °C and a relative humidity of 65 % and tested in a pulling test at 1.2 mm per min.

The amount of straw and silicate solution used for the particleboards was calculated depending on the water content of the straw and the concentration of the solution to keep the actual mass of solids constant. For the given density of 0.68 g cm^{-3} and a given size of 65.712 cm^3 (7.4 cm x 7.4 cm x 1.2 cm), a total amount of solids of 44.68 g was expected.

Where: m_w = mass of wheat straw solids (water content subtracted) [g]

m_{wa} = actual mass of straw [g]

m_{Si} = mass of silica solids in the solution [g]

m_{Sia} = actual mass of silicate solution [g]

m_P = mass of protein solids, constant 1,8 g

p = water content of the wheat straw [%]

c = concentration of the silica solution [%]

Equation 3 to 6 show the mass balance for a straw-silica-board with a constant silica ratio of 15%.

$$m_w+m_{Si}=44,68\text{ g} \tag{3}$$

$$\frac{m_{Si}}{m_w+m_{Si}}=0,15 \tag{4}$$

$$m_{wa}=\frac{m_w}{(1-\frac{p}{100})} \tag{5}$$

$$m_{Sia}=\frac{m_{Si}}{c} \tag{6}$$

For a board with an additional amount of 1.8 g protein the mass balance is slightly different, starting with equation 7 and then following the same procedure as for a straw-silica-board described above in equation 4 to 6.

$$m_w+m_{Si}+1,8\text{ g}=44,68\text{ g} \tag{7}$$

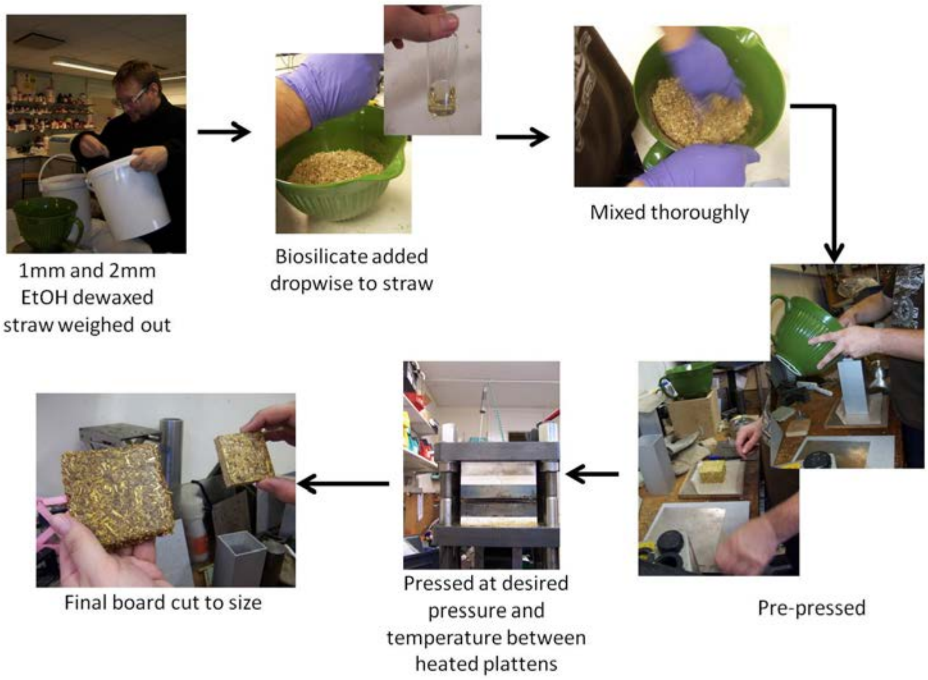

Figure 41. Procedure for formation of test boards using a wheat straw substrate with different binders (Originally in colour)

6.2. Development of binder system (wheat straw)

In a first approach, skimmed milk was chosen as a readily available source of proteins. By using milk powder it was possible to form a more concentrated solution of the protein, to speed up spraying and to reduce the quantity of moisture being introduced to the particle furnish.

Typical bovine milk contains 30 to 35 grams of protein per litre. The αs1-, αs2-, β- and κ-casein proteins are approximately 76-86% of the total protein, with other proteins such as lactoglubulin, which is the most common whey protein. The colloidal nature of the casein proteins is of interest – as κ-casein bears a negative charge, and individual molecules serve to form a micellar structure, similar to surfactant micelles, and such structures are known to influence the deposition process of colloidal silica (Iler, 1979). Typical skimmed milk powder has 49% lactose, 37% protein, 1% lipids, 8% minerals (ash), and 4% moisture; with the mineral content including calcium at 1.2%, magnesium at 0.1% and phosphorous at 0.9%.

Combining raw (waxed) Viscount wheat straw with skimmed milk and K120 silicate, an internal bond strength of about 0.11 MPa was obtained. Given the low internal bond strength obtained using a variety of silicate-hardeners, further improvements were probably better related to the nature of straw-silicate interaction, i.e. incompatibility of the hydrophobic waxes versus the hydrophilic nature of silicate. In a first approach, the latter hypothesis was tested using cold ethanol dewaxed straw, as described earlier. Boards made of a combination of dewaxed straw, skimmed milk and K120 reached maximum internal bond strength of approximately 0.23 MPa. This was about double strength compared to the use of raw (waxed) Viscount wheat straw (0.11 MPa). Note equally, that this result constituted a ten-fold increase in strength compared to the R100/silicate based straw boards made in the early stages of the project.

However, when hot ethanol extracted wheat straw was used, the so-created *'EtOH extracted straw/skimmed milk/K120'* boards reached internal bond strengths of up to 0.34 MPa, constituting an additional increase in strength of over 50% compared to when cold ethanol dewaxed straw was used (0.23 MPa). The densities of the as-synthesised boards typically ranged from 0.7- 0.715 g/cm^3, which was slightly out of the accepted commercial range for particleboards but possibly acceptable for MDF board applications.

6.2.1. Boards made using only ethanol Soxhlet dewaxed straw and biosilicate derived from Ely bottom ash, i.e., K120 mimic

Initially 5 x 5 cm boards were formed in order to test the effectiveness of the biosilicate solutions from Ely bottom ash (as described earlier) in comparison to commercial K120 solution. Visual observations during the board making process identified slightly more spring-back during pre-pressing, along with a darker colouration of the surface of the board following pressing when using the biosilicate solutions compared to K120.

With whey as protein source

Whey powder was tested as a means of increasing the protein present, while reducing the quantity of calcium ions, lactose, other sugars, fats, phospholipids and other components of milk. The whey is the water-soluble protein fraction, left behind when the casein is coagulated into curds during cheese making or similar activities. The main protein is therefore β-lactoglobulin (approx. 65%), and others include α-lactalbumin (approx. 25%) and serum albumin (approx. 8%).

Whey does still contain minerals (in particular calcium and phosphorous), and a significant portion of lactose, however the majority of lipids have been removed from the whey by preferential coagulation with the casein. There is small quantity of lactic acid within the whey solution, and the pH of all whey solutions is below seven, and significantly lower if a lactic acid bacterial culture was used for the whey production process (rather than a neutral or cheese whey process).

During concentration, drying and recovery, the lactose, minerals and fat may be removed. However, the divalent cations such as Ca^{2+} and Mg^{2+} are bound to the negatively charged whey proteins and only partially removed. The whey protein used in this study was purchased from a health food store, marketed as a protein supplement for bodybuilders. Typical whey powder has 73% lactose, 13% protein, 1% lipids, 8% minerals (ash), and 3% moisture; with the mineral content including calcium at 0.6%, magnesium at 0.2% and phosphorous at 0.6%. Delactosed whey powder has 49% lactose, 37% protein, 1% lipids, 8% minerals, 4% moisture. The calcium content is 1.2%, magnesium is 0.1% and phosphorous is 0.9%.

The first set of boards formed was sent to Bangor for internal bond strength testing (Table 24). Another set was tested at the University of York by Dr Mario de Bruyn following the acquisition of a larger load cell (Table 25). The boards tested at Bangor were subject to conditioning for a longer period of time (2 weeks) whilst those tested at York were conditioned for only 1 day. The internal swelling tests were not measured using the appropriate standards, as this requires the formation of larger boards. In addition, only general conclusions can be drawn from the data presented as the production of a much larger sample size would be necessary to produce a statistically significant data set.

Table 24: Strawboard composite properties using different silicate binders (tested at Bangor University)

Binder details		Width (mm)	Breadth (mm)	Density (gcm^{-3})	Maximum Load (N)	Internal bond strength (Nmm^{-2})
No protein	**K120**	50.5	50.3	0.660	185.7	0.07
		50.8	50.7	0.636	207.5	0.08
	Biosilicate 1	50.4	50.6	0.646	398.7	0.16
		50.2	50.1	0.698	479.0	0.19
	Biosilicate 2	50.0	50.1	0.647	388.5	0.16
With whey protein	**K120**	50.6	50.2	0.692	517.7	0.20
		50.6	50.8	nd	662.7	0.26
	Biosilicate 1	50.0	49.7	0.688	525.4	0.21
		49.9	50.2	0.693	690.7	0.28
		49.9	49.8	0.707	620.0	0.25
	Biosilicate 2	49.8	49.7	0.696	828.4	0.33

From Table 24, without the addition of protein, the biosilicate solutions both show a substantially higher bonding strength than the K120 solution. This may be due to the higher total-solids content, reducing the amount of water required to be removed to set the silicate bond via dehydration. On addition of protein, all of the binders display a higher bonding strength. The biosilicate solutions still exhibit slightly higher tensile strength, especially where boards of equal density are compared, however, the disparity is reduced in comparison to the case where no protein is added. Biosilicate 2 demonstrates the highest strength. This may not be reproducible; however, it could indicate the benefit of an increased solids content. The additional strength imbued by the presence of whey protein is perhaps not surprising. It consists of soluble proteins including β-lactoglobulin and α-Lactalbumin. Under the action of heat, these proteins can be denatured causing them to coagulate. In addition, albumin is known to coalesce by the adsorption of polysilicic acid, which then polymerises, although this appears to be promoted at acidic to neutral pH (Langenberg *et al.,*2010).

From the initial set of results it appeared that the biosilicate was showing improved strength in comparison to K120. Therefore, additional KOH was added to K120, based on the characterisation of Biosilicate 1, to produce a silicate of similar composition. The silicate absorption band shape of K120, analysed by IR, was altered by the addition of KOH, being almost identical to that of Biosilicate 1.

Table 25. Strawboard composite properties using different silicate binders (tested at the University of York)

Binder	Additives	Density (gcm^{-3})	Internal bond strength (Nmm^{-2})	Thickness swelling (%)
K120	Whey Protein	0.712	0.49	51
K120 + KOH	Whey Protein	0.721	0.36	48
Biosilicate 1	Whey Protein	0.726	0.41	51

The second set of results analysed at the University of York (Table 25) illustrate an almost universal increase in the internal bond strength in comparison to the first set of boards. The probable cause of this is the difference in the conditioning methods. As can be observed by the thickness swelling, all of the boards are still relatively hydrophilic. Therefore, a longer conditioning time in a high humidity chamber may significantly reduce the internal bond strength. In addition, the densities are slightly higher, which may also be due to swelling occurring in the first set of boards upon conditioning. Within the second set, the boards set using K120, display a higher internal bond strength. Indeed, these are the first to meet the required strength for the particleboard standards. The K120 solution with added base and the Biosilicate 1 boards both exhibit lower tensile strengths. It is impossible to say whether these differences are significant and further testing is required to understand the full impacts of the different variables on the board strength. The water swelling for all of the boards are similar, although greater than the required standard. Nevertheless, these boards do demonstrate promise in producing a novel inorganic composite material utilising low concentrations of alkali silicate binder from biomass combustion residues.

With semi-skimmed milk as protein source

The internal bond strength was found to be approximately 0.24 MPa. Compared to the use of K120 as the silicate source, this corresponded to an overall reduction in internal bond strength of 25%. While the use of milk in a board formulation does raise some concern given its nutritional value – not to mention its cost - an incentive existed to find other more acceptable sources of protein. Through liaising with the National Industrial Symbiosis Programme (NISP) the existence of waste milk streams were discovered. Milk producers, Arla, Leeds, during the separation of raw milk into skimmed milk and cream, generate approximately 5 tonne/day of ‘waste milk’ which is approximately 28 wt % solids. In a comparable experiment to the ones described above for skimmed milk, i.e. keeping the total amount of solids in the aqueous waste milk fraction similar to the solids content in skimmed milk, internal bond strengths between 0.32 – 0.33 MPa were attained with densities around 0.7 – 0.71 g/cm^3. In contrast to skimmed milk, the use of waste milk offered the possibility to increase the total protein content in the board formulation without any further, and necessary, increase of the water content in the formulation. This was of utmost importance as tests at Bangor had shown previously that the presence of water in the board formulation could not exceed an overall 30-(35) wt %. Doubling the amount of “waste milk” used in the formulation and keeping the water content constant – compared to when skimmed milk was used – further increased the internal bond strength to 0.38 MPa with density of 0.715 g/cm^3.

6.3. Summary of Testing and upscaling at Bangor*

A first series of 30 x 30 cm boards with density in the region 0.65 g/cm^3 using raw milled Viscount wheat straw as well as raw milled rapeseed straw were manufactured at Bangor. The solids content of silicate binder (K120) was 99 g and of milk solids was 13.57 g on 561 g oven dry straw. The initial moisture content of the straw was 16.8% (as received/from storage). A variation of the amount semi-skimmed milk added was also tried using the same straw and silicate. In this case, the skimmed milk powder was made up to (a) the equal concentration with true milk, (b) a concentration with 2/3 of the liquid content and (c) a concentration with 1/3 of the liquid content.

Boards were pressed at 190 °C for a 12 minute press schedule (of which 11 minutes was press closure). Two further boards were produced at 200 °C using the 12 minute press schedule, these were (a) semi-skimmed milk and (b) the one-third liquid powdered milk formulation. Samples were cut from the boards for internal bond and thickness swelling tests. On cutting the initial mid line, it was apparent that several of the boards had not sufficiently cured, and spring-back had occurred on exiting the press. These boards were one of the pair of semi-skimmed milk boards pressed at 190 °C (the other was almost acceptable);

- The milk powder board made at full concentration, pressed at 190 °C;
- The milk powder board made with 2/3 of the liquid content, pressed at 190 °C;
- The semi-skimmed milk board pressed at 200 °C.

---

* To be read in conjunction with section 2.6 on “Board pressing technology”

The samples of one semi-skimmed board from 190 °C press, milk powder at 1/3 liquid pressed at 190°C and the same at 200 °C were, therefore, the only three that proceeded to testing for internal bond strength. The first point to notice was that the thickness of the semi-skimmed milk hardened boards was greater than that of the two milk powder boards (with lower total liquid content), resulting in a lower density for the milk board than the milk powder boards. This was possibly a consequence of the higher moisture content, meaning that a greater level of spring-back occurred after press opening for the milk hardener system (even though this was less catastrophic than for the rejected boards). Curing is likely to be more complete in the lower moisture content milk powder boards, thus resisting spring-back and retaining the target density.

There was an appreciable difference in internal bond strength between the full moisture content milk board and the lower moisture milk powder formulation. This also implied more complete bonding in the boards with lower hardener moisture content. There was, however, some variability in strength between samples taken from each board.

The best recipe used was a slight modification of the York-proposed formulation, in that a lower content of total water content was added to the system. For this purpose, dried skimmed milk powder was dissolved in three times less water as can be found in classic skimmed milk (Table 26a). The so obtained Viscount wheat straw board was fairly erratic, reaching internal bond strengths between 0.03 – 0.1 MPa. In contrast, the board made from raw rapeseed straw reached 0.15 and 0.16 MPa but with very low density (0.625 g/cm^3). For practical reasons, the conditioning of these boards was limited to one day. A formulation using a combination of Viscount wheat straw (50/50 1/2mm fractions), whey protein and K120, reached internal bond strength of 0.41 MPa. However, when Viscount wheat straw (25/75 1/2mm fractions), waste milk (the solids fraction) and K120 reached an internal bond strength of 0.46 MPa, thus surpassing P3 standard. Essentially, there seems to be a profound effect of the straw sizes used on the obtained internal bond strength. When a 50/50 mixture of 1 and 2 mm fractions was used, the internal bond strength dropped to 0.31 MPa (compared to 0.46 MPa). The densities of the above mentioned boards were around 0.685 g/cm^3.

Table 26a. Internal bond strengths from 30 x 30 cm boards from Bangor

Sample	Density (kg/m^3)	Max Load (N)	IB strength (N/mm^2) Three weeks conditioning	Average density (kg/m^3)	Average IB (N/mm^2) Three weeks conditioning	IB strength (N/mm^2) 24hr conditioning
120a	973.995	470.72	0.18	712.030	0.1	0.11
120c	725.232	153.12	0.06			
120f	752.97	261.39	0.1			
120h	395.961	155.58	0.06			
122a	712.378	566.27	0.22	711.290	0.18	0.32
122c	717.134	368.92	0.14			
122f	724.115	287.32	0.11			
122h	691.534	631.79	0.25			
123a	695.38	580.01	0.23	699.257	0.2075	0.31
123c	701.193	482.55	0.19			
123f	715.97	410.78	0.16			
123h	684.485	633.45	0.25			
124a	678.973	134.64	0.05	695.138	0.05	not done
124c	715.122	138.77	0.05			
124f	736.18	119.09	0.05			
124h	650.277	133.92	0.05			
125a	662.625	301.01	0.12	702.702	0.14	0.13
125c	724.729	309.01	0.12			
125f	723.268	177.14	0.07			
125h	700.187	642.79	0.25			
126a	675.83	521.42	0.2	755.102	0.155	0.26
126c	779.949	306.06	0.12			
126f	791.802	333.68	0.13			
126h	772.825	438.17	0.17			

Table 26b.Water swelling and bend test results from the 30 x 30 cm boards from Bangor campaign

Board code	Thickness swelling after 24h soak in a water bath (%)	Flexure stress at Maximum flexure Load (N/mm^2)
120	44	13.00
122	34	11.88
123	37	Not tested
124	88	5.72
125	54	14.86
126	35	16.15

Code to samples: biomass/protein/silicate
120: Dewaxed Wheat straw/Whey protein/K-120
122: Dewaxed Rapeseed/Whey protein/K-120
123: Dewaxed Rapeseed/Whey protein/C205
124: Native wheat straw/Whey protein/K-120
125: Dewaxed wheat straw (Bangor milled)/Whey protein/C-205
126: Dewaxed wheat straw (Bangor milled)/Whey protein/C-205/glycerol

From the boards pressed during the Bangor campaign (Table 26), the internal bond strengths and water swelling were not close to the required target. But the dewaxed wheat straw formulations show good bend strength. There was insufficient material left to test a rapeseed board (board code 123) but from this campaign it showed, overall. the best characteristics and was pursued in future experiments.

Initially, two types of whey protein were examined: whey protein (Precision engineered Ltd, 74% wt/wt protein) and high protein Promax (whey protein isolate, 90% wt/wt protein). The latter protein yielded 30% higher internal bond strength in duplicate experiments (1009 N, 0.40 MPa versus 1340 N, 0.51 MPa) with wheat straw as the biomass. Therefore, for any future experiments high protein Promax was used in the formulation.

It has been reported that proteins can be gelled with ribose, or at a slower rate with glucose, which provides additional non-sulphide covalent crosslinks in a protein gel (Iler, 1979). Protein gels can also be formed with calcium chloride and the hardness or elasticity of a gel can be altered by the reaction temperature or by the concentration of calcium chloride. Aggregation of whey protein induced by the addition of calcium chloride can generate hard gels and these are dependent on the aggregate size (Rich and Foegeding, 2000). This gel and aggregate formation was achieved with samples of whey protein isolate at 45 ^{o}C.

Boards pressed from these gel or aggregate formulations did not show any increase in internal bond strength compared to ones with standard whey protein isolate.

However, addition of glycerol can increase the bond strength with a whey protein formulation. Adding 9% glycerol to the formulation increased the bond strength in comparison to whey protein alone (1462 N, 0.58 MPa versus 1185 N, 0.46 MPa). However this addition of glycerol increased the board density considerably to 0.85 g/cm^3 and is beyond the acceptable upper limit of 0.72 g/cm^3. As shown in the results from the Bangor board pressing campaign, glycerol does increase bond strength and reduce water swelling (compare samples 125 to 126 in Table 26) but the board density exceeds the acceptable value.

6.3.1. Scale up to 50 x 50 cm^2 boards

A scale up experiment was undertaken for the milk powder system. However, spraying difficulties were encountered with the silicate and the milk hardener which caused blockages in the spray nozzles due to rapid cure. In order to make use of the straw which had been sprayed with K120 silicate, but which had not received any milk through the blocked spray system, undiluted milk powder was tested for hardener potential. The powder was added to the drum blender, mixed and a mattress of the correct weight was prepared. The bonding of this board was visibly different to all previously pressed boards, being paler but with prominent dark spots where silicate droplets had coalesced and cured during pressing. The integrity of the boards was poorer than the other milk boards, with the edges being more friable. It was concluded that using the milk powder (or other protein systems) undiluted is not an efficient method for hardening the resins in the boards.

Glycerol was trialled as a way of reducing water content. Approximately, 25% of the water – related to the aqueous protein dispersions – was replaced by glycerol. Irrespective of the silicate used, one exception being K-biosilicate, the presence of glycerol lead to a marginal increase of 0.04–0.05 MPa in internal bond strength. In addition, and with respect to the most performing silicates being Britesil C205 and K120, inclusion of glycerol led to increased water resistance. The reason for this is unclear and is likely to be a combination of the following factors:

Less water in the mixture will make the average temperature in the board during pressing higher. This could harden the silicate more thoroughly, hence the higher strengths and increased water resistance.

At higher temperatures and in the presence of base, the glycerol may well transform into acrolein. The latter could polymerize and add to the strength. If this would have happened, it would likely have increased the density of the boards which is not really the case.

Glycerol could decompose beyond the stage of acrolein forming mainly gases, likely including CO_2 and possibly even formaldehyde. Both CO_2 and formaldehyde have the potential of hardening out the silicate.

Economically, at the time of conducting the experiment the use of glycerol was considered cost-effective as it was a very cheap by-product of biodiesel production. However, the economics may be less favourable as more and more applications are developed for the waste glycerol. However, the substitution of 26% of the water present in the aqueous protein dispersions with glycerol did increase the viscosity and may lead to processing difficulties.

The addition of additives to wheat straw, *e.g.* Na-lignosulfonate, vanillin, salts etc., was not very rewarding. Indeed, while some of these did lead to somewhat higher internal bond strengths, they also led often to decreased water resistance. One exception proved to be ferulic acid which is a decomposition product of lignin and hence fully sustainable. Ferulic acid is known to polymerize in the presence of base and, thus, its isolation from lignin is problematic. However, in the manufacture of boards, it may be an interesting future concept because of high alkalinity biosilicate which will aid ferulic acid polymerisation*.* The addition of 600 mg ferulic acid to a formulation comprising K120; EtOH Soxhlet dewaxed wheat straw, and whey protein, gave an internal bond strength of 0.54 MPa for *a* density of 0.715 g/cm^3 and a water resistance of 46%. This represented a moderate improvement compared to classical K120 boards (0.49MPa */*density 0.712 g/cm^3*)* and a water resistance of 51%).

A board made of Britesil C205, whey protein & glycerol and EtOH dewaxed Bangor milled straw broke on the glue at 0.58 MPa and this block did not show any signs of cracking whatsoever. In view of the high internal bond strengths obtained in combining Bangor milled straw (Soxhlet dewaxed) and Britesil C205, it was tried to reduce the total water content in the formulation by lowering the amount of silicate. Instead of using 15 wt% of silicate it was decided to go for 13wt%.

The as-synthesised board gave an internal bond strength of 0.52 MPa for a density of 0.723g/cm^3 and a water resistance of 43%. This formulation used around 13.8% of total binder. While this formulation used less than 15% binder and had a markedly reduced water content, this may well be an interesting way forward for making larger boards.

Interestingly, the internal bond strength of wheat straw and rapeseed straw boards were superior to those made with tomato waste (data not given). Wheat straw was superior to rapeseed straw and tomato waste with the three point bend test (performed manually). However, boards made with tomato waste and rapeseed straw showed superior water resistance compared to those made with wheat straw.

6.4. Summary of best binder formulations for wheat straw

In summary, the three most performing formulations for the making of protein-silicate-Viscount wheat straw boards were based on:
Straw: The formulations presented are all based on a 50/50 combination of the 1 and 2 mm fractions of Bangor milled hot ethanol dewaxed Viscount wheat straw. The advantage of Bangor milled straw over York milled one is that the former contains certain quantity of fibres which adds significantly to the strength of the board – typically 20-25% compared to milled material from York.

Silicate: Commercial Britesil C205 silicate solution was made by mixing 45 g Britesil C205 in 40.9 g of water to afford a 52.4 wt% solution therewith resembling the K120 solution. Britesil C205 is a Na-silicate and contains a molar SiO_2 to Na_2O ratio of ~2 while K120 contains a molar ratio of SiO_2 to K_2O of 2.24. Hence, Britesil C205 contains somewhat more base than K120 – or alternatively Britesil C205 contains somewhat less silicate than K120.

Density: The calculations underlying the formulations presented always aimed at a density of 0.68 g/cm^3. Quite strikingly the silicate-protein boards always seem to shrink substantially during the pressing stage. In fact, there seems to be a proportional relation between the shrinkage of the board and its eventual strength. In practice, boards were typically pressed to 11.75 mm with the plates generally managing to follow the shrinkage to around 11 mm at which point steel blocks prevent the heating plates from going any further. Final blocks with a thickness of around 10.3 mm were obtained thus affecting density.

Formulations:

Formulation 1:

$$\text{Straw: } \frac{36{,}448g\ dry\ straw}{(1-0.107) correction\ for\ water\ content} = 40.8\text{ g}$$

Whey protein dispersion (1): 900 mg + 2.7 g H_2O

Silica source: Britesil C205 solution in water: 12.27 g

Whey protein dispersion (2): 900 mg + 2.7 g H_2O

Density: ***0.71 g/cm***^{3}

Water test: ***32% swelling***

Strength: ***~0.58 MPa***

Formulation 2:

This is a formulation with reduced water content in the sense that part of the water in the protein dispersion is replaced by glycerol as a high boiling and benign solvent – also known as organic water.

$$\text{Straw: } \frac{36{,}448g\ dry\ straw}{(1-0.107) correction\ for\ water\ content} = 40.8\text{ g}$$

Whey protein dispersion (1): 900 mg + 700 mg glycerol (organic water) + 2 g H_2O

Silica source: Britesil C205 solution in water: 12.27 g

Whey protein dispersion (2): 900 mg + 700 mg glycerol (organic water) + 2 g H_2O

Density: ***0.7 g/cm***^{3}

Water test: ***30.6% swelling***

Strength: ***> 0.58 MPa***

Formulation 3:

In this formulation the amount of silicate used was reduced and thus the total water content was also lowered. The lower silicate content allowed more wheat straw to be added.

$$\text{Straw: } \frac{37.3g\ dry\ straw}{(1-0.107) correction\ for\ water\ content} = 41.8\text{ g}$$

Whey protein dispersion (1): 900 mg + 2.7 g H_2O

Silica source: Britesil C205 solution in water: 10.63 g

Whey protein dispersion (2): 900 mg + 2.7 g H_2O

Density: ***0.72 g/cm^3***
Water test: ***43% swelling***
Strength: ***~0.52 MPa***

The correction factor relates to the water content in the straw – and is thus variable, typically ranging around 8-11%.

6.5. Rapeseed straw and binders

A large bale of Dimension oilseed rape straw was supplied and was prepared for board production. Oilseed rape straw was hammer milled (9 mm screen size) with the direct hammer milling process giving good separation of the tubular strong sections, opening the pith region to accept resin and assist with bonding (Figure 42). There was a significant amount of dust generated from the pith material fragmenting which was left in the mixture of feedstock for board manufacturing.

Figure 42 a. Oilseed rape stems in a range of different diameters, as supplied for analysis. b. Oilseed rape particles after hammer milling.

Three binders/hardeners were trialled with rapeseed straw at York: lignosulfonate, tannic acid, and proteins (whey protein, wheat gluten or gelatin). Rapeseed straw was milled, sieved and either, the 1 and 2 mm fractions (used in a 1:1 ratio) or the 1,2 and 2.8 mm fractions (combined as one) were used. The primary filter used in the milling to generate these fractions was wire mesh which had internal diameter measurements of 11.00 x 11.24 mm. The 1,2 and 2.8 mm fractions separated after sieving represented about 75% of the total milled biomass. Unless otherwise stated the internal bond strengths quoted are for boards of 7.4 cm x 7.4 cm (with a total projected mass of 44.68 g).

6.5.1. Sodium/Calcium/Ammonium lignosulfonate binders

Free samples of these materials were obtained from Borregaard UK (Warrington, Cheshire, Jim Buchanan jim.buchanan@borregaard.com). These lignosulfonates (LS) were not characterised for molecular weight, but it has been reported that they have an average molecular weight in the range of 40,000 to 65,000 with greater than 90% ranging from 10,000 to 250,000. The sodium and ammonium lignosulfonates were received as brown powders whilst the calcium lignosulfonate is a 50% (w/v) viscous liquid. This makes the former salts more useful in board production as they can be added as a dry powder, whilst the calcium salt is difficult to add to the biomass evenly and brings a large amount of water to the final binder formulation. Historically these LS materials (also known as spent sulphite liquor, SSL) have been used as sole binder for particle board manufacture (Ju and Kilara, 1998). Albeit that they are relatively inexpensive, this advantage is possibly negated by the low reactivity of the LS towards condensation. Condensation will facilitate cross-linking and may reduce bleeding of this material from the board. A Danish particleboard firm has used acidified SSL as a binder for particleboards. The low reactivity did not permit its use as a direct substitute for formaldehyde-based resins. To develop the full bond properties of SSL a severe autoclaving (200 ^{o}C, 2h) was required. During this treatment the LS thermosets and crosslinking of the LS occurs. Myers (1987) has also reported this necessity when using LS in particleboard manufacture. Hardboards using ammonium lignosulfonate as the binder needed to be heated and 354^{o}F for 4h after pressing. No boards produced in York underwent this process as it was suggested that this will not fit to the current Compak working operations.

Lignosulfonate formulations at York

Sodium lignosufonate (SLS) as the binder showed similar pattern in strengths as those seen for other York binders. That is, only a dewaxing with hot ethanol (using a Soxhlet) delivered a board of suitable strength (Table 27). The wax content of rapeseed is reported as 1.83%. Supercritical CO_2 extracted or native rapeseed stalk yielded considerably weaker boards.

Table 27. Variation of bond strength with extraction method

Extraction method	Sodium Lignosulfonate (wt %)	K120 silicate (wt %)	Water/g (wt %)	Internal bond strength
None (waxed biomass)	12	13.5	9.7 (21%)	328 N (0.14 MPa)
$scCO_2$	12	13.5	6.6 (15%)	474 N (0.18 MPa)
Hot ethanol	12	13.5	9.6 (21%)	>1050 N (0.45 MPa)

Lowering the silicate content below 13.5 wt % (to 7.5%) and thereby adding more SLS (to 18%) reduced the internal bond strength to 769 N. The order of addition should be silicate solution first to the biomass, followed by dry powdered SLS. Ammonium lignosulfonate (ALS) can also be used as a binder and when 13.5% ALS was employed an internal bond strength of >1050 N (0.45 MPa) was achieved.

However, these boards suffered from water stability issues. Offcuts of these boards were immersed in water and rapidly disintegrated (within 1h). Bleeding of the material could be easily observed and it would seem that chemical curing and cross linking had not occurred during pressing. Although it has been reported that ALS condenses at a higher rate than calcium lignosulfonate (CLS), with SLS lying in between these two (Iler, 1979), boards made from all of these binders did not remain stable in water. Boards made from SLS also suffered from reduced internal bond strength with prolonged conditioning (881 N, York, 24 h vs 485 N, Bangor, 14 days for a SLS formulation). However, it should be noted that method of testing between the two sites are extremely different. It would seem that a condensation/crosslinking of the lignosulfonate is important for water stability. It has been reported that a major drawback of SSL as an adhesive for board manufacture, is its hydroscopic nature. One possibility to circumvent this is the use of hydrogen peroxide or sulphur dioxide for oxidative coupling of SSL (Myers. 1987). It is reported that this yields an insoluble resin which favours the use of SSL for board manufacture. But here too, the success of this method on a technical scale has been questioned (Clad, 1983). This oxidative coupling could potentially be achieved using the enzyme laccase, which is known to crosslink lignins. This enzyme requires only oxygen as to perform this, however, in the scope of this project was prohibitively expensive (Viikari *et al.,*1998).

In an attempt to reduce the bleeding from the boards, an alternative method to crosslink the lignosulfonate was explored. The viscosity of lignosulfonate solutions can be increased by using NaOH alone or NaOH/epichlorohydrin. In the latter case, a gel was formed in 24 h. Gelation is observed by the addition of NaOH alone but this can be enhanced by the addition of diepoxides or epichlorohydrin. Difunctional compounds are required as propylene oxide had no effect on viscosity (Collins *et al.,*1977).

A gel could be made from a SLS (42% w/v) aqueous solution, epichlorohydrin and sodium hydroxide, with 6 days of standing at room temperature (SLS-gel). When heating was employed, this reaction was not successful and it is reported that raising the temperature has a significant effect on slowing the rate of gel formation (Myers, 1987). The molecular weight of this gel material has yet to be determined, however it is insoluble in water. A board made from the SLS-gel had a lower IB (723 N), but the swelling in water was significantly reduced and an offcut actually remained intact. Swelling was estimated at 45% for a wet block (after 24 h in water) and 24% after a further period of drying (24h, known as dry). Contraction of offcuts is often observed upon drying. For future studies, the SLS-gel seems to be appropriate. Generation of a dry powder (perhaps after solvent exchange with ethanol) from the SLS-gel would be beneficial. When using the gel it is added to the biomass and afterwards a drying step is required to remove excess water. This could be circumvented by using a powdered form of the SLS-gel.

An alternative silicate can be employed with the SLS-gel. Using Britesil C205 increased the IB to 1028 N (0.44 MPa) but with a slight increase in water swelling (51%, wet). A board made from tomato waste (1 and 2 mm, 50:50 ratio), K-120 silicate and SLS-gel showed moderate strength (796 N, 0.31 MPa) but improved water swelling (31% wet, 8% dry) when compared to rapeseed.

Tannic acid binder

This was selected based on a patent which indicates that it is a suitable binder for paper, straw and roads (Fulton-Tompkins, 1917). According to the patent, tannic acid in combination with soluble silicates has the ability to glue cellulose containing materials. It has previously been reported as a binder for particle board (Roffael, ;Tabarsa *et al*., 2011) but not in combination with silicate. It has also been identified as Green wood adhesive (Langenberg *et al.,* 2010). Further, it is available as a waste product (from pomegranates) from a solventless process (Ensymm).

For these boards, an aqueous solution of tannic acid (32% w/v) was first added to the biomass. The addition of a more concentrated solution or dry tannic acid was not feasible for board production. Hereafter, solid glucose was added to the moist biomass and the excess of water removed by drying at 120 ^{o}C for 1h. This provided an even coating of the binder across the biomass, which is not achieved with dry tannic acid or a concentrated solution of tannic acid. Final addition of K-120 silicate and pressing yielded a board with good strength (>1050, 0.45 MPa). However there are considerable amounts of binder in this formulation (total = 40%). Here again, using either native rapeseed biomass or adding the flour (<1 mm fraction) into the formulation, weakened the board with respect to bond strength. This formulation was also not productive with dewaxed wheat straw (1 and 2 mm fraction, 1:1 ratio), yielding a bond strength of only 394 N (0.15 MPa).

A reduction in the amount of binder was possible when an alternative silicate C205 was employed in the formulation. When a formulation with a total of 24% binder (of which it is 10% tannic acid and 7% each of glucose and silicate) was used, a board of reasonable strength was achieved (1164 N, 0.46 MPa). However the water swelling increased considerably (to 160%).

Reducing the pressing temperature from 235 to 192 ^{o}C reduced bond strength (to 974N, 0.38MPa), but improved the pressing and the appearance of the product. At the higher temperature the appearance of the test board was charred. Again native (waxed) biomass yielded a board with lower strength (753 N, 0.30 MPa). Albeit considerable amounts of binder were used in this formulation, the water swelling was moderate at around 38% (wet). The patent of Tompkins suggested that the addition of calcium carbonate can improve the binding characteristics of tannic acid. Boards pressed with calcium carbonate (4% or 2%) in the formulation resulted in increased water swelling (52%). At a lower temperature (192 ^{o}C) and with 40% binder, boards were made which incorporated polylactic acid (PLA) as a substitute for the tannic acid binder. The aim was to increase strength and water resistance; the total amount of binder remained constant but the levels of tannic acid, glucose and silicate were reduced to allow for polylactic acid. The lower temperature was also chosen as it is reported that PLA decomposes at high temperatures (Garlotta, 2001). This compound had a positive effect on both the bond strength and the water swelling. The bond strength in the PLA/glucose/tannic acid/silicate board increased to 1558 N (0.60 MPa) from 1001 N (0.40 MPa) and the water swelling reduced to 22% (wet) from 46% (wet). This was one of the clearest effects seen in all trials with this formulation. The amount of PLA was about 9%, although the overall amount of binder remained constant. However in terms of this project this approach was probably unfeasible due to cost. The cost of this material (compared to Sigma Aldrich) can be reduced by using a supplier such as icopolymers (Charlie Busceme <cbusceme@icopolymers.com>). However in terms of this project this approach was probably unfeasible due to costs.

Glucose was also replaced with 5-hydroxymethyl furfural (HMF) for board production. Using both C205 and K-120 moderate board strengths were obtained (approx. 1100 N, 0.44 MPa) using the 1 and 2 mm fraction (50:50 ratio). Wet swelling was about 32–34% and dry about 18–19%.

For the glucose/tannic acid/K-120 formulation the influence of particle size on bond strength was examined. The results are outlined below in Table 28. Both the <1mm and 4mm fractions of the milled biomass clearly influenced internal board strength. Removal of these fractions was not in keeping with one of the project's objectives, however the combined 1, 2 and 2.8 mm fractions do still make up some 70–75% of the biomass. These values are for hot Soxhlet extracted biomass.

Table 28. Influence of particle size on properties

Experiment No (size fraction)	Fraction removed	Internal Bond strength	Wet swelling (%)
DVJ I/99 (<1, 1, 2, 2.8, 4mm)	Non-full fraction	894 N (0.37 MPa)	50
DVJ I/103 (<1, 1, 2, 2.8mm)	4 mm	1023 N (0.43 MPa)	26
DVJ I/104 (1, 2, 2.8mm)	<1 and 4 mm	1222 N (0.48 MPa)	23

As a comparison the properties for boards made from cold ethanol dewaxed material are shown in Table 29. As reported with other binders (see earlier), the type of ethanol extraction (hot versus cold) affected bond strength. The values outlined in Table 29 were clearly lower than those in Table 28, which reinstated the need for hot ethanol extraction with this biomass.

Table 29. Tannic acid boards made with cold ethanol dewaxed material.

Experiment No (size fraction)	Fraction removed	Internal Bond strength	Wet swelling (%)
DVJ I/109 (<1, 1, 2, 2.8 mm)	4 mm	876 N (0.37 MPa)	23
DVJ I/104 (1, 2, 2.8 mm)	<1 and 4 mm	881 N (0.35 MPa)	32

A comparison between two biomasses, dewaxed rapeseed and untreated tomato waste, was made for this formulation (using 1 and 2 mm fractions). Tomato waste could be a viable biomass with this formulation, showing moderate strength (0.48 MPa) and acceptable water swelling of 18%, considering the P3 standard target is 14% (Table 30). Also this biomass does not require dewaxing as is the case for rapeseed. For both ligonsulfonate and tannic acid binders the tomato waste showed the best water swelling properties.

Table 30. Comparison of biomasses with Tannic acid formulation.

Experiment	Internal Bond strength	Wet swelling (%)
DVJ I/87 rapeseed dewaxed	1001N (0.40MPa)	46
DVJ/105 tomato waste	1180N (0.48MPa)	18

The 1 and 2 mm fraction of the tomato waste was selected to study the influence of tannic acid/glucose ratios (as weight percent in the formulation, Table 31). Provisionally a 1:1 ratio seemed to give the best water swelling, without dramatically effecting bond strength. However, reduction of the total binder levels to 28% (towards the target 20%) lowered the internal bond strength significantly. It would seem for this, formulation high quantities of binder are required.

Table 31. Comparison of tannic acid/glucose ratios.

Experiment	Composition (%)			Internal Bond strength	Wet swelling (%)
	Tannic acid	Glucose	Silicate		
DVJ I/105	15.5	15.5	11.8	1180 N (0.48 MPa)	18
DVJ I/106	19	9	11.8	1304 N (0.51 MPa)	33
DVJ I/107	9	19	11.8	1317 N (0.52 MPa)	30
DVJ I/114	10	6.7	11.8	917 N (0.36 MPa)	39

With tomato waste, boards were pressed at slightly lower temperatures without affecting board strength, such that a board pressed at 191 ^{o}C yielded a similar strength to one at 181 ^{o}C (0.48 vs 0.49 MPa, respectively), but the appearance of the board was improved at the lower temperature. This was not the case when using rapeseed as the biomass, where the pressing temperature seemed to affect the internal bond strength.

Protein binders

Wheat gluten

Wheat gluten is known to be a natural adhesive and has the potential to be a good binder because of its ability to form films and prepare fibre boards (Tate and Lyle). Wheat gluten is described as a water-insoluble protein and is composed of two proteins fractions, glutenin and gliadin. These proteins have high content of glutamine and proline and a low fraction of charged amino acids which promotes the water insolubility of wheat gluten. This water insolubility makes the wheat proteins stable to high humidity and it was selected as the binder to try and reduce the impact that extended conditioning was having on board internal bond strength. When hydrated, gliadin is soft and has good adhesive properties whilst glutenin is firm and elastic. Wheat gluten has been used as the sole binder for particleboard made form reed (Tate and Lyle) or wood fibres, but not in combination with silicate. Wheat gluten is also a low-cost raw material, annually renewable and readily available. It also has the potential to be described as a waste product with the current drive towards gluten-free foods.

Initial experiments employed an adaptation of the method reported by El-Wakil *et al*. (2007), whereby the 15% w/w wheat gluten adhesive was applied to the biomass followed by silicate solutions. Two experiments (II/15A and 15B) varied the amount of silicate in the formulation (4.5% w/w and 8% w/w). The lower silicate-content formulation obtained higher bond strength and lower water swelling (484 N and 29% water swelling versus 324 N and 42%), hence this lower level (4.5% w/w) was maintained for future experiments. However the method of preparing a wheat gluten adhesive (using urea as the denaturing solution) as per El-Wakil *et al*., then applying that to the biomass brings considerable water into the formulation (33-44 mL for a 7.4 x 7.4 cm board) and this results in a weak board. An adaptation of this method was required.

Wheat gluten can be made into an adhesive by the denaturing action of urea and sodium hydroxide. Hence when a solution of urea (1.5M)/sodium hydroxide (2% w/v) (denaturing solution) was added to the biomass followed by solid wheat gluten, the adhesive is made *in situ* on the biomass and it becomes tacky and adheres easily. The silicate solution is then added to this tacky biomass.

In general for a formulation where the total solids are 45.64 g (approx. 36.44 g of dry biomass, excluding water content), 15 mL is an appropriate volume of denaturing solution (Table 32). Although a lower volume can be used, this reduces the internal bond strength. Increasing the volume may result in a wet and weaker board as noted above. It is well documented that water is plasticiser for wheat gluten and is important to stop the material becoming brittle. Glycerol can also be used as a plasticiser for wheat gluten (Sun *et al.* ,2007).

Table 32. Influence of volume of denaturing solution on internal bond strength

Volume denaturing solution (mL)	Amount of Wheat Gluten (g)	Amount of C205 (g)	Internal bond strength
15	7.2	2	1239 N (0.50 MPa)
8	7.2	2	978 N (0.38 MPa)

The experiments above were performed using wheat gluten with a composition of 70% protein and 15% carbohydrates (Type A). However a wheat gluten with a higher protein content (80% protein, 8% carbohydrate, <1% fat, http://www.lowcarbmegastore.com/ingredients/wheat-gluten-powder-1kg) is available. Employing this higher protein wheat gluten increased the internal bond strength (approximately 16%) to 1451 N (0.58 MPa). This was the preferred source of wheat gluten for all the remaining experiments (Type B). Increasing the amount of total binder to approximately 35% (30% wheat gluten 4.4% silicate) did increase the internal bond strength (to 0.66MPa) but placed it beyond the 20% limit set by the consortium.

Wheat gluten can be defatted by treatment with butanol (Yonezawa *et al.,*1966; Jones *et al.,*1959). Extraction of wheat gluten (Type B) with t-butanol (3 times) and subsequent drying of the powder at room temperature (3 days), returns a defatted powder (wheat gluten type C). Employing this binder, the internal bond strength was further increased to 0.66 N 1745 MPa. Note, a shorter pressing time (3 mins instead of 8 min) or a decrease in press temperature affected the board strength. A press time of 3 mins yielded 0.14 MPa and a pressing temperature of 160 ^{o}C yielded 0.52 MPa. Therefore 8 mins and 180 ^{o}C would be the best combination at present. The best board was also made using the 1, 2 and 2.8mm fractions of rapeseed. Incorporating the 4 mm fraction into the board reduced the bond strength to 0.54 MPa (1384 N).One of the consortium aims was to utilize all the milled mass, though removal of the flour fraction (<1 mm) maybe acceptable. Using the 1, 2 and 2.8 mm fractions was the closest we could get to this aim, whilst still retaining some board strength. Using miscanthus or wheat straw (with 1, 2 and 2.8 mm fraction) yielded lower internal bond strengths (0.36 MPa and 0.13 MPa, respectively). With this formulation, rapeseed would appear to be the preferred biomass. Again using waxed (non-pretreated) rapeseed yielded lower internal bond strength (697 N, 0.27 MPa). When the wheat gluten formulation was applied to tomato waste, a considerably weaker board was obtained (0.37 MPa). However addition of 7.8% lignin (Sigma Aldrich, 471003) in the tomato waste formulation increased the bond strength considerably (to 0.53MPa). Tomato waste has a very low lignin content (approximately 4.1%)(Guutekin *et al.,*2009) whereas rapeseed has a much higher content, 17% (Karaosmanoglu, 1991). It is perhaps this difference which, with respect to internal bond strength and bend strength, makes tomato waste a weaker biomass.

For any future studies, wheat gluten with high protein content should be obtained which should, if necessary, then be defatted using *t*-butanol. Including the flour (<1 mm) or the 4mm fraction from the milling should be avoided as with all binders, this reduces the bond strength. With wheat gluten type C, C-205 silicate yields higher internal bond strength (0.66M Pa, 1745 N) than the silicate K-120 (1249 N, 0.50 MPa).

Wheat gluten formulation

Volume of board = 18 cm x 18 cm x 1.1 cm = 356.4 cm^3
Desired density = 0.68 g/cm^3 therefore total amount of solids = 242.35 g
At 20% binder, amount of binder = 48.47 g, therefore amount of rapeseed = 193.35 g
Adjusted amount of rapeseed (to include water content, 11.8%) = 219.81 g
Amount of denaturing solution (urea 1.5 M, 2% w/v NaOH) = 81 mL
Wheat gluten (Type C) = 37.93g, C205 silicate = 10.54 g dry (=24.34 g aqueous solution)

Wheat gluten with Zein, PLA or glyoxal formulations

Wheat gluten/Zein composite materials have been reported (Kim, 2008). Zein has been reported to possess strong adhesive properties when binding matrix materials and a protein composite can be formed by combining wheat gluten (80%) with Zein (20%). Two boards were pressed whereby 20% of the wheat gluten binder content was replaced with Zein. In contrast to pure wheat gluten boards, the type of silicate did not influence the internal bond strength. Using C205 or K-120 a figure of 0.67 MPa was achieved. To date, these figures remain the highest internal bond strengths obtained where 20% protein binder is used. Increasing the Zein content from 20% to 40% did not increase the internal bond strength. Surprisingly, substitution of some of the wheat gluten by PLA (20%) (hence 80/20 wheat gluten/PLA ratio), did not increase the internal bond strength (0.56 MPa). This was in contrast to the positive influence PLA substitution had on the tannic acid formulation. Even increasing the amount of PLA (hence 60/40 wheat gluten/PLA ratio) did not improve the bond strength (yielding 0.54MPa). Glyoxal, a known cross-linker of proteins, did not improve the bond strength and in fact considerably weakened the board and was no longer pursued. Wheat gluten boards without urea in the formulation were also prepared. Urea, a known hydrogen bond disrupter, is required to make wheat gluten into an adhesive. The boards lacking urea in the formulation were weaker than those where it was included (0.46 MPa versus 0.67 MPa)

Wheat-Gluten boards at Bangor and waxed wheat gluten boards

After the optimisation of the boards in York on a 20 x 20 cm, a pressing campaign was attempted at Bangor. All boards were not successful and all suffered from delamination in the middle. Pressing of 20 x 20 cm waxed rapeseed boards was attempted in York but without success. In fact, this should not be attempted again, both boards suffered explosive failure.

7. BOARD PRESSING TECHNOLOGY (BANGOR)

Discussion between B&Q, Compak and Bangor University led to the definition of suitable grades of panel to meet performance requirements and the target service environment of the product range and manufacturers and secondary processor companies present within the consortium. The main target products were profiled panels for kitchen drawer and door fronts, and kitchen work-surfaces. This meant that various thicknesses of panel were required for different tasks: 12, 15 and 18 mm, with the worktop being likely to be a laminated pair of panels to give sufficient thickness.

In order to perform in the kitchen environment over the target lifespan, a performance class of P3 (non-load-bearing boards for use in humid conditions) according to BS EN 312:2003 was selected. The P2 category (boards for interior fitments for use in dry conditions) was also considered, as some applications require this more general performance level.

P3 grade particleboard is suitable for general use, in humid areas such as kitchens, and the specific properties such as modulus of elasticity in bending, modulus of rupture and thickness swelling parameters are set out in Table 33.

Table 33. Specified values for relevant performance properties for P3 grade particleboard of thicknesses >6 to 13 and >13 to 20mm, under BS EN 312.

Property	EN Test	Units	Specified value for >6-13 mm	Specified value for >13-20 mm
Bending strength	EN 310	N/mm^2	15	14
Modulus of elasticity in bending	EN 310	N/mm^2	2050	1950
Internal bond strength	EN 319	N/mm^2	0.45	0.45
Thickness swelling, 24 h	EN 317	%	14	14
OPTION 1				
Internal bond after cyclic test	EN 321	N/mm^2	0.15	0.13
Thickness swelling after cyclic test	EN 321	%	14	13
OPTION 2				
Internal bond after boil test	EN 1087-1	N/mm^2	0.09	0.08

It was also discussed that for the international market, the American grade of M2 (ANSI A208-1) could be considered. This is broadly equivalent in strength to EN 312 requirements for P3 panels, but differs in the types of test (hardness and screw holding are additional requirements) and the MOE specification is a bit higher (Table 34). The ANSI classification does not alter the requirements with board thickness in the way that the European standard does.

Table 34. Specified values for M2 grade boards under ANSI A208.1-1999 standard

Property	ASTM test	Units	Specified value
Modulus of rupture	D 1037	N/mm^2	14.5
Modulus of elasticity	D 1037	N/mm^2	2250
Internal bond	D 1037	N/mm^2	0.45
Hardness	D 1037	N	2225
Screwholding (face)	D 1037	N	1000
Screw holding (edge)	D 1037	N	900
Linear expansion max avg.	D 1037	%	0.35
Formaldehyde	E1333	ppm	0.30

The defined performance meant that three key tests were selected for initial benchmarking and comparison between early development panels: MOE and MOR in bending; internal bond strength and thickness swelling. Later in the project, prototype panels would be subjected to the fuller suite of tests, such as internal bond strength after boil, screw holding, machine blunting, cutting, drilling and routing, outlined in the diagram (Figure 43). Once panels for pilot scale production were selected, the full testing for verification of performance under EN 321 would be performed.

For prototype panels in the first phase, a thickness of 12 mm was agreed, to enable preparation of sufficient samples while keeping the quantities of straw, silicate and trial hardener systems to reasonable levels in the early stages. The three point bend specimens require a test length which is proportional to their thickness, so 12 mm allowed samples to be cut from 30 x 30 cm panels on the smallest Bangor press.

During the first phase, the test panels are produced in order to optimise the press schedule, (temperature, press closure rate, press time) while also monitoring press related properties such as internal gas pressure and core temperature. This is in addition to monitoring the effect of these parameters on panel strength, and simple effects of binder quantity and selected panel density.

Secondary testing to fine tune the quantity of resin and of hardener, the panel density, and the optimal combination of pressing conditions will follow. At this stage, any feedstock related issues such as surface preparation or dewaxing, addition of other additives or extra steps to increase specific properties as required can be investigated. Similarly the exchange of the mineral silicate for the biosilicate, and any necessary alterations which accompany this transition.

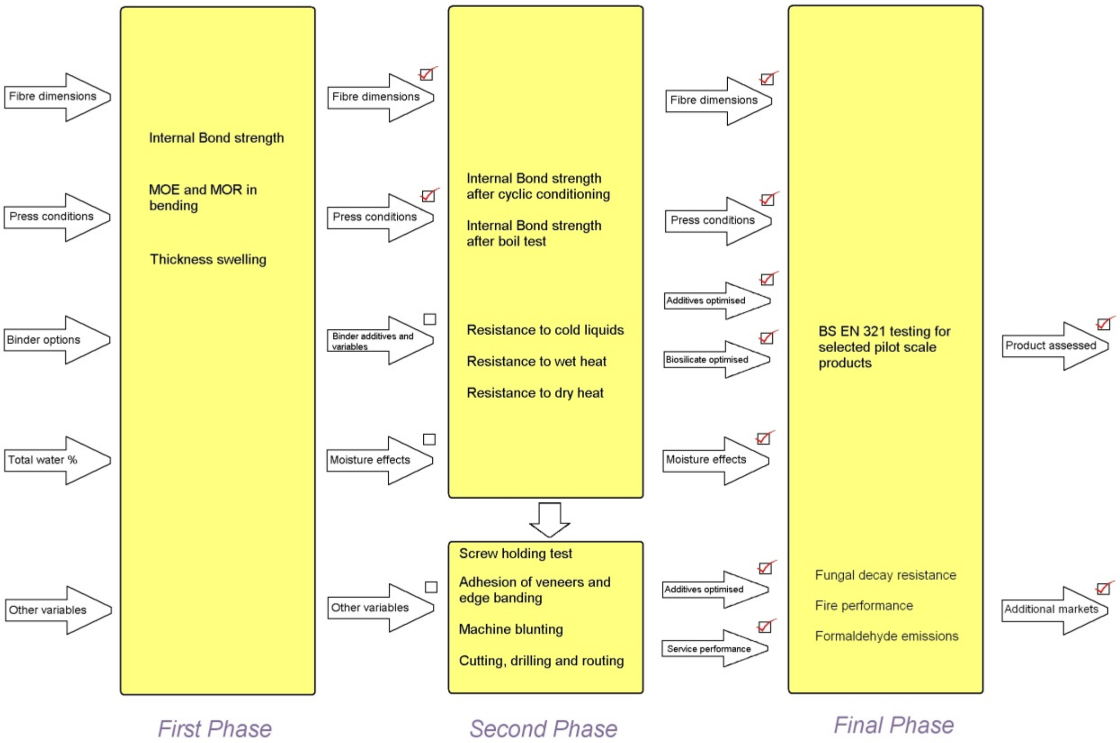

Figure 43. Testing types to be used during screening at the first phase, to optimise during the second phase, and to demonstrate full saleability during the third phase of product development.

The final stage, transfer to pilot scale, is intended to be as simple as possible, having optimised all the input parameters and the processing conditions. Therefore, the testing is intended to be a sweep of the necessary tests for performance, and to include options which demonstrate a market potential.

7.1. Silicate and R100

An initial trial was conducted using Crystal 0120, a sodium silicate, and R100, a dibasic acid hardener. The resin content of the boards was set at 20% and this silicate was assumed to have 65% solids content. The hardener was used at 8% of total resin solids. The straw had been chopped to 25 mm lengths, and hammer milled on a 9 mm screen. The target density was 650 kg/m^3, and panels were 300 mm x 300 mm and 12 mm thick.

The press was closed to a fixed aperture of 12 mm, rather than a fixed pressure. The press temperature was 220 °C for the majority of this batch, but a small number of panels were prepared at 210 °C, and a few at 230 °C. Panels were produced from a range of different press times; 8, 9, 11 and 13 minutes total press closure time. All of these durations are longer than would be typical for a standard MDI bonded panel, but the extra time was necessary to allow cure to develop within the silicate binder, where water content is proportionally greater.

The straw chips were either used at ambient conditions (measured to be 14% moisture content) or after drying to 4% moisture content. At both temperatures, the adhesion was shown to be poorer in the panels made with the drier chips. In the 220 °C samples, the difference was only relatively small, see Figure 44 , however when pressed at 210 °C, the difference in adhesion was marked, with straw poorly adhered to the surface Figure 44b, right hand side. This result was surprising, in that the lower moisture content of the chips in the panel was expected to lead to faster cure and moisture loss than the high moisture content panels, especially at this low temperature and fast press time.

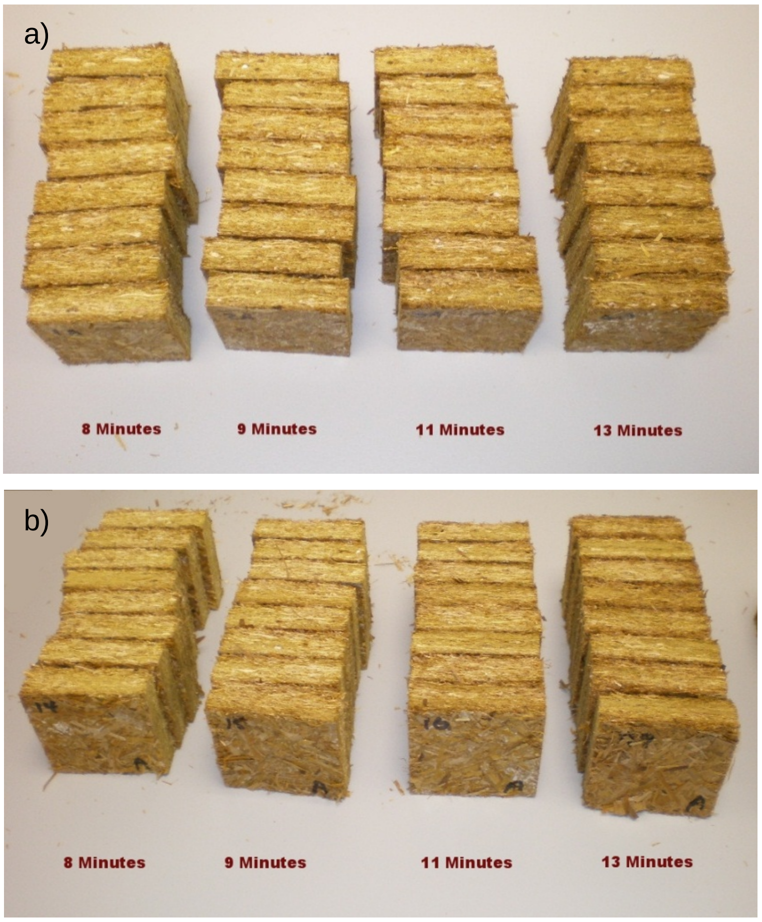

Figure 44. a) Samples cut from panels pressed at 220 °C with straw of 14% moisture content, for four different press times. b) Samples cut from panels pressed at 220 °C with straw of 4% moisture content, for the same four press times.

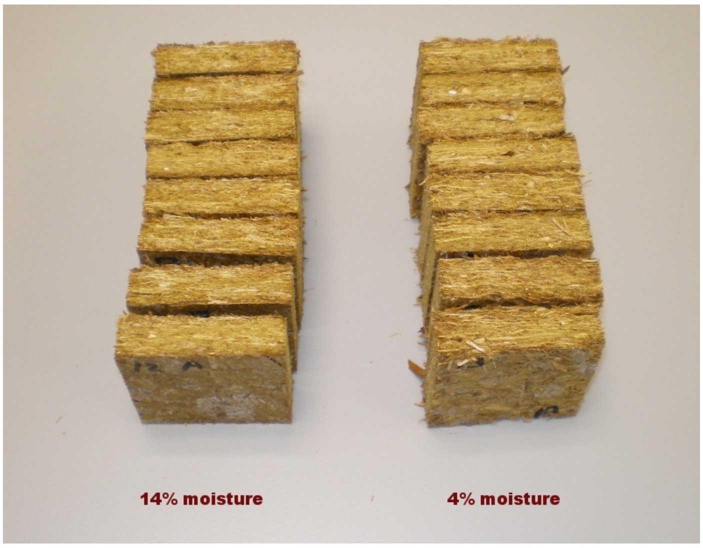

Figure 45. Samples cut from two panels pressed at 210 °C for 8 minutes, using chips of higher (left) and lower (right) moisture contents.

The internal bond strengths for panels were all poor, however the weakest were the panels with low moisture content (14 N at maximum load), even the strongest sample (11 minutes pressing at 210 °C) was too weak (34.45 N at max load*, i.e.* 0.014 N/mm^2) to compare with the performance required in the standard (0.45 N/mm^2). The board density values were observed in the test specimens cut for internal bond strength. It was noticeable that all panels produced with straw at low moisture content (4%) had lower densities (circa 570 kg/m^3) than the panels produced with straw at ambient conditions (circa 660 kg/m^3). This again indicated the poor cure for the drier furnish.

Bending strength and modulus of elasticity in bending were poor, and again showed that the low moisture chips gave weaker boards than the straw at ambient conditions. The thickness swelling tests were very poor, and the low moisture content chips showed the greatest disintegration. It is possible that the chip moisture is required in order to hydrolyse the hardener in situ, initiating the reaction between the acidic units generated with the alkaline silicate binder system. It was therefore decided that chips did not require drying before use with this binder system. Alternative hardeners would also be considered.

The density profile of these boards was evaluated. It is worth noting that most panels had sprung back somewhat after pressing to the initial 12 mm thickness, and ranged in thickness from 12.36 to 13.14 mm. A small number of panels appeared to have lower spring-back, and samples measured 11.98 to 12.56 mm (e.g. IP24, IP25 and IP26, the only connection between these was that they were the first three pressed on one day of the trial, press conditions were 210°C for 11 mins. 220°C for 9 mins and 220°C for 12 mins). The panels produced with lower straw moisture content (IP28-33) had spring-back of a similar level to that of the 14% moisture content straw panels (excluding the three low spring-back panels listed above).

Interestingly, some of the boards showed density profiles which were fairly typical of MDF or particleboard. For example, Figure 46 shows a sample from panel IP11, which was pressed for 9 minutes at 220 °C, and made with straw with normal moisture content. This sample had a bulk density of 658.02 kg/m^3, and a thickness of 12.28 mm when measured for thickness swell testing. However the density profiler showed that internally it had a minimum density of 588 kg/m^3, and the two face layers were 815 and 946 kg/m^3. This compaction at the surface would be typically due to good thermal transfer in this layer, coupled with effective action of the press being intensified in this region where the particles are sufficiently warm to behave in a plastic manner during the early stages of press closure.

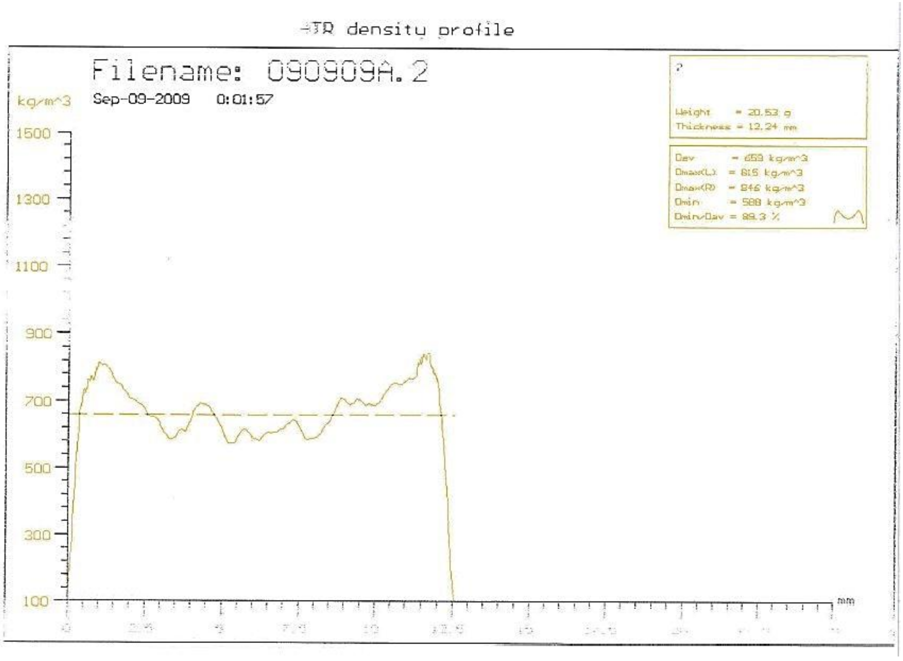

Figure 46. Density profile through the thickness of sample IIA, showing higher density material at the two surfaces of the panel.

Similarly, samples from panel IP33 which was made with dried straw at a lower moisture content showed typical density profiles (Figure 47). Here, the difference in density between the surface and the core appears even more pronounced, with the minimum density being 461 kg/m^3, while one face is 763 kg/m^3. It is also clear that the two face layers are of significant thickness (over 2 mm each). This panel showed a greater amount of spring-back (this sample was 12.5 mm thick), which may be partially the cause of the very low density core material. If the compacted and well bonded surface layers are less likely to relax once the press opens, the level of bonding, and the presence of steam within the core of the panel, make the core more likely to attempt to return to a less compressed state once the pressure is released.

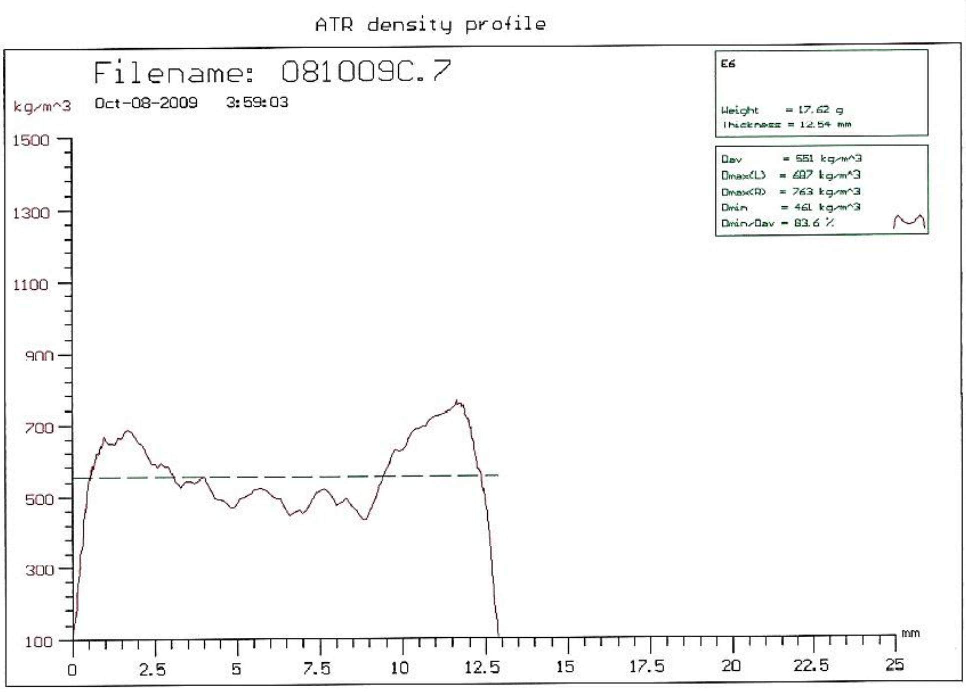

Figure 47. Density profile for sample IP33C, from a panel made with low moisture content straw at 220 °C for 8 minutes press time.

Other samples showed very large spikes and troughs in density through the cross section of the panel, for example, panel IP27 (Figure 48a-d). The four samples were adjacent to each other on the left hand side of the panel. The location of deep troughs in density in sample 27A is different to those in sample C and D, whereas sample B shows an almost normal density profile. It is clear that regions prone to poor bonding (which are then able to spring back and obtain very low density values after pressing) are randomly located within the furnish when it is laid up.

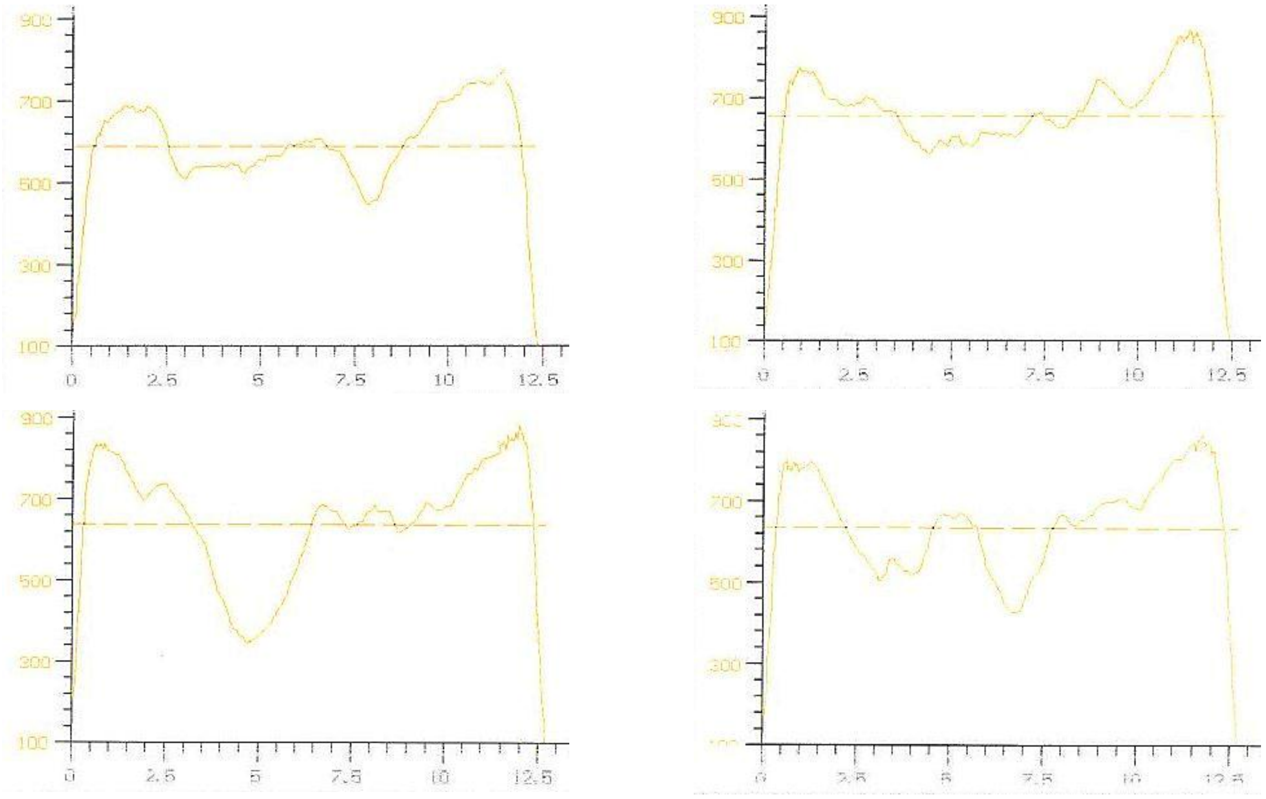

Figure 48a-d. Samples A, B, C and D from panel IP27 showing the difference in density profile across one side of the panel.

It does seem noticeable that the samples in Figure 48a-d (above) tend to have higher density face material in the second face (at 12 mm) than the start of the measurements. This can also be seen in Figures 46 and 47 for other panels. This difference relates to the face which is in contact with the press prior to press closure having slightly longer time for moisture to evaporate, and therefore slightly different curing conditions during the press schedule. Such differences can be evened out in scale up to the more continuous industrial process. However, it corresponds with observations of slight difference in the appearance of the upper and lower face, both in level of compaction, and type and texture of silicate droplets.

For the low spring-back panels, the density profile was much more flat than the other examples. In panel IP24 there was very little evidence of the typical compaction of particles at the surface, and lesser degree of compaction in the core. The profile is much more uniform, and the minimum density value detected by the density profiler was 709 kg/m^3, with the two faces being 833 and 850 kg/m^3 (Figure 49). This sample measured 11.92 mm when prepared for the density profiler, indicating negligible spring-back. When tested for internal bond strength, this individual sample registered 77.42 N, which was the highest recorded for this set of tests, however other samples from the same panel sprung back more (minimum density values showed 575 for A, 608 for C and 584 kg/m^3 for D).

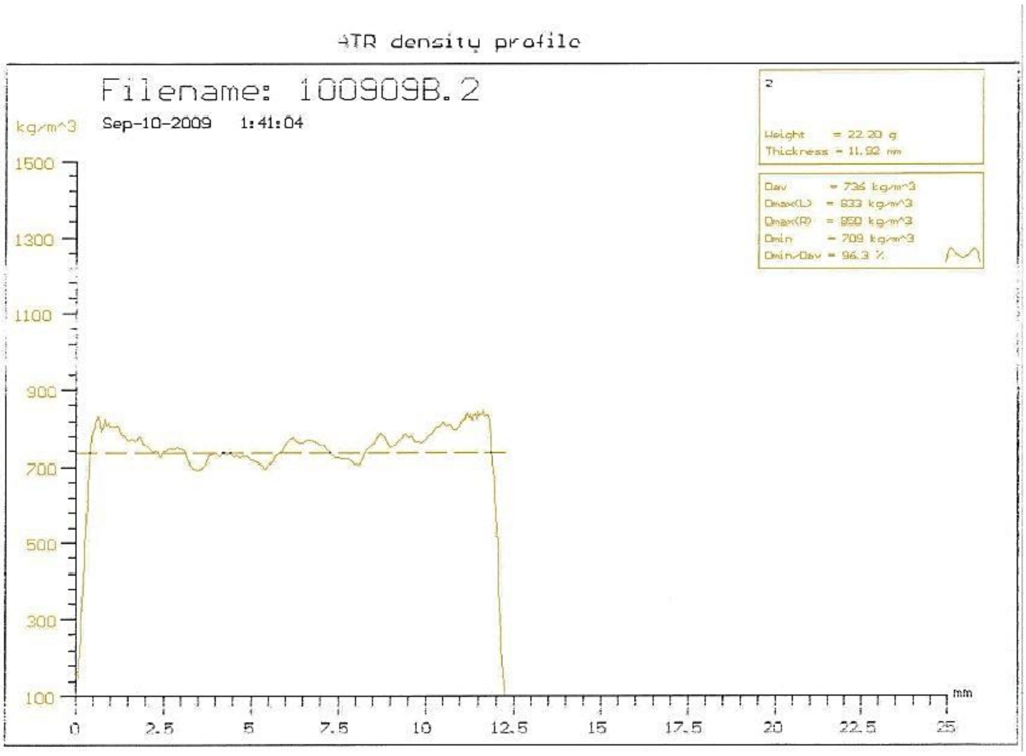

Figure 49. Density profile for sample IP24B, pressed at 210 °C for 11 minutes.

Bonding is clearly a critical issue for strength development within the boards and for good integrity of each panel in retaining its structure after pressing, and, for example, during the water soak necessary for thickness swelling tests.

7.2. Batch 2 using lower viscosity Silicate and R100 binder

The second batch of panels pressed used two different silicates, which had lower viscosities (250-500 cP compared to 2,000 cP for the binder used previously). One was a sodium silicate (C0079) and the other was a potassium silicate (K120). It had been shown from the development of biosilicate using ash from straw-fired electricity generation, that a potassium silicate would be a better model for the final product.

Once again, the panels formed were tested in three point bending and internal bond strength, and no significant improvement was seen. Although the IB strength of panels IP34 to IP44 was improved (now ranging from 32 to 66 N at maximum load) this was still too small an IB strength (0.023 N/mm^2) for the target particleboard grade. These panels are made with potassium silicate. The Crystal 0079 binder gave rise to lower IB values, more consistent with those seen for C0120 in the previous experiment. This confirmed the move to potassium silicate for future studies.

The K120 panels had been produced using pressing times ranging from 7 to 12 minutes at 200 °C. The strength did appear to increase with press time, although the difference was very small. In addition, another set of panels using K120 used 180 and 190 °C at 12 minutes press time, to compare the influence of temperature. Boards pressed at 180 °C (23.8N at max load) were significantly weaker than those pressed at 190 °C (39.65 N) and at 200 °C (43.72 N). This low strength for panels produced at 180 °C was despite these samples having the highest density of the three groups under comparison (701.9 kg/m^3 compared to 660.4 kg/m^3 and 670.1 kg/m^3). Density is often correlated to strength, so the lack of commensurate improvement indicated issues with bond development in these boards.

When K120 binder was used with a 10 minute press time, the difference in strength with temperature increased its effect, as the 190 °C samples had strengths of 18.85 N at max load. An experiment using C0079 at 210 °C had also been conducted, which showed a decrease in strength for panels pressed for 12 minutes at this temperature. For future studies the optimal temperature range is considered to be 200 °C, with press times of at least 10 minutes but preferably longer. This is not ideal for an industry where conventional press times are considerably shorter than this.

A further set of samples were tested using a higher level of hardener addition, at equivalent conditions to regular boards, to attempt to improve strength. These high hardener content boards were made at 190 °C for 10 minutes, and at 200 °C for 10 minutes. The internal bond strength remained low for the boards with additional hardener (Table 35), and in fact was lower than had been observed in boards pressed with a normal hardener addition rate at 200 °C for 10 minutes.

Table 35. Mean values for maximum load during internal bond strength test, and density for panels made with regular and high hardener quantity. Standard deviation shown in parenthesis.

Temp (^{o}C)	Max load (N)		Density (kg/m^3)	
	Normal	High hardener	Normal	High hardener
190	18.84 (5.93)	16.99 (3.51)	625.48 (28.09)	623.08 (64.60)
200	43.30 (15.78)	20.17 (4.76)	664.31 (82.19)	630.24 (60.25)

It became obvious that alternative hardener systems, and various options for particle surface improvement, were needed to make progress in terms of strength, and to produce a competitive press schedule.

7.3. Alternative hardener types[*]

Work at the University of York led to investigation of milk (full and semi skimmed) and milk powder as a bio-derived hardener for the silicate binder. It was proposed that the protein would react at elevated temperature, and along with other components within the milk such as lactose and calcium ions, would initiate the hardening process. Small panels produced in York showed higher internal bond strengths than had been recorded thus far; values between 122 N to 471 N were recorded at maximum load, which equate to IB strengths of approx. 0.0488N/mm^2 to 0.1884N/mm^2. This is a step change compared to the panels produced with R100, and a full trial was devised. Semi-skimmed milk was selected for trials in Bangor.

A trial was conducted on the small press using a 300 x 300 mm former in Bangor. Semi-skimmed milk and milk powder were used as the hardener. The press temperature was 190°C and a time of 12 minutes for the first set of boards, and then the temperature was increased to 200 °C for additional panels. Boards made with semi-skimmed milk, and with milk powder made up as per the packet instructions, blew apart within the press (Figure 50), indicating high core gas pressure, and poor bond strength within the core of the panel. The milk powder was then used at high concentration, first by omitting one third of the required liquid, then by omitting two thirds of the liquid.

Figure 50. Delamination in the midline of a milk hardener board which had blown when the press opened. This is sometimes only visible once the panel is cross cut for quality checks, as shown.

---

[*] to be read in conjunction with section 2.4.5

Where the milk powder was used at the highest concentration, no blow was detected, whereas the intermediate with only two thirds liquid still blew. A board with milk produced at 200 °C also blew, so only the low liquid content milk powder option was tested at 200°C, and made a good panel. The furnish moisture content, evaluated just prior to pressing, was 34% for the panels with semi-skimmed milk, but only 26% for the one third liquid milk powder recipe. This is a significant reduction in total liquid present, reducing the potential for delamination or blows during pressing.

Internal bond strength tests showed that the milk powder with one third liquid worked well, giving and average IB strength of 0.074 N/mm^2 for the 190 °C press, and 0.084 N/mm^2 for the 200°C press. The recipe used for this set of panels used 16.71% resin solids, with milk solids being 12% for the total resin solids. The target density was 624 kg/m^3.

A second trial was done using wheat straw and oilseed rape straw using the University of York recipe; all panels were produced at a temperature of 200 °C and for 12 minutes press time. A typical press temperature and pressure graph for one of the wheat panels is shown in Figure 51. The core temperature increased steadily to approx. 125 °C within the first 150 s after press closure (closure occurs at 60 s on the horizontal axis). Within that period, the core gas pressure increased to approx. 0.3 psig.

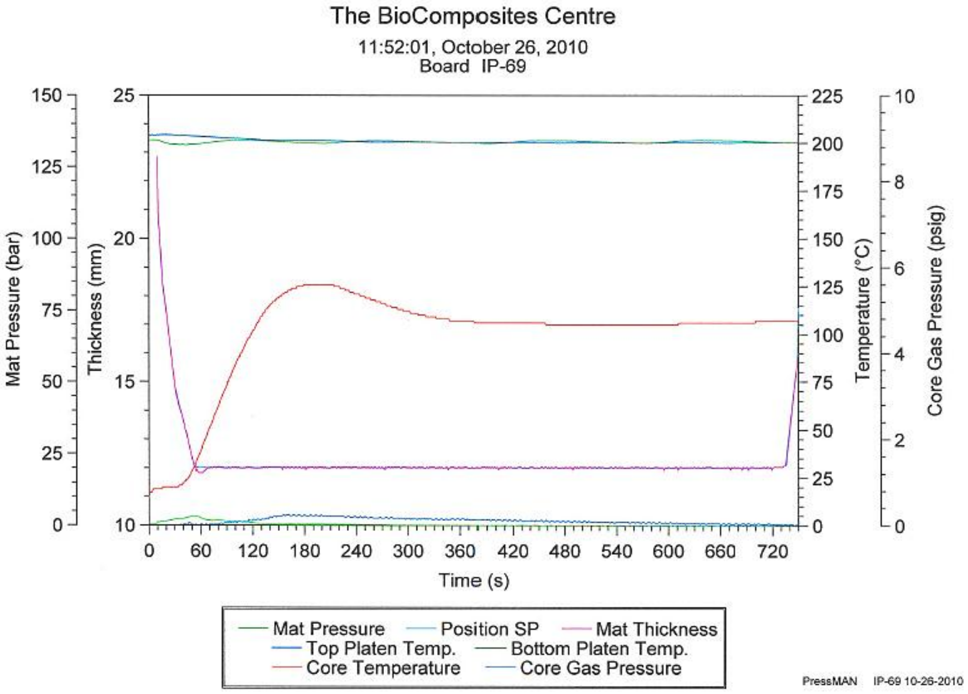

Figure 51. Press profile for wheat straw board produced with potassium silicate and milk as hardener.

This temperature and pressure profile was fairly typical for 300 x 300 mm panels. The decrease in core temperature which follows is due to evaporation and loss of the initial influx of steam as this travels to the board edges to exit, with subsequent temperature remaining near 100 °C due to steady movement of new steam evaporating from the particles and binder. Thus although press closure time can be controlled, the temperature in the core will remain near the boiling point of water until all the moisture is liberated.

Table 36. Internal bond strength and density for panels produced with milk as hardener. Standard deviation shown in parenthesis.

	Internal Bond strength (N/mm^2)	Density (kg/m^3)
Wheat	0.0425 (0.005)	631.56 (29.94)
Oilseed rape	0.18 (0.014)	625.80 (25.94)

Note that the internal bond strengths had improved sufficiently to use the correct units in reporting this parameter by using milk as hardener (Table 36). Two samples which had been produced on the York press were also tested and recorded IB strengths of 0.27 (C062, using whey protein) and 0.45N/mm^2 (C068 using waste milk).

The samples in the above table were conditioned for two weeks at 20°C and 65% relative humidity as is standard for particleboard tests. Two additional samples from each of the same panels were tested on the day of pressing, and showed average IB strengths of 0.035 N/mm^2 (wheat) and 0.155 N/mm^2 (OSR). It appears that the conditioning period may assist with continued bond cure, so testing under the standard conditioning regime will continue.

On transferring the milk powder recipe to the large press and drum blender system at BC's Tech Transfer Facility, it was found that the milk was a very efficient hardener for silicate, and blockages rapidly occurred in the spray system for the drum blender. A twin bomb system was therefore used to spray the binder and the hardener through separate nozzles into the straw particles within the drum blender.

The 500 x 500 mm panels produced on the larger press showed similar internal bond strengths to the 300 x 300 mm panels reported above. The highest internal bond strength was seen for the panel pressed at 200 °C for 10 minutes (0.034 N/mm^2). However comparable performance was seen in panels produced at 190 °C with 12 minutes in the press (Table 37).

Table 37. Mechanical properties of samples cut from panels made with potassium silicate and milk powder as hardener in the large press.

Press temperature (^{o}C)	Press time (minutes)	Panel(s)	Average density (kg/m^3)	Internal bond strength (N/mm^2)	MOR (N/mm^2)	MOE (N/mm^2)
190	10	IP78, IP79, IP80	628.74	0.035	6.24	1297.90
190	12	IP76, IP77	674.37	0.028	6.07	1244.45
200	10	IP81	722.43	0.040	5.52	1208.95
MDI binder		IP73, IP74, IP75	617.268	0.450	15.79	2198.37

Three panels were produced with polymethylene diisocyanate (pMDI or MDI) using 190 °C and 5 minutes. These conditions are not idealised for MDI binders, but for simplicity the press schedule was kept to a truncated version of the schedule used for silicate systems for comparability. The mechanical properties for these panels are reported in the same table.

7.4. Optimising for two substrate types – wheat and oilseed rape

A large production trial was planned using the K120 potassium silicate binder, and milk powder made up with one third water as hardener. For this trial, the straw was sourced from a single large bale of Viscount straw (Figure 38). A second matrix was drawn up for preparing boards with the same binder formulation in oilseed rape straw (Table 39), sourced from a single half tonne bale.

Table 38. Press time and temperature for wheat straw panels, percentage values indicate the moisture content of the furnish, measured after resination.

Temp (^{o}C)	Time (minutes)				
	7	8	9	10	12
190			IP95 35.3% IP96 35.3%	IP94 35.3%	
200	IP101 35.1% IP102 35.1%	IP99 34.1% IP100 35.1%	IP97 34.1% IP98 34.1%	IP91 33.9% IP103 35.1% IP104 35.1%	IP92 33.9% IP93 33.9%
210		IP107 32.3%	IP105 32.3% IP106 32.3%		

Table 39. Press parameters for the oilseed rape straw panels with silicate and milk powder as the binder and hardener system.

Temp (°C)	Time (minutes)		
	9	10	12
190	IP-84 36.6% m.c.	IP-82 36.6% m.c. IP-83 36.6% m.c.	
200	IP-89 38.6% m.c. IP-90 38.6% m.c.	IP-87 40.3% m.c. IP-88 38.6% m.c.	IP-85 40.3% m.c. IP-86 40.3% m.c.

A further study was performed using whey powder as the hardening agent in potassium silicate bound wheat straw boards. The main formulation used 18.4% resin solids, with the hardener being 21.87% of the total resin weight. For the low hardener formulation, the resin solids content dropped slightly to 17.70%, and hardener was set to 17.79% of the total resin weight.

Table 40. Press parameters for wheat straw panels produced with whey protein as the hardening agent for potassium silicate.

Temp (°C)	Time (minutes)		
	8	9	10
190		IP-110 37.8% m.c.	IP-108 37.8% m.c. IP-109 37.8% m.c.
200	IP-118 38.0% m.c. IP-119 38.0% m.c.	IP-113 37.8% m.c. IP-117 38.0% m.c.	IP-111 37.8% m.c. IP-112 37.8% m.c.
200 low whey recipe		IP-116 26.6% m.c.	IP-114 26.6% m.c. IP-115 26.6% m.c.

Further wheat straw panels using higher target densities or different ratios of milk powder were also investigated. One set of boards were also made using straw which had been dewaxed on the large scale. The furnish moisture content was measured as 46.6% using the same bench-top moisture meter as had been used for all production batches reported in the Tables 38–40. There was no physical difference in the moisture content of the straw, or the quantity of binder and hardener added, so the difference in apparent furnish moisture is possibly related to differences in the rate of moisture loss (related to differences in cure characteristics).

7.5. Testing and physical properties

7.5.1. Wheat straw boards with milk powder as the hardener

The data from the optimisation study using milk powder as the hardener did not reveal large changes in mechanical properties within the range of parameters tested. For example, the Modulus of Rupture and Modulus of Elasticity data from three point bend tests are presented in Tables 41 and 42. The values observed for both bending strength properties were consistently lower than the target value for a 12 mm panel. The requirement for a P3 panel is 15 N/mm^2 (MOR) and 2050 N/mm^2 (MOE), and for P1 is 12.5 N/mm^2 (at this grade only the MOR is specified). The MOE observed in 500 x 500 mm panels was also lower than had been seen in 500 x 500 mm panels produced for the initial milk experiments. No reason for this difference could be found.

Table 41. Modulus of rupture for wheat straw boards using milk powder as the hardener system.

Temp (^{o}C)	Time (minutes)				
	7	8	9	10	12
190			4.20 sd 0.44	4.17 sd 0.26	
200	3.62 sd 0.30	4.49 sd 0.52	4.98 sd 0.43	4.27 sd 0.29	4.06 sd 0.57
210		3.76 sd 0.34	4.07 sd 0.25		

Table 42. Modulus of elasticity for wheat straw boards with the potassium silicate and milk powder binder system.

Temp (^{o}C)	Time (minutes)				
	7	8	9	10	12
190			881.75 sd 145.45	879.25 sd 33.98	
200	749.88 sd 87.60	827.88 sd 93.05	946.00 sd 89.62	832.08 sd 65.25	853.25 sd 118.89
210		819.75 sd 74.15	887.25 sd 48.58		

Unfortunately, the level of scatter within sample populations, combined with relatively small differences in the average values for each population, mean that there is no outstanding option for increasing panel performance within the matrix of parameters studied. For example, it may be possible to reduce the press time to 9 minutes using a temperature of 200 °C, however there will be no additional strength benefit, simply a process efficiency benefit.

The data from internal bond strength tests showed a similar lack of trends and, as all values ranged from 0.02 to 0.04 N/mm^2 (compared to a target value of 0.45 N/mm^2), the problem of poor internal bond strength for wheat straw boards remained a concern.

Thickness swelling tests (24 h, according to EN 317) were done for these panels and due to previously observed high swelling levels, a two hour swelling test was also used. The two hour test was included to attempt to identify the more promising boards and press conditions, *i.e*. those with some degree of resistance to short term moisture uptake.

All panels, including the three made with MDI binder in the preliminary study, failed the 24 hour thickness swelling test. The MDI panels had thickness swelling of 27.17% (standard deviation 1.52). Swelling seen in wheat straw panels was higher, with individual values ranging from 39 to 60%. There was also significant scatter within the sample population from each set of panels, making analysis of trends between pressing conditions difficult. Unfortunately, there was also significant scatter in the thickness swelling data from 2 hour swelling tests, which prevented selection of optimal conditions.

7.5.2. Oilseed rape boards with milk powder as the hardener

The internal bond strength data for the oilseed rape panels showed very little difference with the pressing conditions. Values for individual samples ranged from 0.01 to 0.05, however, no panel contained more than two high values (often at the central locations within the panel). The panels produced with 200 °C press and 10 minutes press time had the greatest average value for IB strength, 0.028 N/mm^2, however this remains too low to meet performance requirements.

No difference was seen between different pressing conditions for oilseed rape particleboard Modulus of Elasticity (MOE) and Modulus of Rupture (MOR) in three point bending tests. Average values of MOR ranged from 4.18 N/mm^2 to 4.24 N/mm^2 for times of 9 and 10 minutes at 190 °C and 200 °C. For MOE the average values were also close, 853 to 891 N/mm^2, which is very low. A small decrease in bending strength was seen for the 12 minute panels, MOR 4.11 N/mm^2 and MOE 843 N/mm^2.

24 hour thickness swelling in oilseed rape straw panels was lower than in wheat straw panels, and many values compared favourably with the MDI wheat panels produced as control samples (Table 43, compared with 27.17%, SD 1.52).

Table 43. Percentage thickness swelling after 24 hour water soak, standard deviation shown in parenthesis.

Temp (^oC)	Time (minutes)		
	9	10	12
190	26.67 (3.35)	27.76 (5.17)	
200	24.22 (4.75)	21.57 (5.13)	26.32 (5.10)

However, in the 2 h thickness swelling tests, the oilseed rape straw panels swelled to a greater extent than the MDI control samples, typically 14 to 16% compared to 5.59% (SD 1.32) for the MDI panels.

If the reduced thickness swelling for OSR panels is indicative of a better cure, this is likely to relate to particle geometry – with thicker particles leading to a more permeable mattress during pressing, to enable transport of moisture across the thickness and through the width of the panel, facilitating cure. In the case of silicate, the cure relies on driving moisture out of the binder during precipitation or gelling. The rate can be limited if vapour pressure around the curing binder droplets is already high, tipping the equilibrium and limiting the rate of extra moisture evaporating.

However, note that the improved thickness swelling was not accompanied by improvement in internal bond strength or bending strength, so some of the effect may relate to the oilseed rape particles forming a mattress which will naturally swell less. This is due to a smaller number of thicker particles requiring a different quantity of binder or reduced inherent spring-back due to easily compressible pith regions within the oilseed rape straw.

A trend was seen within the 24 h oilseed rape thickness swelling data, for samples from specific locations within the panel to swell more than samples from elsewhere in the panel. This trend was clearer in oilseed rape panels than in wheat straw panels, where other factors may influence bond quality. It also contributed to the relatively high standard deviation values reported in Table 19 above, as the difference based on location was up to 12%.

Samples for thickness swelling were taken from two 50 mm strips, 50 mm away from the midline, one on each side of the panel (Figure 52).

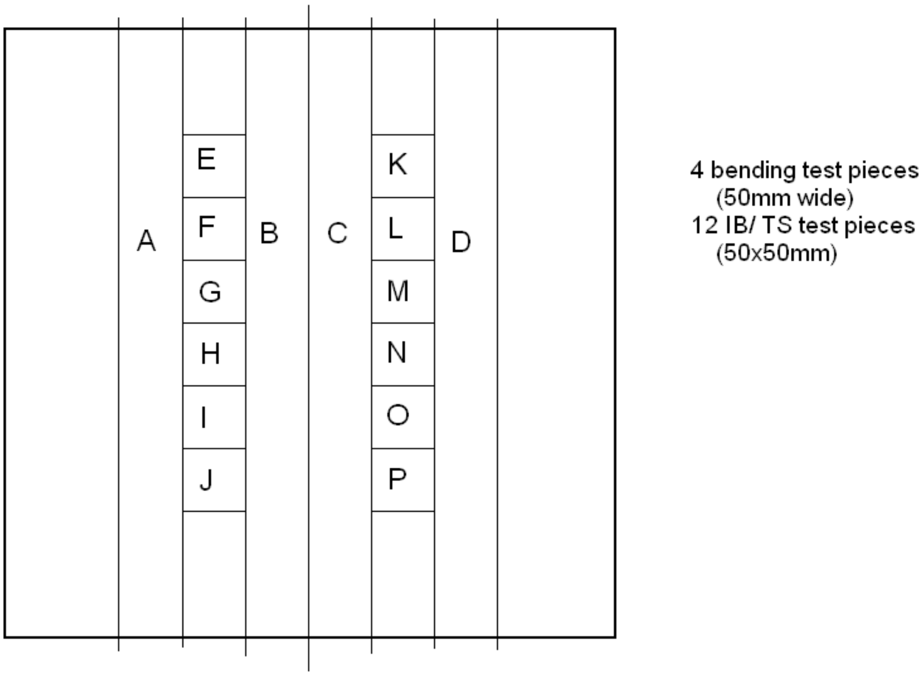

Figure 52. Cutting pattern for 500 x 500 mm boards used in this study.

Of the available six pieces in one row, three were used in internal bonding, but samples F, H, J, K, M and P were soaked for thickness swelling. Of these, F, J, K and O (further from the centre) tended to have higher swelling values than H and M. The degree of resin cure may, therefore, be highly dependent on location within the panel, and more importantly, the distance from the edge (relating to the dominant moisture transport route).

Comparing the average values from the centre-most samples of each batch indicated that the 200 °C pressed panels performed best, with the 10 minute press schedule being 17.01%, the 9 minute schedule 21.69% and the 12 minute schedule being 22.42%. There is therefore little scope for further improvement in properties by altering press conditions, as the better option is already in use. The intention of shortening press time to increase productivity will rely on alterations in hardener, additives or straw pre-treatment.

7.5.3. Wheat straw with whey powder as the hardener

A set of panels were also produced with whey powder as the hardener, and these gave only a very small improvement in internal bond strength (ranging from 0.02 to 0.05 N/mm^2), and had lower thickness swelling than the milk powder hardener set of boards (individual values ranged from 34 to 39%). While both of these observations are an indication of progress, the values remained outside the acceptable limit for particleboard. Also, the thickness swelling values remained higher than for oilseed rape panels, potentially indicating that the wheat straw substrate is a contributor to the difficulties encountered.

7.5.4. Other milk powder experiments

Various other experiments, with different quantities of milk powder in wheat straw panels and different concentrations of the milk powder solution, all failed to show any significant alteration in internal bond strength or thickness swelling.

7.6. Trials with dewaxed straw

Trials were conducted with dewaxed wheat straw. The trials in both the 300 x 300 mm press and the 500 x 500 mm press showed a reduction in panel performance rather than the intended improvement. Panels on the 500 x 500 mm press had almost delaminated in the core, but retained some strength. The three point bending tests did show and increase in MOR to 8.12 N/mm^2 and MOE of 1481.88 N/mm^2. These values are just over half of the target performance value, which is a great achievement.

There was however, a relatively low density core, which meant that while some samples in internal bond strength tests reached values of 0.07, others remained low at 0.01 or 0.02 N/mm^2. The average for panels pressed at 200 °C for 10 minutes was 0.038 N/mm^2. This represents a significant improvement compared to early board results, but remains symptomatic of very poor stress transfer between upper and lower faces. The patchiness of internal bond strengths indicates that localised good bonding is occurring, but that issues relating to core gas pressure or issues such as spring-back after press opening are still significant.

Thickness swelling in dewaxed straw panels was the worst seen to date, with the lowest value being 47%, and the highest 92%.

7.7. Press conditions, moisture content and core gas pressure

As the various options for hardener systems for silicates in wheat straw particleboard had led to only a mid-range improvement in properties, it is important to consider the effects that this novel binder system is having on the structure of the panel during pressing. Examination of the press profile graphs from the large scale experiments revealed that the core gas pressure had been significant at the time of the press opening (Figure 53).

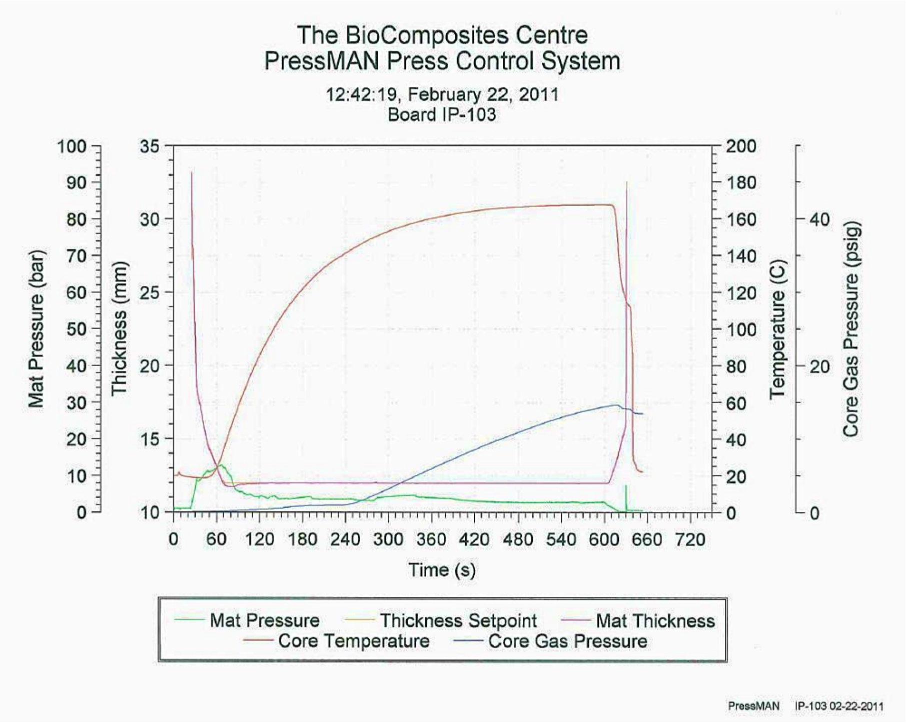

Figure 53. Press profile for wheat straw panel pressed at 200 °C for 10 minutes.

The steady build-up of core gas pressure in this panel accompanies a core temperature of 160°C, which is higher than had been seen in the earlier reported studies where temperature dropped to equilibrium with moisture evaporating from the binder at just over 100°C (relating to latent heat of evaporation). This data was gathered from the larger press, and a freshly purchased probe was used for the experiments.

A high core gas pressure at the end of the press cycle leads to the likelihood of blows developing when pressure is released. In this panel the delamination was not severe enough to prevent testing, but a very low density middle region was visible in all panels from this large scale experiment. Issues with core gas pressure gain increased severity as panel size increases, due to the additional distance required for moisture to travel from the centre to the edges (first order), and the proportionally larger increase of moisture present (a function of area, i.e. second order).

Part of the issue is the dimensions of the straw particles, which lead to a very lightweight, but lamellar lay-up, with relatively small gaps between particles in any vertical cross section. The second is the quantity of moisture present in the panel, and although the reduction in milk liquid had brought this as low as possible and remained within the working range for a 300 x

300 mm panel, this (combined with the large quantity of liquid in the silicate) is likely to lead to core gas pressure issues on a larger scale.

The development of core gas pressure shown does indicate that moisture is being driven out of the silicate successfully, so the obvious question is whether additional time would complete the necessary de-watering for good cure to develop. This was not tested as early studies had shown that over-drying of the surface regions of the panel (in good contact with the plattens which are at 200 °C) led to darkening, and brittleness/problems in cutting.

7.8. Thoughts on adhesion, silicate cure state and reversibility

Sodium and potassium silicates are solutions containing SiO_2 and Na_2O or K_2O in various ratios. The solids content (or moisture content) can have a strong influence on the behaviour of the material during drying, as can the temperature experienced during drying and the duration of that temperature. For example, Roggendorf *et al.* (2001) reported experiments where different temperatures and durations led to formation of transparent solid product, a cracked solid or a crystalline solid, at temperatures from 30 to 100 °C and a period of up to 100 days. They concluded that the colloidal sols experience gradual solidification within this temperature range and may retain a moisture content of 45 to 12% while in the glassy transparent solid state. The size of colloidal particles differed with drying rate and initial moisture content, as is further explained in Iler (1979)

During adhesion experiments for direct bonding of straw pieces at atmospheric conditions, and in the oven at 105 °C, the silicate was observed to form a white, slightly granular but also flakey solid structure. This is consistent with drying in a situation where the material passes into the solid cracked state described by Roggendorf *et al.* (2001). Board faces were also observed to contain silicate aggregate droplets on the surface which adopted various forms during the board cure process. Immediately after leaving the press these droplets may have been glassy in structure, but after a period continuing to cure at room temperature, the form changed to a granular white structure.

The data collected by Roggendorf *et al.(*2001) for sols which had been dried to just inside the solid state, with a density determined as 1.56 g/cm^3. This information was used to calculate the density of the solid silicate colloidal material as 2.24 g/cm^3 present within in a material which still also contained a solution phase, and where the solution density was estimated to be 1.05 g/cm^3. This glassy material, at the point of solidification had been observed to have a water content of 50%. Further loss of solvent requires a reorganisation of the aggregate structure, and a disappearance of the voids between the primary colloids. As loss of water continues, this reorganisation may lead to cracking (at higher temperatures) or a crystalline form if drying is slow. The cracking could be one explanation for the observed increase in whiteness of the silicate droplets on the surface of the panels, upon aging.

Density data for all generic types of silicate are presented in Iler (1979) and are known to range from 1.99 to 2.93 g/cm^3 with melanphlogite being the lowest density, closely followed by amorphous silica and ranging through tridemite, crystobalite, keatite and quartz to coesite. Stishovite is a much higher density silica material, at 4.30%. Both melanphlogite and amorphous silica have a range of densities rather than an absolute value, and the value calculated by Roggendorf falls within the expected range for colloidal silicas (2.1 to 2.3 g/cm^3). Quartz, tridemite and crystabolite have two crystalline forms, and therefore two densities. However, in this project, the silicate of interest is the amorphous form, colloidal silicates and silicate anions, all of which exist in equilibrium in high pH solutions.

$(SiO_2)_x + 2\ H_2O = Si(OH)_4 + (SiO_2)_{x-1}$

$Si(OH)_4 + OH^- = Si(OH)_5^-$ (or $HSiO_3^-$)

$Si(OH)_4 + OH^- = H_3SiO_4^- + H_2O$

The polymerisation behaviour of monosilicic acid ions is known to be similar to that of the gelling of sols, in respect of the effects of pH, presence of salts, and temperature (Iler, 1979). The formation of colloidal sols from higher molecular weight silicate solutions and dissolution/deposition of solid silicate can therefore be considered together within this project. The addition of an ester as hardener for the first set of experiments (R100) uses a change to lower pH as the solidification mechanism, coupled with elevated temperature within the particleboard during pressing.

There is, therefore, some interest in establishing the form of silicate which is induced under these conditions in order to understand the durability, performance and longevity of the adhesive bond. One experiment was to create small samples bonded directly with silicate (C0079) and hardener (R100) between straw particles. A second was to form droplets of catalysed silicate for curing under different conditions. A third was the use of straw particles generated during board manufacture to investigate by eye and using microscopy.

Samples of sodium silicate were dried at laboratory temperature to complete dryness during the course of the project (i.e. circa three years) and finished with a short spell in the oven at 105 °C. The white granular flaky material was then subjected to helium pycnometry to determine its density. This material was similar in appearance (and likely in crystal type) to the white resin spots which had been seen on the surface of panels pressed with R100 as hardener. It was suspected that this white form was a low strength material, with poor bonding to the straw particles.

Two samples were tested, and values of 2.0806 $g/cm^3$and 2.0730g/cm^3 were recorded. This value was of a similar magnitude to that calculated by Roggendorf *et al.* (2001) for the colloid phase. The small difference may relate to this being potassium silicate or indicate that during this very slow mode of drying, other effects, such as the formation of carbonates, have also occurred.

The particle to particle bonding experiments also generated this white form of silicate when bonding was left to occur at room temperature and the pieces of straw were easily detached from one another. Particle to particle samples which were formed in the 105°C oven were initially of transparent nature, but also aged to a white state on standing before it was possible to complete microscopy studies. The colour change indicated that there is some extent of reversibility in the silicate state if it insufficiently solidified. One hypothesis is that partial cure of the silicate in the press (for example due to incomplete moisture removal due to panel dimensional issues) has led to a reversible solidification reaction, where on ageing the silicate bonds convert to the low strength white state and lose integrity – leading to ageing effects seen in internal bond samples. The full experiment has not been reported, but populations of additional samples cut from adjacent pieces of panel at a later date tended to perform more poorly than the initial samples in the main cutting plan.

7.8.1. Resin distribution via Scanning electron microscopy

Particles of straw stem and leaf were observed for Humber, Gladiator and Viscount straws, to confirm the structural components present in the inner and outer faces (Figure 53a-b). Later, Scanning Electron Microscopy (SEM) was used to investigate resin distribution on sprayed particles from the batches prepared for board manufacture. Fracture faces from internal bond strength tests and segments cut from particleboard samples were also observed.

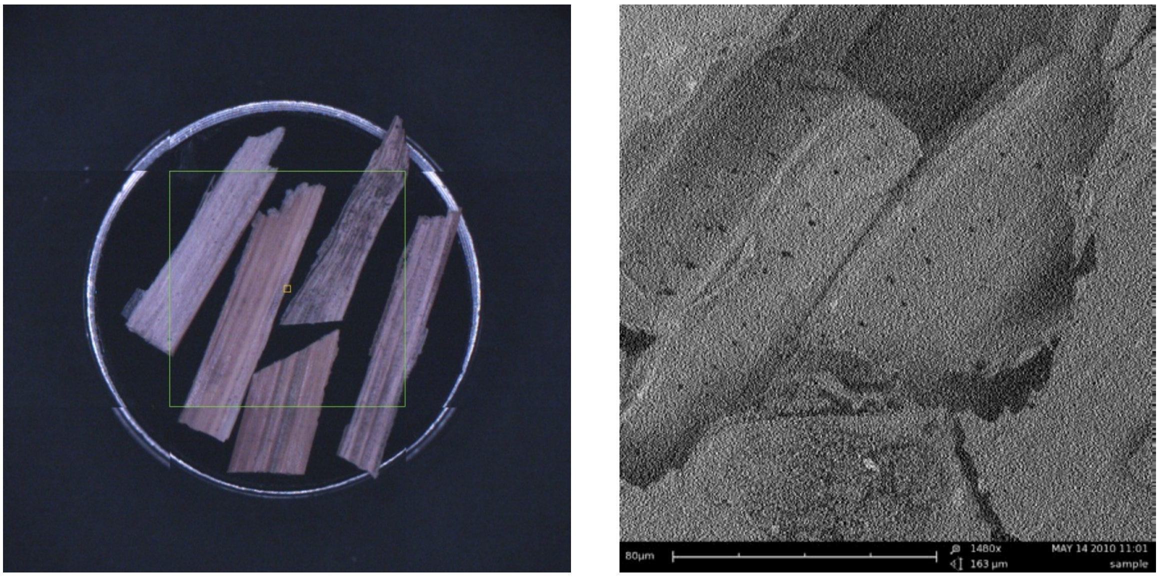

Figure 53a. Pieces of stem and leaf for Viscount straw prepared for scanning electron microscopy. 53b. Vessel and phloem cells within the stem piece, visible due to fracture of the surface.

The distribution of droplet sizes in particleboard is an important consideration in board manufacture, as the increasing fineness of resin mist applied to the chips or particles has a direct correlation with increase in number of particle to particle bond sites within the board. The droplet size was measured by SEM for several samples of straw which had been sprayed with silicate solution within the drum blender, for example see Figures 54, 55 and 56.

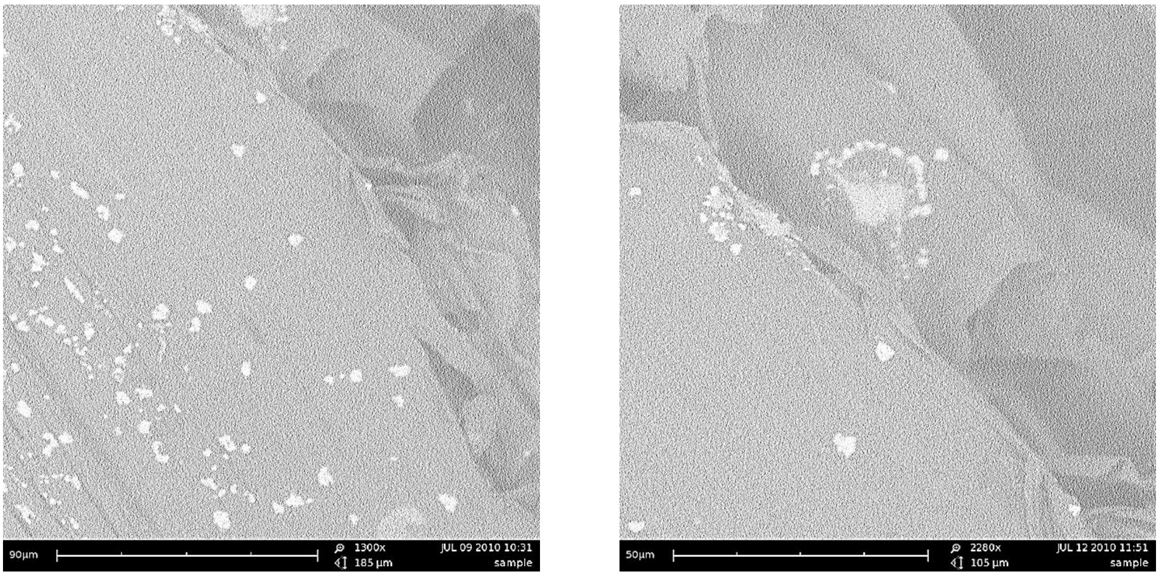

Figure 54a. Droplets of resin on the inner face of a straw particle. 54b. In some cases the droplet had splattered on landing to give a ring of smaller droplets.

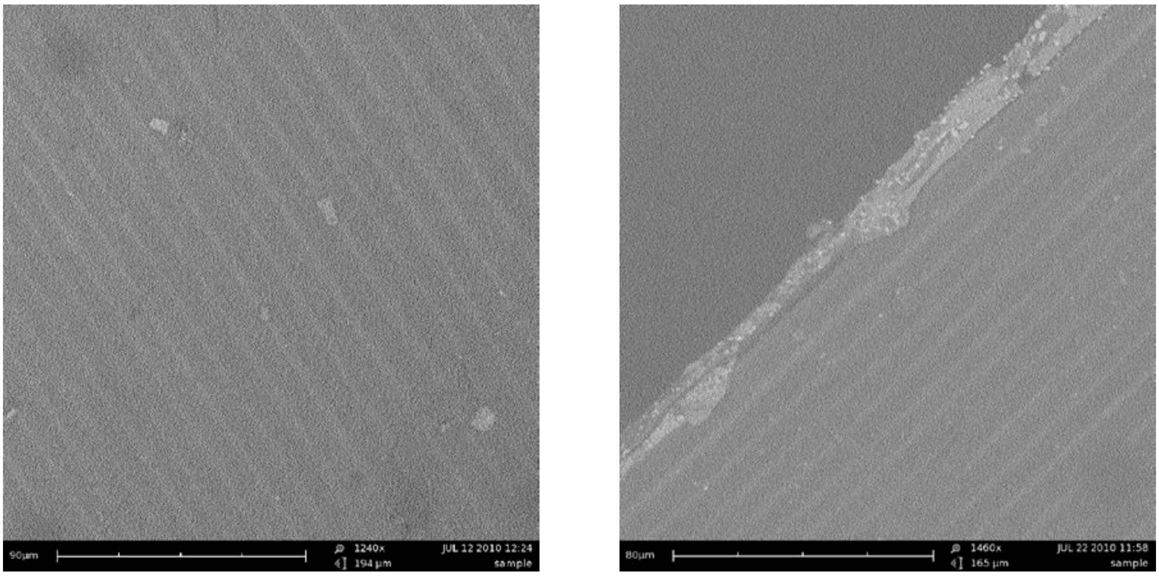

Figure 56a. Stem outer surfaces frequently showed no droplets of resin at all. 56b. Resin was sometimes observed preferentially adhered to features such as particle edges, or damaged locations on the particle.

The spraying of resin onto particles in the drum blender is dependent on the nozzle design, but also the viscosity of the resin itself. In the case of silicates used in this study, the viscosity was relatively high (e.g. C0120 at 2,000 cP at 20 °C and C0079 at 250 to 500 cP). Given this high viscosity and the shear thickening behaviour of sodium silicates(Kamke *et al.,* 2000), the droplets measured on the particles were surprisingly small. The median area for resin spots on the stem inner surface was 19.8 µm^2 (Figure 58). This is considerably smaller than the ideal droplet size for a typical UF resin. For this median droplet, a flattened droplet on the stem inner surface using an estimated value of 0.5µm as the thickness, would have a volume of 9.9µm^3, while the typical ideal range for a droplet in softwood particleboard would be 10 to 35µm^3(Yang *et al.,*2008). Droplets smaller than this, *i.e.,* all of the lower 50% of the population, are thought to be at risk of getting lost in the cell lumena of the particles and droplets larger than this waste resin by forming thick or inefficient bonds.

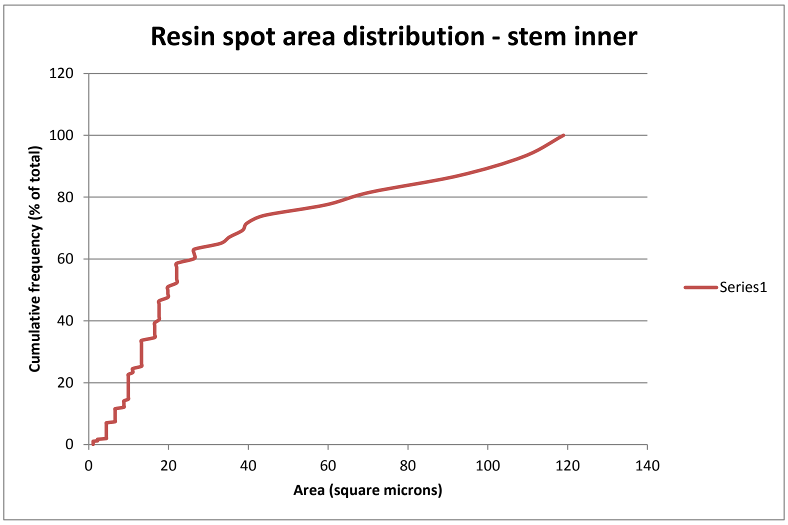

Figure 58. Area of resin spots as measured using SEM for a section of stem inner.

However, the droplets on the stem inner surfaces (Figure 24) were the exception to the rule. Droplets on the stem outer tended to be larger and much more varied in size and shape (longer thinner ellipses were typical, as were non-elliptical patterns). Often stem outer surfaces had no resin visible at all (Figure 56). On the leaf surfaces, the presence of a greater number of texture features, such as ribs and stomata (Figure 57), led to droplets forming shapes which adapted to the contours present and were, again, larger than those seen on the stem inner. It appears likely that many droplets, if hitting a stem outer face or a leaf face, would be shaken off during the tumbling process unless they collided with a textured portion of the substrate.

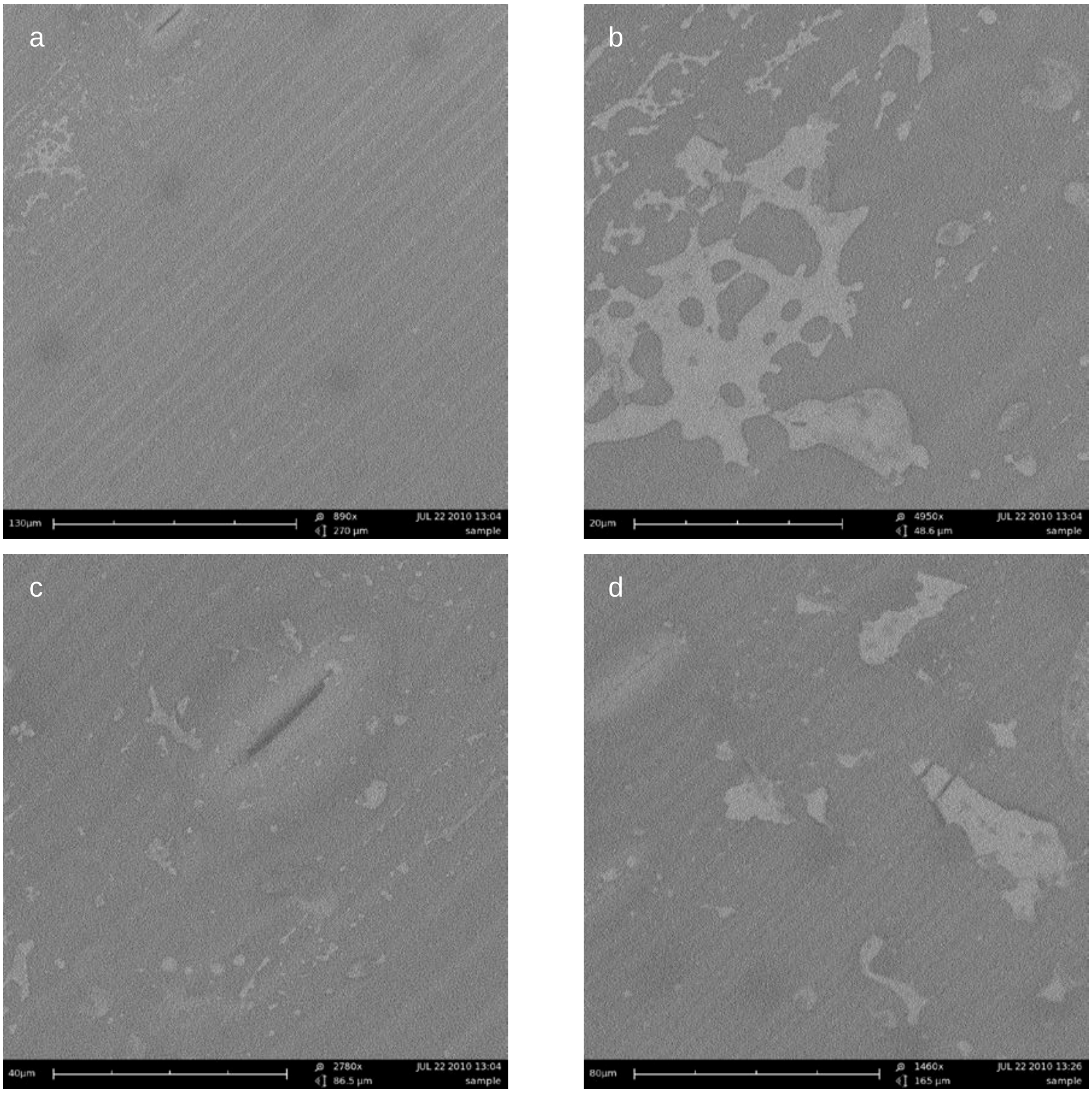

Figure 57a. Resin on leaf particles was observed more frequently than on stem outer, but was again associated with textural elements such as stomata. 57b. The resin was sometimes distributed as a smear rather than a single droplet, as if wiped off, and only the portion which could adhere to a textured region had remained. 57c. close up of stomata with resin. 57d. binder droplets adhered across ribbed structure of leaf, which led to linear crack formation.

It was mentioned previously it was known that some very large droplets of silicate formed during drum blending, which led to large silicate spots on the panel surface (Figure 59). These were too large to measure using the microscope, and ranged in size from approx. 6 x 4mm to 24 x 20 mm, with the more frequent size range being 11 x 9 mm.

Figure 59. Surface of particleboard sample, showing size of resin spots formed due to snowball effect within drum blender.

The lack of textured features for adhesion, or of surface energy to allow good contact, on the waxy straw outer face are likely to have contributed to this, with droplets being shed easily during blending. The large droplets could also be due to the high viscosity leading to some problems in atomisation at the nozzle, or due to collisions between resin droplets or resinated particles during flight, giving rise to a snowball effect. Dust and particle fragments were frequently observed to be intimately mixed with these resin spots on the board faces and the resin droplet clumps seen during handling the furnish to make the panel. This issue can be resolved by adjusting flow rate and nozzle design once the ideal resin and combination has been defined and resin solids content of the panel optimised for board properties. It is also likely to be better controlled in a blowline situation as may be used in the more MDF-based process in some straw board production units.

8. COMMERCIAL MANUFACTURE OF BOARDS (COMPAK)

The conclusion of the work conducted at York and Bangor enabled Compak to manufacture boards at their operation in China.

CS Process Engineering's Compak System board making production System is the only fully proven technology for the manufacture of board products using agri-waste materials. To date over 30 Compak System production lines have been delivered worldwide, of which seven are in China. As part of the LINK project, CS Process Engineering had arranged for production trials of York University's silica based resin to be carried out on a Compak line in China (Figure 60).

Figure 60. Compak line in Tongling, China

A silica based resin was received at the Compak System agri-board plant located at Tongling, China. The resin was to be used in production board making trials as a partial replacement for MDI resin using wheat straw as board raw material. Percentage resin mix was discussed with Bangor University and agreed as follows:

- 2.5% solids MDI
- 2% solids silica resin
- Board pressing cycle was to be as MDI.

Boards of 12 mm and 18 mm thickness were to be made (Figure 61). Production preparation, actual production and then subsequent cleaning of equipment took approximately one week per board thickness. Particular care had to be taken cleaning resin systems after use of the silica resins because of their alkalinity – risk to metal pipework. Two thicknesses of boards were produced and prepared for shipment from China to UK. Unfortunately B & Q were unable to arrange a China Customs export permit for the boards and so only small samples could be hand carried to UK. It should be noted that additional board samples still remain in stock in Shanghai for carriage to UK if required/carriers can be arranged.

Figure 61. Finished boards from production line

9. CONCLUDING REMARKS

The overall aim of this project was to study the reutilisation of the major ash components, predominantly silica and potassium, in wheat straw combustion residues to form alkali silicate binders for novel inorganic composite boards comprising agricultural straws.

Initial tests on a laboratory scale were carried out on one variety of wheat straw. This work showed, for the first time, that the inherent alkali in unleached wheat straw was sufficient to solubilise up to 25% of the silica in the ash at room temperature. Combustion of wheat straw at temperatures below 600 °C gave the highest silica extraction by producing the most alkaline solutions, preventing calcium solubility and maintaining silica in a less crystalline form. Silica extraction was significantly increased by leaching under reflux. Optimised silica extraction, using only the inherent alkalinity, was achieved at combustion conditions of 500 °C for 2 h, with leaching under reflux giving a silica extraction of 36%. Under these optimised conditions comparisons were made between different wheat straw varieties and straw collected in different years. This demonstrated that the straw varied in its initial inorganic composition, mainly dependent on their year of growth and, specifically, the level of rainfall causing the *in situ* leaching of soluble species. This initial composition influenced their combustion and pyrolysis decomposition, mineralogical ash composition, leaching of inorganic components, silica structure and alkalinity, which further affected silica extraction.

Wax extraction by Soxhlet and supercritical CO_2 ($scCO_2$), water washing and acid washing were successfully applied as pretreatment methods to study the impact on the thermochemical, mineralogical and ash extraction analysis. Water washing and acid leaching demonstrated similar results to those found by previous researchers with substantial removal of inorganic species, however, acid leaching was required to significantly increase the ash fusion temperature. $scCO_2$ treatment had the smallest impact on the straw for thermochemical purposes, whilst ethanol extraction produced a reduction in K and Cl content similar to that achieved by water washing. This is believed to be the first reported observation of this effect. Pretreatment of straw by ethanol extraction prior to combustion therefore potentially provides an economic benefit by removing salts which could be recovered as fertilisers and valuable lipids without reducing the extraction of silica utilising the inherent alkalinity of the ashes.

The extraction of silica from the combustion residues from a commercial facility burning miscanthus straw was achieved utilising a highly alkaline potassium hydroxide solution. The extraction could be controlled to produce a solution of similar concentration and ratio to the commercially available potassium silicate solutions. Initial tests also suggested that a concentrated alkaline solution could be formed from the fly ash. This could dissolve some of the silica within the bottom ash; however, it was not sufficiently alkaline to dissolve the majority. The solutions produced using potassium hydroxide were tested as binders for the formation of inorganic composite boards with a wheat straw substrate. The results for the internal bond strength and water swelling were promising.

Overall, it has been demonstrated that alkali silicate solutions can be formed from biomass combustion residues and that these can be used as a binder for inorganic composite boards, however, there may be insufficient inherent alkalinity within the biomass to form entirely bioderived solutions. In addition, the straw must be dewaxed and the formulation must contain a hardener/binder most likely derived from a waste protein-containing source.

10. REFERENCES

Al-Akhras, M. and Abu-Alfoul, B.A. *Cement Concrete Res.*, 2002, **32**, 859-863.

Anastas, P. and Warner, J. *Green Chemistry: Theory and Practice*, Oxford University Press, Oxford, 1998.

Arvelakis,S., Frandsen, F.J. and Dam-Johansen, K. *J. Therm. Anal. Calorim.*, 2003, **72**, 1005-1017.

Arvelakis, S., Gehrmann, H., Beckmann, M. and Koukios, E.G. *J. Therm. Anal. Calorim.*, 2003, **72**, 1019-1030.

Arvelakis, S., Jensen, P.A. and Dam-Johansen, M. *Energ. Fuel.*, 2004, **18**, 1066-1076.

Barneto, A., Carmona, J., Alfonso, J.E. and Alcaide, L. *Bioresour. Technol.*, 2009, **100**, 3963-3973.

Bass, J.L. and Turner,G.L. *J. Phys. Chem. B*, 1997, **101**, 10638-10644.

Bass, J.L., Turner, G.L and Morris, M.D. *Macromol. Symp.*, 1999, **140**, 263-270.

Baxter, L.L., Miles, T. R., Miles, T.R, Jenkins, B.M., Milne, T., Dayton, D., Bryers, R.W. and Oden, L.L. *Fuel Process. Technol.*, 1998, **54**, 47-78.

Belle-Oudry and D. Dayton, in *Impact of Mineral Impurities in Solid Fuel Combustion*, ed. R. Gupta, Kluwer Academic / Plenum Publishers, New York, Editon edn., 1999, pp. 569-579.

Bio-based Chemicals, Renewable Feedstocks, Green Polymers, Less-toxic Alternative Chemical Formulations, and the Foundations of a Sustainable Chemical Industry; 2Q 2011, © 2011 Pike Research LLC, Boulder, CO 80302 USA.

Biomass Energy Centre, http://www.biomassenergycentre.org.uk/portal/page?_pageid=75,18521&_dad=portal&_schema=PORTAL, Accessed 15/03/11.

Biricik, H., Aköz, F., Berktay, I.I., and Tulgar, A.N. *Cement Concrete Res.*, 1999, **29**, 637-643.

Blander, M. and Pelton, A.D. *Biomass Bioenerg.*, 1997, **12**, 295-298.

Brown, I.D. and Shannon, R.D. *Acta Crystallogr. A*, 1973, **29**, 266-282.

Bryers, R.W. in *Impact of Mineral Impurities in Solid Fuel Combustion*, eds. R. Gupta, T. Wall and L. Baxter, Kluwer Academic / Plenum Publishers, New York, Editon edn., 1999, pp. 105-131.

California Air Resources Board, *Fact Sheet: Airborne Toxic Control Measure (ATCM) to Reduce Formaldehyde Emissions from Composite Wood Products*.

Casey, W.H., Kinrade, S.D., Knight, C.T.G., Rains, D.W. and Epstein, E. *Plant Cell Environ.*, 2004, **27**, 51-54.

Chindaprasirt, P. and Rukzon, S. *Constr. Build. Mater.*, 2008, **22**, 1601-1606.

Chung-Yun, H., Feng, F. and Hui, P. *Forest Prod. J.*, 2008, **58**, 56-61.

Clad, *Int. J. Adhesion and Adhesives*, 1983, 3 (2), 127-131

Collins, J.W., Torkelson, J.M. and Webb, A.A. *J. Agric. Food. Chem*., 1977, **25**(4), 743-746.

Columbia Forest Products, *PureBond: Formaldehyde-Free Hardwood Plywood* http://www.columbiaforestproducts.com/product/purebond-classic-core/

Copeland, J. and Turley, D. *National and Regional Supply/Demand balance for agricultural straw in Great Britain*, Central Sciences Laboratory, 2008.

Dayton, C., Jenkins, B.M., Turn, S.Q., Bakker, R.R., Williams, R.B., Belle-Oudry, D. and Hill, *Energ. Fuel.*, 1999, **13**, 860-870.

Della, V.P., Kuhn, I. and Hotza, D. *Mater. Lett.*, 2002, **57**, 818-821.

Demirbas, *Prog. Energy Combust. Sci.*, 2004, **30**, 219-230.

Dutta, P.K. and Shieh, D.C. *Zeolites*, 1985, **5**, 135-138.

Elliott and T. Mahmood, *Tappi J.*, 2006, **5**, 9-16.

El-Wakil,N.A., Abou-Zeid, R.E., Mohamed, A.Y. *Journal of Applied Polymer Science,* 2007, **106**, 3592-3599.

Engelhardt and D. Michel, *High-Resolution Solid-State NMR of Silicates and Zeolites*, John Wiley, New York, 1987.

Engelhardt, D., Zeigan, D., Jancke, H., Hoebbel, D. and Wieker, W. *A. Anorg. Allg. Chem.*, 1975, **418**, 17-28.

English, The National Institute of Environmental Health Sciences (NIEHS), Edition edn., 1994, vol. 102, pp. 168-170.

Ensymm "abstract for solvent free production of tannic acid from fruit peels and organic waste", www.ensymm.com.

Environment Protection Agency, *An Introduction to Indoor Air Quality*, http://www.epa.gov/iaq/formalde.html

Ergudenler and A.E. Ghaly, *Applied Biochemistry and Biotechnology*, 1992, **34**, 75-91.

Falcone Jr, S., Bass, J.L., Krumrine, P.H., Brensinger, K. and Schenk, E.R. *J. Phys. Chem. A*, 2010, **114**, 2438-2446.

Falcone, J.S., Bass, J.L., Angelella, M., Schenk, E.R. and Brensinger, K.A. *Ind. Eng. Chem. Res.*, 2010, **49**, 6287-6290.

FAOSTAT, *ForesSTAT*, http://faostat3.fao.org/faostat-gateway/go/to/home/E

Ferraro and M.H. Manghani, *Journal of Applied Physics*, 1972, **43**(11), 1972, 4595-4599.

Frías,M., Villar-Cociña, E. and Valencia-Morales, E. *Waste Manage.*, 2007, **27**, 533-538.

Fulton-Tompkins, *Binding and cohering composition*, 1917, patent number 1, 247,595

Galeener, F.L. *Phys. Rev. B*, 1979, **19**, 4292.

Garlotta, D., Journal of Polymers and the Environment, 2001, 9(2), 63-84.

Gervais, F., Blin, A., Massiot, D. and Coutures,J.P *J. Non-Cryst. Solids*, 1987, **89**, 384-401.

Ghosh and M. Sain, *Polym. Polym. Compos.*, 2006, **14**, 217-227.

Giancaspro, J., Papakonstantinou, C. and Balaguru, P. *Compos. Sci. Technol.*, 2008, **68**, 1895-1902.

Gibbs, G.V., Boisen, M.B., Hill, F.C., Tamada, O. and Downs, R.T. *Phys. Chem. Miner.*, 1998, **25**, 574-584.

Gill, P.M. *Bulletin 9: Environmentally Safe Binders for Agglomeration*, PQ Corporation, USA, 1997.

Gill, P.M. *Environmentally Safe Binders for Agglomeration*, PQ Corpration, 1997.

Gomes,J.R.B., Cordeiro, M. and Jorge, M. *Geochim. Cosmochim. Ac.*, 2008, **72**, 4421-4439.

Gómez-Barea, Vilches, L.F., Leiva, C., Campoy, M. and Fernández-Pereira, C. *Chem. Eng. J.*, 2009, **146**, 227-236.

Greiner-Wronowa,E., Paluszkiewicz, C. and Stoch, L. *J. Mol. Struct.*, 1999, **512**, 199-204.

Gupta, R., Wall, T. and Baxter, L. *Impact of Mineral Impurities in Solid Fuel Combustion*, Kluwer Academic / Plenum Publishers, New York, 1999.

Guuntekin, Uner, B. and Karakus, B. *Journal of Environmental Biology*, 2009, **5**, 731-734.

Halasz and A. Derecskei-Kovacs, *Mol. Simul.*, 2008, **34**, 937-942.

Halasz, Agarwal, M., Li, R. and Miller, N. *Catal. Lett.*, 2007a, **117**, 34-42.

Halasz, Agarwal, M., Li, R. and Miller, N. *Catal. Today*, 2007, **126**, 196-202.

Halasz, Agarwal, M., Li, R. and Miller, N. *Micropor. Mesopor. Mat.*, 2010, **135**, 74-81.

Hald, P. Technical University of Denmark, 1994.

Halvarsson, S., Edlund, H. and Norgren, M. *Ind. Crop. Prod.*, 2008, **28**, 37-46.

Hanna and Su, G. J.*Journal of the American Ceramic Society*, 1964, **47**, 597-601.

Hareau, W., Oliveira, F.B., Grelier, S., Siegmund, B., Frollini, E. and Castellan, A. *Macromol. Mater. Eng.*, 2006, **291**, 829-839.

Hodson, M.J., White, P.J., Mead, A. and Broadley, M.R. *Annal. Bot.-London*, 2005, **96**, 1027-1046.

Iler, R.K. *The Chemistry of Silica*, Wiley & Sons, New York, 1979.

Iler, R.K. *The chemistry of silica: solubility, polymerisation, colloid and surface properties, and biochemistry*. 1979, John Wiley and Sons.

Isaksson, Z.E., Bruze, M. J*. Occup. Environ. Med.*, 1999, **41**, 261-266.

Janos, P., Buchtová, H. and Rýznarová, M. *Water Res.*, 2003, **37**, 4938-4944.

Jenkins, M., Bakker, R.R. and Wei, J.B. *Biomass Bioenerg.*, 1996, **10**, 177-200.

Jensen, P.A. and Dam-Johansen, K. *Energy & Fuels,* 1998, **12**, 1998, 929-938.

Jensen, P.A., Sander, B. and Dam-Johansen, K. *Biomass Bioenerg.*, 2001, **20**, 447-457.

Jensen, P.A., Frandsen, F.J., Dam-Johansen, K. and Sander, B. *Energ. Fuel.*, 2000, **14**, 1280-1285

Jiang, H., Zhang, Y. and Wang, X. *Industrial Crops and Products*, 2009, **30**, 304-310.

Jones, J.M, Darvell, L.I., Bridgeman, T.G., Pourkashanian, M. and Williams, A. *P. Combust. Inst.*, 2007, **31**, 1955-1963.

Jones, J.M., Nawaz, M., Darvell, L.I., Ross, A.B., Pourashanian, M. and Williams, A. in *Science in Thermal and Chemical Biomass Conversion*, ed. A. Bridgewater, Blackwell Science Ltd, Oxford, Edition edn., 2006, pp. 331-339.

Jones, R.W., Taylor, N.W. and Senti, F.R. *Arch. Biochem. Biophys*., 1959, **84**, 363.

Ju, Z.Y. and Kilara, A. *Journal of Dairy Science*, 1998, **81**(4), 925-931.

Jung, H.G. and Himmerlsbach, D.S. *J. Agric. Food Chem*., 1989, **37**, 81-87.

Kalapathy, J., Proctor, A. and Shultz, J. *Bioresource Technol.*, 2000, **73**, 257-262.

Kalapathy, J., Proctor, A. and Shultz, J. *Bioresource Technol.*, 2000, **72**, 99-106.

Kalapathy, J., Proctor, A. and Shultz, J. *Ind. Eng. Chem. Res.*, 2003, **42**, 46-49.

Kamke, F.A., Sizemore, H., Scott, K.A., Ra, J.B. and Kamke, C.J.C. *Advances in adhesive detection and measurement in panel products.* In: Proceedings of the 4th European Panel Products Symposium, Ed. Hague et al., 11-13 October 2000, Llandudno, Wales, U.K.

Karaosmanoglu, E., Tetik, B., Gurboy and I. Sanli, I., *Energy Sources*, 1991, **21**, 801-810.

Khan, A., de Jong, W., Jansens, P.J. and Spliethoff, H. *Fuel Process. Technol.*, 2009, **90**, 21-50.

Kim, S. *Bioresource Technology*, 2008, **99**, 2032-2036.

Kinrade, S.D. and Pole, D.L. *Inorg. Chem.*, 1992, **31**, 4558-4563.

Kirk, C.T. *Phys. Rev. B*, 1988, **38**, 1255.

Klass, L. *Biomass for Renewable Energy, Fuels and Chemicals*, Academic Press, California, 1998.

Knight, T.G., Balec, R.J. and Kinrade, S.D. *Angew. Chem., Int. Ed.*, 2007, **46**, 8148-8152.

Knudsen, J.N., Jensen, P.A. and Dam-Johansen, K. *Energ. Fuel.*, 2004, **18**, 1385-1399

Knudsen, N.O., Jensen, P.A., Sander, B. and Dam-Johansen, K. in *Biomass for Energy and Industry*, eds. H. Kopetz, T. Weber, W. Palz, P. Chartier and G. L. Ferrero, Centrales Agrar Rohstoff Mkt & Entwicklung Netzwerk, Rimpar, Editon edn., 1998, pp. 224-228.

Llorente, M.J.F. and Garcia, J.E.C. *Fuel*, 2005, **84**, 1893-1900.

Lubi, M. and Thachil, E.T. *Polym. Polym. Compos.*, 2007, **15**, 75-82.

Martinez, J.R., Ruiz, F., Vorobiev, Y.V., Perez-Robles, F. and Gonzalez-Hernandez, J. *J. Chem. Phys.*, 1998, **109**, 7511-7514.

McCormick, A.V., Bell, A.T. and Radke, C.J. *J. Phys. Chem-US.*, 1989, **93**, 1733-1737.

McDonald and LaRosa Thompson, J. *Sodium Silicate a Binder for the 21st Century*, PQ Corporation.

McKendry, *Bioresource Technology.* 2002, **83**, 37-46.

Mecfel, J., Hinke, S., Goedel, W.A., Marx, G., Fehlhaber, R., Bäucker, E. and Wienhaus, O. *J. Plant Nutr. Soil Sci.*, 2007, **170**, 769-772.

Miles, T. R., Miles, T.R., Baxter, L.L., Bryers, R.W., Jenkins, B.M. and Oden, L.L. *Biomass Bioenerg.*, 1996, **10**, 125-138.

Monti, A., Di Virgilio, N. and Venturi, G. *Biomass Bioenerg.*, 2008, **32**, 216-223

Mora-Fonz, M.J., Catlow, C.R.A. and Lewis, D.W. *J. Phys. Chem. C*, 2007, **111**, 18155-18158.

Munoz Aguado, M.J. and Gregorkiewitz, M. *J. Colloid Interface Sci.*, 1997, **185**, 459-465.

Myers, G.C. Forest products Journal, 1987, **37**(10), 63-67.

Nair, G., Fraaij, A., Klaassen, A.A.K. and Kentgens, A.M.P. *Cement Concrete Res.*, 2008, **38**, 861-869.

Nasr-El-Din, H.A. and Taylor, K.C. *J. Pet. Sci. Eng.*, 2005, **48**, 141-160.

Nemli, G. and Öztürk, I. *Build. Environ.*, 2006, **41**, 770-774.

Obernberger, Brunner, T. and Barnthaler, G. *Biomass Bioenerg.*, 2006, **30**, 973-982.

Olanders and Steenari, B.M. *Biomass Bioenerg.*, 1995, **8**, 105-115.

Osswald, J. and Fehr, K.T. *J. Mater. Sci.*, 2006, **41**, 1335-1339.

Perry, C.C., Li, X. and Waters, D.N. *Spectrochim. Acta A-M.*, 1991, **47**, 1487-1494.

Pettersson, Amand, L.E. and Steenari, B.M. *Fuel*, 2009, **88**, 1758-1772.

Phair, J.W. and Van Deventer, J.S.J. *Int. J. Miner. Process.*, 2002, **66**, 121-143.

Pitman, R.M. *Forestry*, 2006, **79**, 563-588.

PQ Corporation, Bulletin 12-31*: Bonding and Coating Applications of PQ Soluble Silicates, PQ Corporation*, 2006.

PQ Corporation, *Sodium Silicates: Liquids and Solids*, PQ Corporation, USA, 2004.

Provis, P. Duxson, G. C. Lukey, F. Separovic, W. M. Kriven and J. S. J. van Deventer, *Ind. Eng. Chem. Res.*, 2005, **44**, 8899-8908.

Rabbii, *Iranian Polymer Journal*, 2001, **10**, 229-235.

Rajamma, R., Ball, R.J., Tarelho, L.A.C., Allen, G.C., Labrincha, J.A. and Ferreira, V.M. *J. Hazard. Mater.*, 2009, **172**, 1049-1060.

Rammon, R.M. in *Proc. 31st Inter. Particleboard and Composite Materials Symp.*, Washington State Univ., Pullman, Washington, Editon edn., 1997, pp. 177-181.

Rao, T.R. and Sharma, A. *Energy*, 1998, **23** (11), 973-978.

Raveendran, K., Ganesh, A. and Khilar, K.C. *Fuel*, 1996, **75** (8), 987-998.

Rees, C.A., Provis, J.L., Lukey, J.C. and van Deventer, J.S.J. *Langmuir*, 2007, **23**, 9076-9082.

Rich, L.M and Foegeding, E.A. *J. Agric. Food. Chem*., 2000, **48**, 5046-5052.

Rodrigues, A. *Cement Concrete Res.*, 2003, **33**, 1525-1529.

Roffael and Dix, B. *Holz als Roh- und Werkstoff,* 1991, 49, 199-205.

Roffael, Process for the manufacture of particle-board and fibreboard, patent number 5,866,057,

Roggendorf, Böschel, D. and Trempler, J. *Journal of Non-Crystalline Solids*, 2001, **293-295**, 752-757.

Ross, B., Jones, J.M., Kubacki, M.L. and Bridgeman, T. *Bioresour. Technol.*, 2008, **99**, 6494-6504.

Salisbury, F.B. and Ross, C.W. *Plant Pysiology*, Fourth edn., Wadsworth, California, 1992.

Sanchez, J. and McCormick, A. *Chem. Mater.*, 1991, **3**, 320-324

Sander, M.L. and Andren, O. *Water Air Soil Pollut.*, 1997, **93**, 93-108.

Sarenbo, S. *Biomass Bioenerg.*, 2009, **33**, 1212-1220.

Schiemenz, K. and Eichler-Lobermann, B. *Nutr. Cycl. Agroecosyst.*, 2010, **87**, 471-482.

Simatupang, M.H. and Geimer, R.L. Wood Adhesives, Wisconsin, 1990.

Staiger, Unterberger, S., Berger, R. and Hein, K.R.G. *Energy*, 2005, **30**, 1429-1438.

Sun, Lawther, J.M. and Banks, W.B. *Carbohydrate Polymer*, 1996, **29**, 1996, 325-331.

Sun, S., Song, Y. and Zheng, Q. Food Hydrocolloids, 2007, **21**, 1005-1013.

Svensson, L., Sjoberg, S. and Ohman, L.O. *J. Chem. Soc. Farad. T. 1*, 1986, **82**, 3635-3646.

Tabarsa, Jahanshahi, S. and Ashori, A. *Composites, part B*, 2011, 176-180; A. Pizzi*, Holz als Roh- und Werkstoff*, 1982, **40**, 293-301

Tamai, K. and Ma, J.F. *New Phytol.*, 2003, **158**, 431-436.

Tangchirapat, W., Saeting, T., Jaturapitakkul, C., Kiattikomol, K. and Siripanichgorn, A. *Waste Manage.*, 2007, **27**, 81-88.

Tate and Lyle, Method for preparing composite materials containing natural binders, US patent 7387756

Tatzber, M., Stemmer, M., Spiegel, H., Katzlberger, C., Haberhauer, G. and Gerzabek, M.H. *Environ Chem Lett*., 2005, **5**, 9-12.

Thy, P., Jenkins, B.M., Lesher, C.E. and Grundvig, S. *Fuel Process. Technol.*, 2006, **87**, 383-408.

Thy, P., Jenkins, B.M., Grundvig, S., Shiraki, R. and Lesher, C.E. *Fuel*, 2006, **85**, 783-795.

Tianinen, M.S., Ryynanen, J.S., Rantala, J.T., Tapio Patrikainen, H. and Laitinen, R.S. in *Impact of Mineral Impurities in Solid Fuel Combustion,* eds Gupta, R., Wall, T. and Baxter, L. Kluwer Academic/Plenum Publishers, New York, Edition edn., 1999, pp.

Trinh, T.T., Jansen, A.P.J. and van Santen, R.A. *J. Phys. Chem. B*, 2006, **110**, 23099-23106.

Ubukata, Mitsuhashi, S., Ueki, A., Sano, Y., Iwasa, N., Fujita, S. and Arai, M. *J. Agr. Food Chem.*, 2010, **58**, 6312-6317.

USA Pat., 6524543, 1998.

Vamvuka, Troulinos, S. and Kastanaki, E. *Fuel*, 2006, **85**, 1763-1771.

van Dam, van den Oever, M.J.A. and Keijsers, E.R.P. *Ind. Crop. Prod.*, 2004, **20**, 97-101.

van der Lans, R.P., Pedersen, L.T., Jensen, A., Glarborg, P. and Dam-Johansen, K. *Biomass Bioenerg.*, 2000, **19**, 199-208.

Van Langenberg, Grigsby, W. and Ryan, G. Green Adhesives: options for the Australian industry-summary of recent research into green adhesives from renewable materials and identification of those closest to commercial uptake, June 2010 (downloaded from www.fwpa.com.au).

Vesterinen, P. *Wood Ash Recycling: State of the Art in Finland and Sweden*, **2003** http://www.cti2000.it/solidi/WoodAshReport%20VTT.pdf.

Viikari, L., Annelia, H. *et al*., Lignin-based adhesives for particle board manufacture, W/O 1998/031764

Vogelsberger, W., Seidel, A. and Rudakoff, G. *J. Chem. Soc. Faraday T.*, 1992, **88**, 473-476.

Wang, S. and Baxter, L. in *Science in Thermal and Chemical Biomass Conversion*, ed. A. Bridgewater, Blackwell Science Ltd., Oxford, Edition edn., 2006, pp. 325-330.

Weber, F. and Hunt, R.D. *Ind. Eng. Chem. Res.*, 2003, **42**, 6970-6976.

Werther, J., Saenger, M., Hartge, E.U., Ogada, T. and Siagi, Z. *Prog. Energy Combust. Sci.*, 2000, **26**, 1-27.

Wu, Y.Q., Wu, S.Y., Li, Y. and Gao, J.S., *Energ. Fuel.*, 2009, **23**, 5144-5150.

Yang, X., Zhu, W. and Yang, Q. *J. Solution Chemistry*, 2008, **37**, 73-83.

Yao, Y., Xu, X. and Feng, Y. *Spectroscopy and Spectral Analysis*, 2003, **23** (1), 58-60.

Yin, Rosendahl, L.A. and Kaer, S.K. *Prog. Energy Combust. Sci.*, 2008, **34**, 725-754.

Yonezawa, D., Miwa, T., Awo, Y. and Shimomura, H. *Bull. Univ. Osaka. Pref. Ser. B.,* 1966, **18**, 61-68;

Zhang, J., Khatib, J.M., Booth, C. and Siddique, R. in *Excellence in Concrete Construction through Innovation*, eds. M. C. Limbachiya and H. Y. Kew, Crc Press-Taylor & Francis Group, Boca Raton, Editon edn., 2009, pp. 517-521.

Zolin, Jensen, A., Jensen, P.A, Frandsen, F. and Dam-Johansen, K. *Energ. Fuel.*, 2001, **15**, 1110-1122.

Zotov and Keppler, H. *Chem. Geol.*, 2002, **184**, 71-82.